**VILNIUS UNIVERSITY**
**NATURE RESEARCH CENTRE**

**ILMA JANUTYTĖ**

# UPPER MANTLE STRUCTURE AROUND THE TRANS-EUROPEAN SUTURE ZONE

Doctoral dissertation
Physical Sciences, Geology (05P)

Vilnius, 2014

Dissertation preparation period 2010-2014 in Vilnius University.

*Scientific supervisor:*

Dr. Elena Kozlovskaya (University of Oulu, Finland, Physical Sciences, Geology – 05P)

*Scientific advisor:*

Dr. Gediminas Motuza (Vilnius University, Physical Sciences, Geology – 05P)

**VILNIAUS UNIVERSITETAS**
**GAMTOS TYRIMŲ CENTRAS**

**ILMA JANUTYTĖ**

# VIRŠUTINĖS MANTIJOS SANDARA TRANSEUROPINĖS SANDŪROS ZONOS SRITYJE

Daktaro disertacija
Fiziniai mokslai, geologija (05P)

Vilnius, 2014

Disertacija parengta 2010 – 2014 m. Vilniaus universitete.

*Mokslinis vadovas:*
Dr. Elena Kozlovskaya (Oulu universitetas, Suomija, fiziniai mokslai, geologija – 05P)

*Mokslinis konsultantas:*
Prof. dr. Gediminas Motuza Matuzevičius (Vilniaus universitetas, fiziniai mokslai, geologija – 05P)

# ABSTRACT

This manuscript is a result of four year studies based on the teleseismic body-wave tomography. The presented study aims to resolve the upper mantle structure around the Trans-European Suture Zone (TESZ) which is the major tectonic boundary in Europe marking transition between the old Proterozoic lithosphere in Northern-Eastern Europe (East European Craton, EEC) and the younger Phanerozoic lithosphere in Central-Western Europe.

We used data of the temporary and permanent seismic stations operated within the study area from May 2006 to June 2008 when the passive seismic experiment PASSEQ 2006-2008, which aimed to study the lithosphere and asthenosphere, was carried out around the TESZ. From data of 183 seismic stations we compiled a dataset of manually picked 8308 arrivals of P-waves from teleseismic earthquakes. We selected the top quality data in order to perform inversions for the entire study area, and we divided the dataset in order to perform investigations focused on different parts of the study area. One division of the dataset was based on data quality, while the other one was based on regional distribution of the seismic stations. The non-linear teleseismic tomography algorithm TELINV was used to perform inversions with the real and synthetic datasets. As a result, we obtain a model of P-wave velocity variations up to about ±3 % compared to the IASP91 velocity model around the TESZ from 70 km (from 60 km for the EEC) down to 350 km. We find that the higher values of seismic velocities to the east of the TESZ correspond to the older EEC, while the lower ones to the west of the TESZ correspond to younger Western Europe. The seismic lithosphere-asthenosphere boundary (LAB) is more distinct beneath the Phanerozoic part of Europe than beneath its Precambrian part. To the west of the TESZ beneath the eastern part of the Bohemian Massif, the Sudetes Mountains and the Eger Rift the lower velocity anomalies are observed from the depth of 70 km, while under the Variscides an average depth of the seismic LAB is about 100 km. We do not

observe the seismic LAB beneath the EEC, but we indicate that the lithosphere thickness in the EEC increases across the TESZ from about 180 km beneath Poland to 300 km or more beneath Lithuania where we indicate the thickest lithosphere in our study area. The LAB on the western edge of the TESZ is at a depth of 150 km, while on the eastern edge it is at a depth of 180 km. The results show that the LAB has a shape of a ramp dipping to the NE direction at an angle of about 30 degrees in the northern part of the study area. In this region we also observe values of seismic velocities close to those of the craton down to about 150 km. In the northern part of the TESZ we do not recognize any clear contact between Phanerozoic and Proterozoic lithosphere, because we investigate the lithosphere while the boundary is more significant in the crust. Further to the south we may refer to a sharp and steep contact on the eastern edge of the TESZ. In the southern part of the TESZ the LAB is shallower most probably due to younger tectonic processes. Beneath Western Lithuania down to 90 km we observe a lower velocity area which could be related to the upper mantle dome which might have originated due to delamination processes. Moreover, at the depth of 120-150 km we find a lower velocity area which follows the proposed palaeosubduction zone between the East Lithuanian Domain (EL) and the West Lithuanian Granulite Domain (WLG), and here we may indicate a slab of the proposed "frozen" palaeosubduction as well. In our results we find some correlation between the crustal thickness and the upper mantle which could be related to either the imperfect crustal travel time corrections used or with different geological conditions. We also indicate that the EL and maybe the WLG crustal units terminate in Northern Lithuania and do not continue to the territory of Latvia.

# REZIUMĖ

Disertacija apibendrina ketverius metus trukusių teleseisminių tūrinių bangų tomografijos tyrimų rezultatus. Šios studijos tikslas yra sudaryti Žemės viršutinės mantijos modelį tyrimų plote, kuris sutampa su pasyvios seismikos projekto PASSEQ 2006-2008 teritorija ir apima Transeuropinę sandūros zoną (TESZ) bei aplinkinius plotus, naudojant teleseisminių bangų tomografijos metodą. Taip pat atlikta atskira studija PV Rytų Europos kratono (EEC) dalyje; šios studijos metu siekta nustatyti plutos struktūrų ir viršutinės mantijos koreliaciją bei sudaryti tikslesnį viršutinės mantijos modelį ir nustatyti litosferos storį EEC.

Šioje studijoje naudoti PASSEQ projekto, kurio tikslas buvo tirti litosferos ir astenosferos sandarą TESZ ir aplinkinėse teritorijose, metu užregistruoti seismologiniai duomenys. TESZ – tai svarbi tektoninė riba, skirianti seną proterozojaus laikų Šiaurės ir Rytų Europos litosferą nuo palyginti jaunos fanerozojaus laikų Vakarų ir Centrinės Europos litosferos. PASSEQ projekto metu buvo įrengtos 139 trumpaperiodės ir 49 plačiajuostės laikinos seisminės stotys 1200 km ilgio ir 400 km pločio teritorijoje tarp Vokietijos ir Lietuvos. Seisminės stotys registravo žemės drebėjimų signalus iš viso pasaulio nuo 2006 m. gegužės iki 2008 m. birželio mėn. Duomenų rinkinys iš 8308 išrinktų teleseisminių P-bangų atvykimų sudarytas naudojant PASSEQ projekto seisminių stočių bei nuolatinių seisminių stočių, veikusių regione projekto laikotarpiu, seismologinius duomenis. Duomenų analizei naudota Seismic Handler programinė įranga. Sudarytas duomenų rinkinys buvo suskaidytas ir atliktos inversijos su atskiromis duomenų rinkinio dalimis. Vienas duomenų rinkinio skaidymas atliktas atsižvelgiant į duomenų kokybės faktorių, kitas – pagal seisminių stočių geografinę padėtį. Netiesinis teleseisminių bangų tomografijos algoritmas TELINV naudotas inversijoms atlikti.

Tyrimų metu buvo gautas teleseisminių P-bangų variacijų pasiskirstymas viršutinėje mantijoje iki 350 km gylio TESZ ir aplinkinėse teritorijose. Tyrimų

plote nustatytos ±3 % seisminių bangų greičių variacijos, lyginant su IASP91 seisminių greičių modeliu. Didesni seisminių bangų greičiai į rytus nuo TESZ siejami su senu EEC, o mažesni greičiai į vakarus nuo TESZ – su jaunesne Vakarų Europa. Nustatyta, kad seisminės litosferos-astenosferos riba (LAB) ryškesnė fanerozojinėje negu proterozojinėje Europos dalyse. Į vakarus nuo TESZ po rytiniu Bohemijos pakraščiu, Sudetais ir Egero riftu žemesnių greičių sritis matoma nuo 70 km gylio. Po Variskidais vidutinis seisminės LAB gylis siekia apie 100 km. Po EEC seisminė LAB nebuvo rasta. Litosferos storis EEC didėja einant į ŠR nuo TESZ nuo 180 km Lenkijoje iki beveik 300 km ar daugiau Lietuvos teritorijoje. TESZ srityje LAB yra 150-180 km gylyje. Rezultatai rodo, jog šiaurinėje tyrimų ploto dalyje LAB yra rampos formos ir gelmėja ŠR kryptimi beveik 30 laipsnių kampu, o seisminių bangų greičiai iki maždaug 150 km gylio yra artimi greičiams kratone. Šiaurinėje TESZ dalyje nerasta ryškaus kontakto tarp fanerozojinės ir proterozojinės Europos, tačiau pietinėje TESZ dalyje, rytiniame pakraštyje, galimai aptiktas ryškus, status ribos kontaktas. Pietinėje TESZ dalyje LAB yra sekliau greičiausiai dėl jaunesnių tektoninių procesų. Vakarų Lietuvos teritorijoje matoma žemų seisminių greičių sritis susieta su galimu viršutinės mantijos kupolu, kuris galimai susiformavo dėl delaminacijos procesų. 120-150 km gylyje aptikta žemesnių seisminių greičių sritis, einanti galima paleosubdukcijos riba tarp Vakarų Lietuvos granulitų domeno (WLG) ir Rytų Lietuvos domeno (EL). Be to, rezultatai rodo, jog EL ir galbūt WLG plutos domenai užsibaigia Šiaurės Lietuvoje ir nesitęsia toliau į Latvijos teritoriją.

# CONTENTS

ABBREVIATIONS ..... 11

INTRODUCTION ..... 12

1 OVERVIEW OF TECTONIC SETTINGS AROUND THE TRANS-EUROPEAN SUTURE ZONE ..... 16

1.1 Tectonic settings ..... 16

1.2 Crustal structure ..... 19

1.3 Review of previous studies ..... 23

2 THEORETICAL BACKGROUND ..... 28

2.1 Theory of ray propagation ..... 28

2.2 Seismic waves at teleseismic distances ..... 32

2.3 Teleseismic tomography inversion ..... 34

2.4 Resolution estimates ..... 37

2.5 Simulation filtering ..... 41

3 DATASET ..... 43

3.1 Data acquisition ..... 43

3.2 Earthquake data and picking of the P-wave arrivals ..... 46

3.3 Compilation and analysis of dataset ..... 52

4 MODEL PARAMETERIZATION ..... 58

5 CRUSTAL TRAVEL TIME CORRECTIONS ..... 62

6 RESOLUTION ..... 67

6.1 Resolution assessment for the top quality dataset ..... 68

6.2 Resolution assessment for datasets of different parts of the study area ..... 72

7 P-WAVE VELOCITY VARIATIONS OBTAINED FOR THE ENTIRE STUDY AREA ..... 79
8 DETAILED STUDY OF THE CRATONIC PART OF THE STUDY AREA: P-WAVE VELOCITY VARIATIONS ..... 84
8.1 Dataset and model parameterization ..... 85
8.2 Crustal travel time corrections ..... 86
8.3 Resolution ..... 87
8.4 Distribution of P-wave velocity variations ..... 97
9 DISCUSSION ..... 100
9.1 Amplitudes of velocity variations ..... 101
9.2 Structure of lithosphere in the study area ..... 102
9.3 Traces of crustal units in the SW part of the EEC ..... 108
10 INTERPRETACION AND CONCLUSIONS ..... 109
AKNOWLEDGEMENTS ..... 114
REFERENCES ..... 117
APPENDIX 1 ..... 132
APPENDIX 2 ..... 135

# ABBREVIATIONS

| | |
|---|---|
| AMCG | anorthosite-mangerite-charnockite-granite |
| BPG | Belarus–Podlasie Granulite Belt |
| CB | Central Belarus Belt |
| DSS | deep seismic sounding |
| EEC | East European Craton |
| EL | East Lithuanian Domain |
| EQ(s) | earthquake(s) |
| Ga | billion years |
| LAB | lithosphere-asthenosphere boundary |
| MLSZ | Middle Lithuanian Suture Zone |
| NE | northeast |
| RMS | rout-mean-square |
| SNR | signal-to-noise ratio |
| STZ | Sorgenfrei-Tornquist Zone |
| SVD | singular value decomposition |
| TESZ | Trans-European Suture Zone |
| TT | travel time |
| TTZ | Teyssere-Tornquist Zone |
| SW | southwest |
| WLG | West Lithuanian Granulite Domain |

*„Supylė svajoklis aukštą kalną...“*

*Romas Lileikis* [1]

# INTRODUCTION

This manuscript is a result of four year studies based on the teleseismic body-wave tomography. The teleseismic tomography is not a novel method, but it has never been used in Lithuania before. Moreover, this study is the first one which applies the teleseismic tomography method for data of the passive seismic experiment PASSEQ 2006-2008 (Wilde-Piórko et al., 2008) which was carried out around the Trans-European Suture Zone (TESZ) and provided a unique possibility to image the upper mantle structure of the area.

**The aim of this study is to obtain a model of P-wave velocity variations in the upper mantle and the seismic lithosphere-asthenosphere boundary (LAB) around the TESZ, and to present a robust model of the upper mantle.** The entire study area coincides with that of the PASSEQ 2006-2008 project. Moreover, a separate study focused on the SW part of the East European Craton (EEC) (i.e. the NW part of the entire study area) was carried out. **This special study aims 1) to estimate in more details the structure of the upper mantle and the lithosphere thickness beneath the SW part of the EEC, and 2) to define whether there is a correlation between the major geological units in the crust and the velocity heterogeneities in the upper mantle.** The special study is important to geosciences in Lithuania, because it is the very first attempt to reveal a possible structure of the deeper parts of the Earth beneath Lithuania. Moreover, it is an important contribution to the other investigations of the

[1] *“The dreamer built up the high mountain...” Romas Lileikis*

Precambrian lithosphere while its structure is still not very well understood and sometimes difficult to resolve.

A compiled dataset of 8308 manually picked P-wave arrivals from teleseismic earthquakes and the non-linear teleseismic tomography algorithm TELINV (Weiland et al., 1995) with optimal inversion parameters and crustal travel time corrections were used. The results obtained during this study may help to improve our knowledge about the upper mantle structure and shape of the seismic LAB beneath the TESZ which is one of the major discussion topics in the geoscientific community, and to provide a deeper understanding of tectonic evolution of Western-Central and Eastern Europe.

---

This manuscript has ten chapters with presented results, two appendixes and several additional parts. In **Chapters 3** to **7** we present results obtained for the entire study area, which coincides with the area of the PASSEQ 2006-2008 experiment, while in **Chapter 8** we present a special study which is focused on the cratonic part of the study area.

In **Chapter 1** called *Overview of tectonic settings around the Trans-European Suture Zone* we present an overview of the tectonic settings and previous studies carried out in the study area.

In **Chapter 2** called *Theoretical background* we present some theory about seismic ray propagation, signal processing, teleseismic tomography inversion method and different tools to evaluate quality of the inversion results.

In **Chapter 3** called *Dataset* we describe the used dataset. We present some information about data collection, selection criteria for the earthquakes, procedure of picking of the P-wave arrivals and compilation of the dataset.

In **Chapter 4** called *Model parameterization* we describe how optimal parameters of the model and teleseismic tomography inversion were determined.

In **Chapter 5** called *Crustal travel time corrections* we present the crustal models used to estimate the crustal effects.

In **Chapter 6** called *Resolution* we describe assessment of resolution.

In **Chapter 7** called *P-wave velocity variations obtained for the entire study area* we present results obtained for the entire study area using different datasets.

In **Chapter 8** called *Detailed study of the cratonic part of the study area: P-wave velocity variations* we present results of the special study which is focused on the SW part of the study area.

In **Chapter 9** called *Discussion* we convey discussion on the results while comparing our results with the results obtained from other studies.

In **Chapter 10** called *Interpretation and conclusions* we present a robust model of structure of the upper mantle in the study area and general conclusions of our study.

In **Abbreviations** we elaborate the most frequently used abbreviations.

**Acknowledgements** contain additional information about other contributions while writing this manuscript.

**References** contain all references of the literature used.

**Appendix 1** contains a list of the earthquakes used in this study.

**Appendix 2** contains a list of the seismic stations used in this study.

# Chapter 1

# OVERVIEW OF TECTONIC SETTINGS AROUND THE TRANS-EUROPEAN SUTURE ZONE

## 1.1 Tectonic settings

The East European Craton (EEC), the Baltica segment, has formed during a collision of three paleocontinents: Sarmatia, Volgo-Uralia and Fenoscandia 2-1,7 Ga (Bogdanova et al., 2001) resulting in the Central Russian Rift System, the Pachelma Rift and the Volyn-Orsha Aulacogen (Fig. 1.1). The EEC in the east is bordered by the Uralides orogen and the Timan Ridge and in the west by the Trans-European Suture Zone (TESZ). The NE part of the EEC is composed of several Svecofennian crustal domains extending to the SW direction throughout the Baltic States, Belarus and Poland down to the TESZ (Bogdanova et al., 2006) (Figs. 1.2, 1.3).

The TESZ is a major lithospheric boundary in Europe (Pharao, 1999) which is well manifested in geophysical data. Due to long evolution and complex tectonic structure the TESZ has always been a subject of great interest in geosciences. The TESZ is 150 – 200 km wide and more than 2000 km long boundary between the old Proterozoic lithosphere of Northern-Eastern Europe and the younger Phanerozoic lithosphere of Central-Western Europe. It has formed after a breakup of Rodinia during accretion of suspect terrains along the SW margin of the Precambrian EEC (Nolet and Zielhuis, 1994). The TESZ contains two large linear segments: the Sorgenfrei-Tornquist Zone (STZ) in the NW part of the TESZ

between Sweden and Denmark–Germany, and the Teisseyre-Tornquist Zone (TTZ) stretching from the Baltic Sea in the NW to the Black Sea in the SE. The territories around the TESZ have formed during four major geological stages: 1) Caledonian collision tectonics, 2) Variscan orogeny, 3) Mesozoic rifting, and 4) Alpine orogenic events (Thybo, 2000).

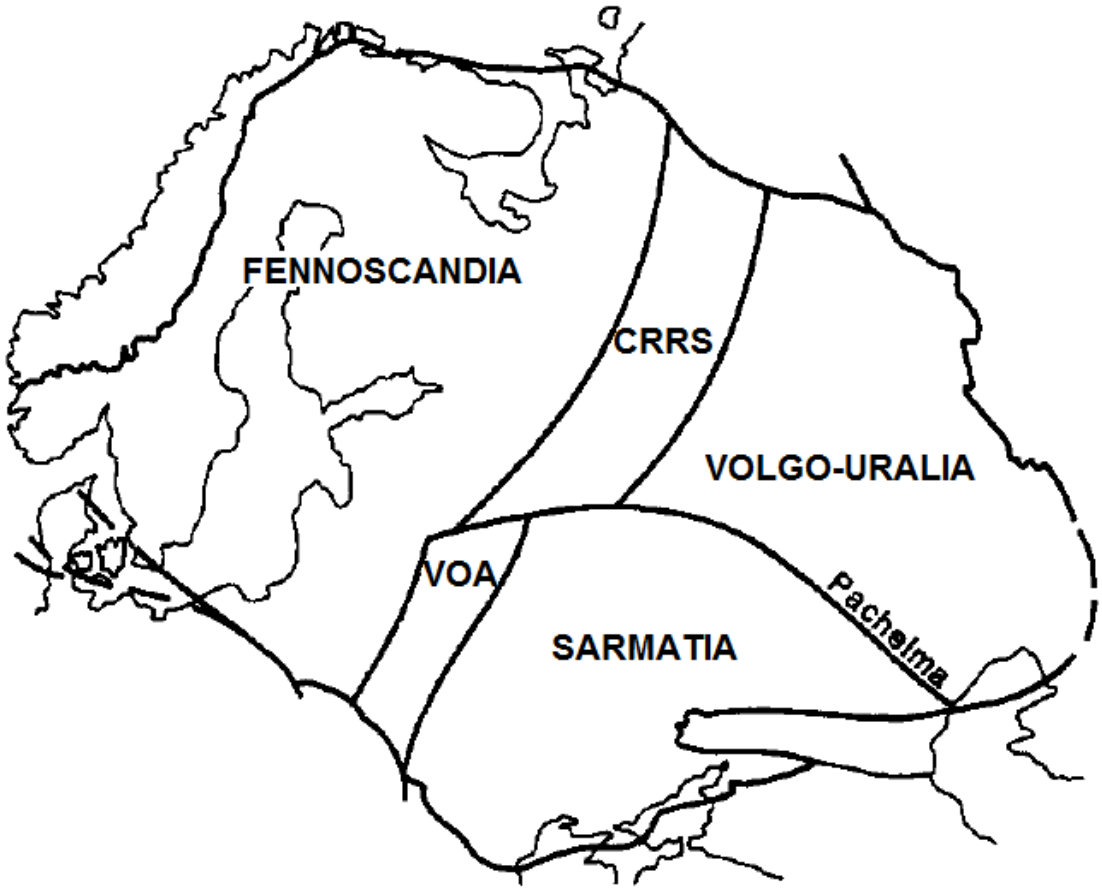


Fig. 1.1 Sketch of major tectonic units of the EEC (after Bogdanova et al., 1996). Notations: CRRS – Central Russia Rift System; VOA – Volyn-Orsha Aulacogen.

The lithosphere to the east of the TESZ is a stable block since at least 1.45 Ga (Bogdanova et al., 2006), while to the west of the TESZ structure of the

lithosphere is much more complex (Dadlez et al., 2005; Knapmeyer-Endrun et al., 2013; Babuška and Plomerova, 2001). The Western-Central Europe consists of various continental fragments that were subsequently rifted off the northern margin of Gondwana and accreted to Baltica during a number of orogenic events (Pharaoh, 1999; Winchester and the PACE TMR Network Team, 2002; Banka et al., 2002). During the Cambrian period the terrains of Lysogory, Malopolska and Bruno-Silesian accreted to Baltica forming southern Poland and the eastern edge of the Bohemian Massif (Belka et al., 2000) (Fig. 1.2). During the Caledonian orogeny the Avalonian segment closing the Tornquist Ocean accreted to the eastern margin of Baltica (Pharaoh, 1999). The Variscan orogeny from late Silurian to early Carboniferous resulted in a junction of three paleomicrocontinents of the Saxothuringian, the Moldanubian and the Tepla-Barrandian in the territory of Vogtland and NW Bohemia (Franke and Zelazniewicz, 2000). The Saxothuringian is juxtaposed against the Moldanubian in a broad contact indicating a paleosubduction of the Saxothuringian, possibly with a piece of oceanic lithosphere beneath the Moldanubian (Plomerova et al., 1998). The "triple junction" resulted in thinning of a crust and lithosphere as well as a tectono-sedimentary evolution of the Cheb Basin situated above the junction. The basin formed between the late Oligocene and Pliocene by reactivation of the Variscan junction of the three lithospheric blocks (Babuška et al., 2007). During the Cretaceous to Cenozoic periods a number of terrains accreted to Western Europe resulting the Alpine and Carpathian orogenies. In middle to late Eocene rifting processes took place in Central Europe followed by the quaternary volcanism (Wagner et al., 2002; Babuška et al., 2007) which was possibly related to the upper mantle reservoir (Babuška and Plomerova, 2001; Zhu et al., 2012). The developed Tertiary Eger Rift continues 300 km in ENE–WSW direction and follows the late Variscan mantle transition between the Saxothuringian and the Tepla-Barrandian (Fig. 1.2).

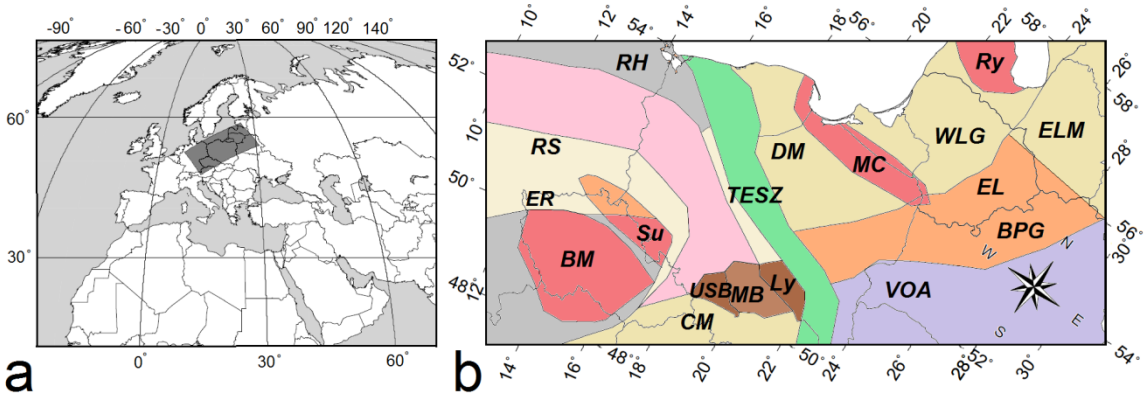


Fig. 1.2 (a) Location of the study area (grey rectangle). (b) Tectonic sketch of the study area compiled from Skridlaite and Motuza (2001), Malinowski et al. (2008), Guterch et al. (1999), Bogdanova et al. (2001), and Gee and Stephenson (2006). Units: BM, Bohemian Massif; BPG, Belarus–Podlasie Granulite Belt; CM, Carpathian Mountains; DM, Dobrzyn Massif; EL, East Lithuanian Domain; ELM, East Latvian Massif; ER, Eger Rift; Ly, Lysogory; MB, Malopolska Block; MC, Mazury Complex; RH, Rhenoherzynian Front; RS, Rheic Suture; Ry, Riga batholit; Su, Sudetes Mountains; TESZ, Trans-European Suture Zone; USB, Upper Silesian Coal Basin; VOA, Volyn–Orsha aulacogen; WLG, West Lithuanian Granulite Domain.

## 1.2 Crustal structure

Crustal thickness varies significantly in the study area: from 28–35 km beneath the Palaeozoic Platform (Guterch and Grad, 1996; Pharaoh et al., 1997; Guterch et al., 1999) to 40-50 km beneath the western part of the EEC adjoining the TESZ (Grad et al., 2006; Guterch et al., 2004) and more further to the NE. Moreover, there were reported some steep changes in the Moho depth and seismic velocity values in some parts, e.g. step-like increase in the Moho depth from 42 to 44 km (which is comparable with resolution of the method) was found along the P5 profile between the Mazury Complex and the Mazowsze Massif (Czuba et al.,

2001), which may be related to the different crustal units. The thickest sedimentary cover up to 16-20 km is beneath some parts of the Polish Through (Guterch et al., 1999).

Grad et al. (2006) and Motuza et al. (2000) summarized results of the deep seismic sounding (DSS) projects (Fig. 1.3) that were conducted in the SW part of the EEC, and distinguished several tectonic domains in the upper lithosphere along the EUROBRIGDE profile: the Vestervik-Gotland block (partly occupied by the Trans-Scandinavian Igneous Belt), the West Lithuanian Granulite Domain (WLG), the East Lithuanian Domain (EL), and the Belarus–Podlasie Granulite Belt (BPG) (Fig. 1.4). The Moho boundary in the WLG is 42-44 km, while in the EL and the BPG it varies from 50 to 57 km. The 35-40 km wide zone in between the WLG and the EL with an abrupt change in crustal thickness, seismic velocity values and other physical parameters is known as the Middle Lithuanian Suture Zone (MLSZ) – the area is interpreted as a palaeosubduction zone along which the terrain in the east subducted under the terrain in the west (Motuza, 2004; Motuza, 2005; Motuza and Staškus, 2009). Motuza (2005) also interpreted the rocks of the crystalline crust of the WLG as a back-arc complex of the Svecofennian orogeny, rocks of the MLSZ as volcanic arc complex, and the rocks of the EL as an accretionary complex, which are related to collision between Fennoscandia and Sarmatia. The contact between the EL and the BPG further to the NE is not so prominent (Motuza, 2005). In the WLG the seismic velocities in the uppermost mantle vary from 8.65 to 8.9 km/s and increase along the EUROBRIDGE profile from the west to the east (Motuza et al., 2000). The crustal features of the EL show lineaments extending to the NE-SW direction which coincide with the direction of collision with Sarmatian palaeocontinent (Motuza, 2005; Bogdanova et al., 2001; Motuza and Staškus, 2009).

Anorogenic magmatism took place in Lithuania and adjacent areas 1.6–1.46 Ga resulting in a number of intrusions of granite and anorthosite-mangerite-charnockite-granite (AMCG) type (Bogdanova et al., 2006) (Fig. 1.2). The largest

AMCG-type intrusion present in our study area is the Riga batholith in Western Latvia. The intrusions of the Mazury Complex form an igneous belt extending the W-E direction along the border of the Kaliningad District of Russia and NE Poland up to SW Lithuania and NW Belarus (Rämö et al., 1996; Dörr et al., 2002).

The junction between Fennoscandia and Sarmatia is significant in Belarus (e.g. Bogdanova et al., 1996) (Figs. 1.3, 1.4). A crustal pattern in the area shows crustal units with alternating granulite and amphibolite facies which vary in age and origin. The structural features suggest that an accretion was driven by several events of subduction and collision, while an accretionary tectonics prevailed 2.0-1.8 Ga (Bogdanova, 1999; Claesson at al., 2001). The Volyn-Orsha Aulacogen (VOA) of Meso- to Neoproterozoic age follows the junction of Fennoscandia and Sarmatia while the Osnitsk-Mikashevichi Igneous Belt (OMIB) represents an active continental margin along the NW edge of Sarmatia (Bogdanova et al., 1996). The 200-250 km wide OMIB consists of various rocks of amphibolite facies (Aksamentova and Naydenkov, 1991) and contains large batholiths of age 2.02-1.95 Ga, which are only slightly metamorphosed and deformed, and younger rapakivi-type granites of age 1.0-1.75 Ga (Skobelev, 1987). At the edge of Sarmatia there are the Central Belarus Belt (CB) and the Vitebsk Granulite Domain (VG) of the Palaeoproterozoic age (about 2.0 Ga). The VG adjoins the CB in the east and NE. Bogdanova et al. (1996) and Stephenson et al. (1996) indicated the complex crustal structures along the Fennoscandia-Sarmatia junction with the VG and the CB slightly dipping to the SE direction beneath the edge of Sarmatia. The CB consists of bodies of amphibolite and granulite facies (Bogdanova et al., 2001) with significant tectonic faults separating the units of different composition. Claesson et al. (2001) showed that the supracrustal rocks of the VG are similar to the ones of the southeastern CB.

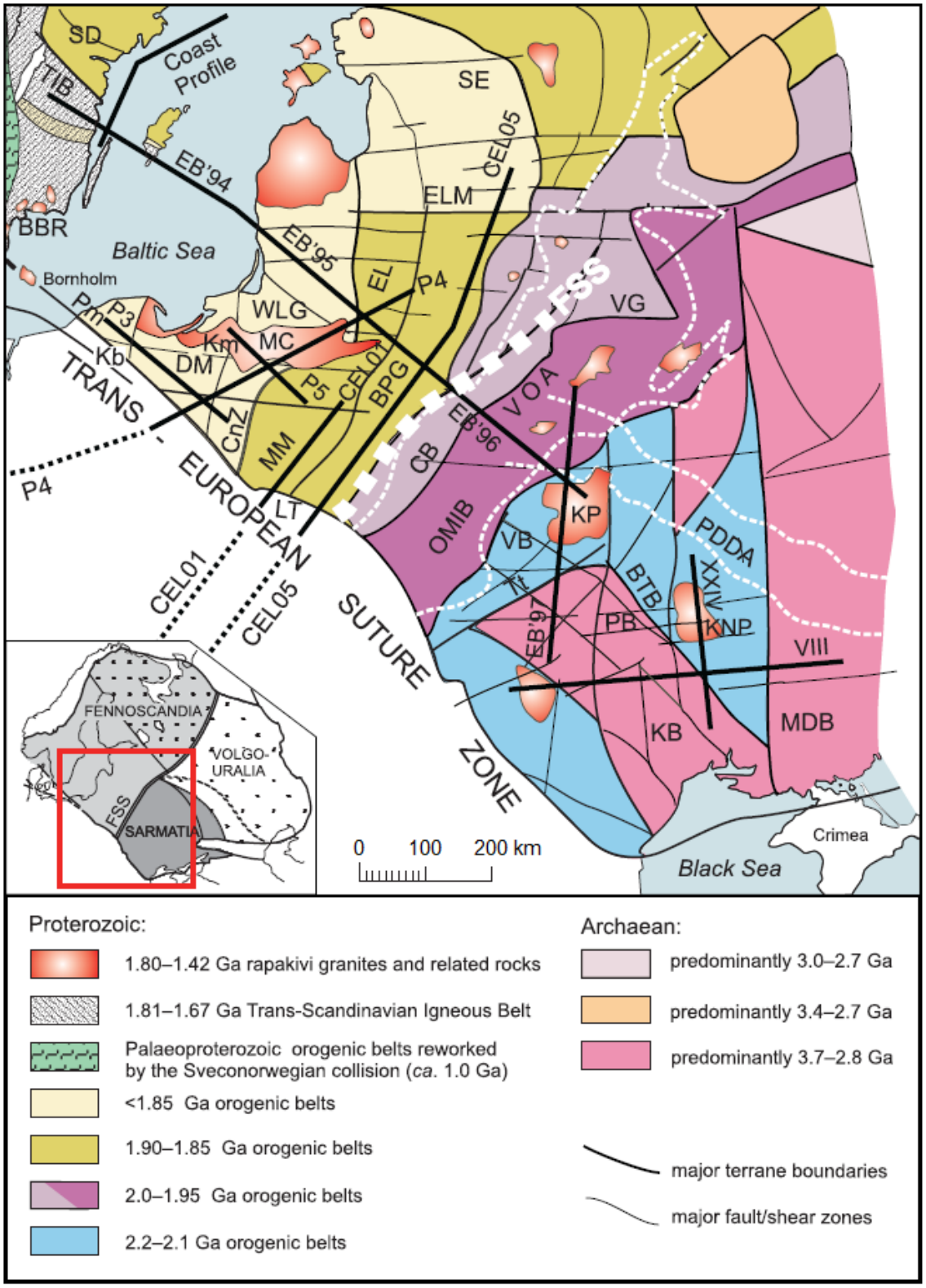


Fig. 1.3 Simplified tectonic map (after Bogdanova et al., 2001) of the SW margin of the EEC and locations of refraction and wide-angle reflection DSS profiles.

Solid straight lines — DSS profiles EUROBRIDGE (EB'95, EB'96 and EB'97), POLONAISE'97 (northern part of P4, P3 and P5), VIII and XXIV profiles; dashed lines — parts of profiles in the TESZ and the Carpathians; and white dashed lines show boundaries of aulacogens. Units: BBR — Blekinge–Bornholm region; BTB — Belaya–Tserkov Belt; CB — Central Belarus Belt; CnZ — Ciechanów Zone; FSS — Fennoscandia–Sarmatia Suture; KB — Kirovograd Block; Kb — Kaszuby Block; Km — Kętrzyn Massif; KNP — Korsun–Novomirgorod Pluton; KP — Korosten Pluton; LT — Lublin Trough; MDB — Middle Dnieper Block; MM — Mazowsze Massif; OMIB — Osnitsk–Mikashevichi Igneous Belt; PB — Podolian Block; Pm — Pomorze Massif; PDDA — Pripyat–Dnieper–Donets Aulacogen; SD — Svecofennian Domain; SE — South Estonian Granulites; TIB — Trans-Scandinavian Igneous Belt; Tt — Teterev Belt; VB — Volyn Block; VG — Vitebsk Granulite Domain. For other explanations see Fig. 1.1.

## 1.3 Review of previous studies

Structure of the crust and the uppermost mantle around the TESZ has been studied intensively during the controlled-source seismic experiments – long-range DSS profiles (e.g. Guterch et al., 1999; Grad et al., 2002; Guterch et al., 2004; Grad et al., 2006; EUROBRIDGE Seismic Working Group, 1999; Pharaoh et al., 2000) and provided detailed models of the crust and the uppermost mantle (e.g. Czuba et al., 2001; Malinowski et al., 2008). The obtained results show large variations of the average thickness of the continental crust. Using data of the DSS projects EUROBRIDGE Working Group (1999), Czuba et al. (2001), Yliniemi et al. (2004) and Grad et al. (2002) in Fennoscandia found the reflectors in the upper mantle just beneath the Moho going down to 75 km. Similar subhorizontal lithospheric reflectors were observed beneath the TESZ (Grad et al., 2002;

Guterch et al., 2004) and the Baltic Sea (Hansen and Balling, 2004). However, depth of resolution of the DSS profiles is usually limited to about 50-80 km. Thus, structure of the deeper lithosphere and the LAB is usually resolved using different methods. But before talking about the deeper lithosphere we present different practical definitions of the LAB regarding different physical properties and geophysical techniques (Eaton et al., 2009):

1) seismic LAB defines transition between the solid outer layer of the Earth, which is characterized by higher seismic velocity values, and its low-viscous interior, which is characterized by lower seismic velocity values;
2) thermal LAB defines transition between the outer layer with dominating conductive heat transfer above the convective mantle which usually coincides with a depth of a constant isotherm of about 1300 ˚C (McKenzie, 1967);
3) electrical LAB is a transition between generally electrically resistive outer layer of the Earth and conductive layer in the upper mantle.

Compared to the crust, the structure of the lithosphere and the LAB around the TESZ is poorly known. The studies show that the lithosphere differs much on both sides of the TESZ (e.g. Majorowicz et al., 2003; Artemieva et al., 2006; Koulakov et al., 2009). The cratonic lithosphere extends much deeper than that of the younger continental regions (e.g. Plomerova et al., 2002b; Eaton et al., 2009; Shomali et al., 2006; Gregersen et al., 2010). The studies by Majorowicz et al. (2003) and Artemieva et al. (2006) based on global tomography and heat flow measurements shows that beneath the EEC the thickness of thermal lithosphere is about 180-200 km, while thickness of the seismic lithosphere is more than 250 km. The study by Artemieva et al. (2006) includes results from some seismic reflection and refraction profiles for the EEC (e.g. Vinnik and Ryaboy, 1981; Garetskii et al., 1990; Grad and Tripolsky, 1995; Kostyuchenko et al. 1999; EUROBRIDGE Working Group & EUROBRIDGE'95, 2001; Grad et al., 2002;

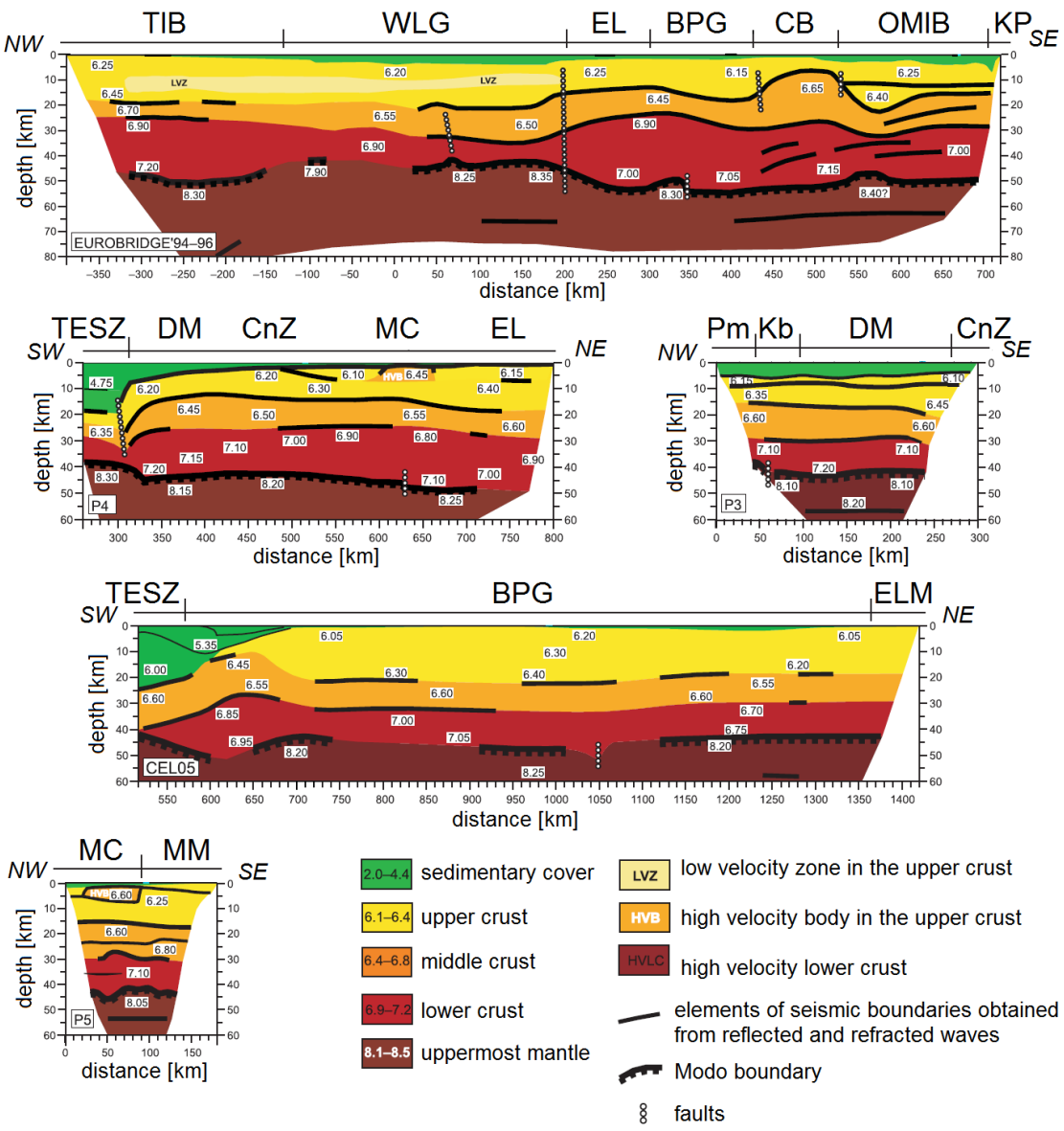


Fig. 1.4 Models of the crust and the uppermost mantle along the EUROBRIDGE transect (EB'94 and EB'96), the POLONAISE'97 profiles P4 (northern part), P5 and P3, and CELEBRATION 2000 profile CEL05 (after Grad et al., 2006). Values of P-wave velocities are given in km/s. For other explanations see Fig. 1.2. Locations of the DSS profiles in Fig. 1.3.

Thybo et al., 2003), P- and S-wave tomography and mantle anisotropy (e.g. Matzel and Grand, 2004), and the data is quite sparse and resolution is questionable, however, it provides an important insight to the lithosphere thickness of the EEC. Even deeper, down to at least 300 km, the positive P-wave anomalies are found beneath the EEC by Koulakov et al. (2009). Legendre et al. (2012) find no indications of a deep cratonic root below about 330 km for the EEC, while Geissler et al. (2010) do not observe any clear indications of the deep LAB beneath the EEC either.

In Central-Western and Northern Europe the passive seismic array project TOR, which was carried out across the STZ in 1996–1997, provided a detailed model of the upper mantle and the LAB (Gregersen et al., 1999; Wilde-Piórko et al., 2002; Plomerova et al., 2002a, Shomali et al., 2006; Artlitt, 1999; Cotte et al., 2002). The results show that an average thickness of the seismic lithosphere is about 100 km in Central Europe, which coincides with global tomography studies by Artemieva et al. (2006) and the studies of the S-receiver functions by Geissler et al. (2010). The results obtained from the TOR data indicate that beneath the TESZ the thickness of the seismic lithosphere is about 120 km, which is an intermediate value between that of the EEC and Western Europe (Shomali et al., 2006; Wilde-Piórko et al., 2010), while transition beneath the STZ is near-vertical with only a weak tendency to the NE slope (Gregersen et al., 2010). Geissler et al. (2010) indicate a lithosphere thickness of about 115–130 km in the vicinity of the TESZ, while the LAB beneath the SW part of the Variscan Bohemian Massif is estimated at the depth of about 115 km, and thin lithosphere of only about 75 km is reported beneath parts of the Pannonian Basin. Beneath the Bohemian Massif an extensive both P and S-waves low-velocity heterogeneity in the upper mantle is found (Koulakov et al., 2009; Karousova et al., 2013), while the high-resolution tomography studies indicate the most distinct low-velocity perturbations along the Eger Rift down to about 200 km (Karousova et al., 2013). Plomerova et al. (2007)

interpret the broad low-velocity anomaly beneath the Eger Rift by an upwelling of the LAB, while they also find different orientations of seismic anisotropy corresponding to the major tectonic units in the Bohemian Massif (i.e. the Saxothuringian, the Moldanubian and the Tepla-Barrandian). The studies of shear-wave splitting (e.g. Wüstefeld et al., 2010; Vecsey et al., 2013; Sroda et al., 2014) show that anisotropy in the Bohemian Massif is higher compared to the one observed in the TESZ and even smaller, but still noticable, for the EEC (Plomerova et al., 2008).

Jones et al. (2010) performed comparison between the delineation of the LABs for Europe based on seismological and electromagnetic observations and concluded that the LABs, as an impedance contrast from receiver functions, a seismic anisotropy change and an increase in conductivity from magnetotellurics, are consistent with the deeper LAB beneath the EEC and the shallower LAB beneath Central Europe, which coincides with conclusions by Korja (2007) who made a review of studies of magnetotelluric imaging of the European lithosphere. Jones et al. (2010) found that the seismic and electric LABs beneath the Phanerozoic Europe are at a depth of about 90–100 km, while for the EEC they differ and the electric LAB is at a depth of about 250 km. The studies also indicate anomalously thick electrical LAB beneath the TESZ, whereas the seismic LAB should be much shallower. This difference could be due to increased partial melting or hydration.

# Chapter 2

*"Nebeprisikiškiakopūsteliaujantiesiem"* [//]

# THEORETICAL BACKGROUND

## 2.1 Theory of ray propagation

Huygens's Principle describes geometry of a wavefront. It states that every point on a propagating wavefront can be considered as a source of secondary wavefronts when it meets heterogeneity on its way. Propagation of a secondary wave follows a surface tangent, and velocity of a ray propagation depends on density of a medium. When a propagating ray meets discontinuity with different density, it results in temporal distortion of a shape of a wavefront.

Fermat's Principles describes geometry of a raypath. It states that ray (energy) follows the minimum time path.

Snell's Law describes refracted waves when a ray enters from one media to another and its path changes due to different velocities:

$$\frac{\sin i_1}{v_1} = \frac{\sin i_2}{v_2}, \qquad (2.1.1)$$

where $i_1$ and $i_2$ are angles of incidence in two media, and $v_1$ and $v_2$ are velocities of ray propagation in two media (Fig. 2.1). A parameter inverse to velocity is defined as slowness:

[//] *(the longest Lithuanian word)*

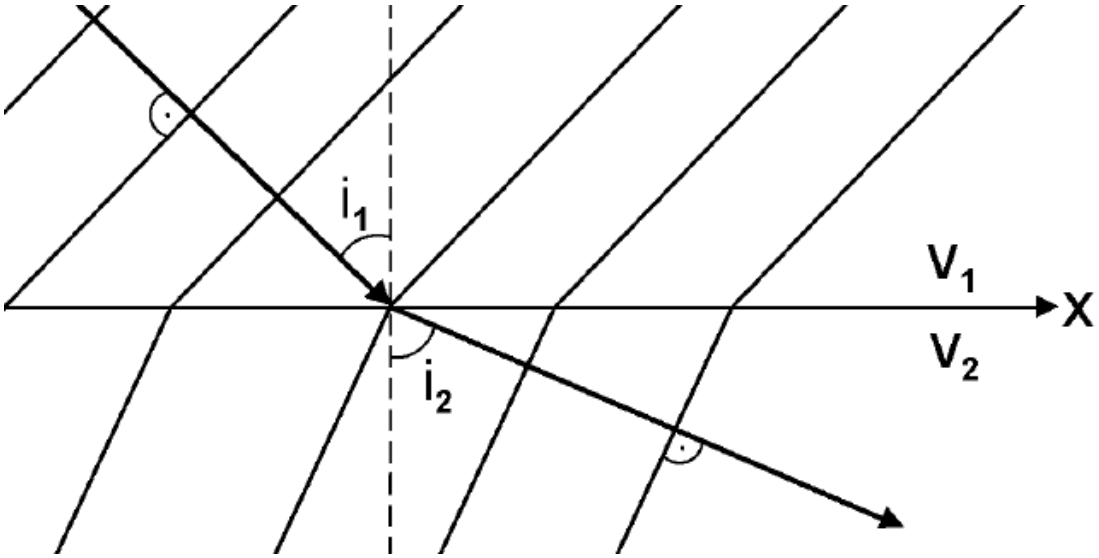


Fig. 2.1 A plane wavefront with an associated ray crossing a boundary of two media with $v_2 > v_1$ (after Bormann, 2002)

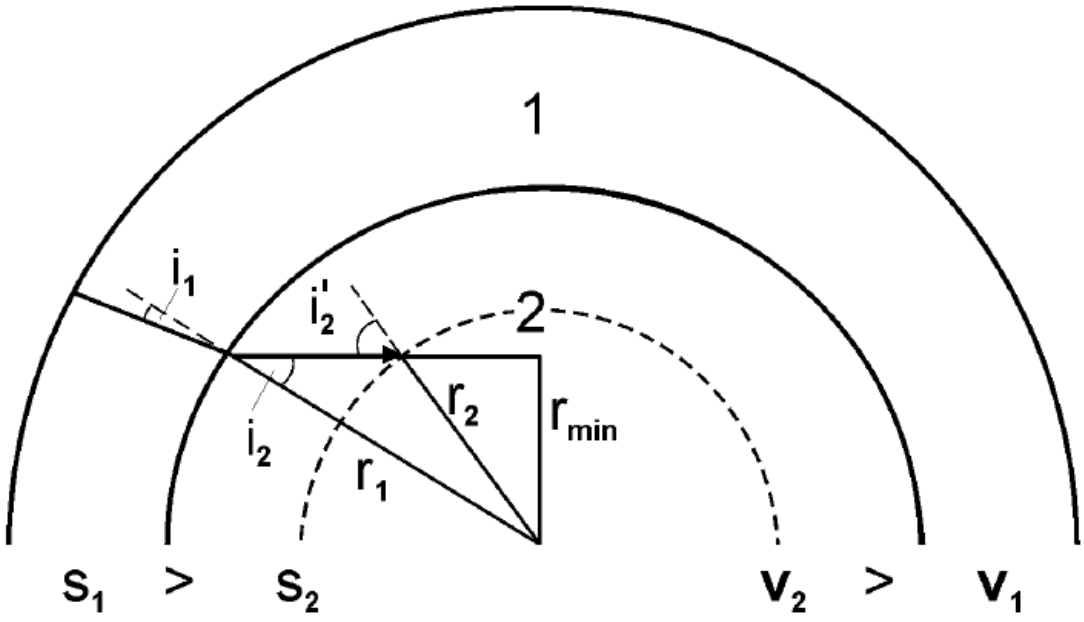


Fig. 2.2 Ray geometry for an Earth model consisting of two spherical shells of constant but different velocities $v_1$ and $v_2$ (after Bormann, 2002).

$$s = \frac{1}{v}, \tag{2.1.2}$$

where *v* is velocity in a media. Then Snell's Law can be rewritten:

$$s \sin i = p, \tag{2.1.3}$$

where *p* is a ray parameter; which represents an apparent slowness of a wavefront in a horizontal direction (Bormann, 2002).

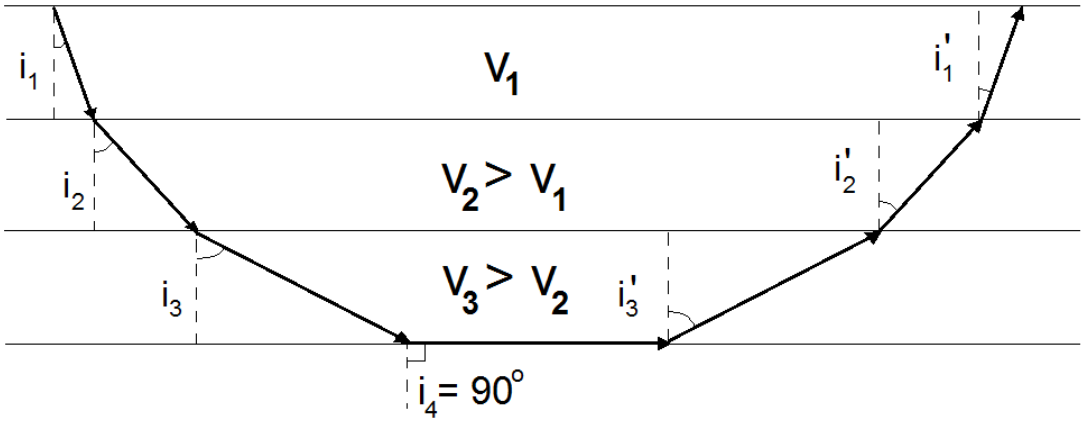


Fig. 2.3 Ray propagation through a multi-layered model with constant velocity within the layers but increasing velocity with depth of the layers.

At distances >12 degrees the Earth's curvature must be taken into account, and a ray parameter must be modified as well. Consider velocity structure as showed in Fig. 2.2. Snell's Law must be satisfied locally:

$$s_1 \sin i_1(r_1) = s_2 \sin i_2(r_2) \tag{2.1.4}$$

for $r_1$=$r_2$, where $r_1$ and $r_2$ are radiuses of two spherical shells. An incidence angle changes as a ray progresses, but the relation holds:

$$s_1 r_1 \sin i_1 = s_2 r_2' \sin i_2', \tag{2.1.5}$$

and can be generalized to the modified Snell's Law for the spherical Earth:

$$s\, r \sin i = \frac{r \sin i}{v} \equiv p, \tag{2.1.6}$$

where *p* is constant for laterally homogeneous media only (Bormann, 2002).

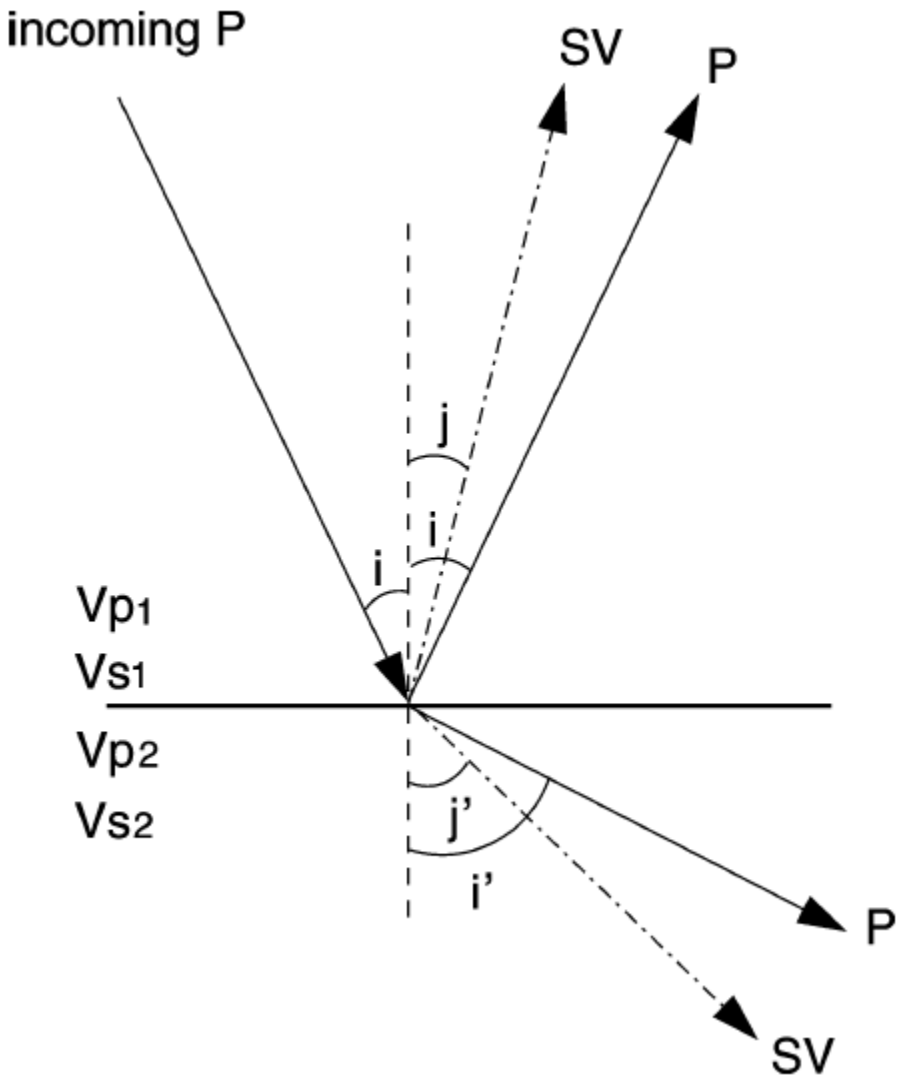


Fig. 2.4 An incident P-wave at a solid-solid boundary with $v_1 < v_2$ generates a reflected and a transmitted P-waves and a reflected and a transmitted SV-waves (after Bormann, 2002).

Due to compaction of material a seismic velocity increases with depth in most parts of the Earth. Consider a ray travelling downwards through a stack of layers

with constant slowness $s_i$ and increasing velocities with depth (Fig. 2.3). Snell's Law must be satisfied for all layers:

$$p = s_1 \sin i_1 = s_2 \sin i_2 = s_3 \sin i_3 = \cdots \quad (2.1.7)$$

In such velocity structure an incidence angle $i$ is continuously increasing with depth, and finally approaching 90°, which is called the turning point (Bormann, 2002). From the turning point a propagating seismic ray is headed towards the surface.

When a propagating seismic ray meets heterogeneity a part of seismic energy is transmitted, reflected or/and converted. If a P-wave hits a boundary between layers with different seismic velocities, four different waves may be generated: a transmitted P-wave; a converted transmitted S-wave purely polarized in the vertical plane of propagation (SV-wave); a reflected P-wave; and a reflected converted SV-wave (Fig. 2.4). Geometry of these waves is governed by Snell's Law (Bormann, 2002):

$$\frac{\sin i}{v_{p1}} = \frac{\sin j}{v_{s1}} = \frac{\sin i'}{v_{p2}} = \frac{\sin j'}{v_{s2}}. \quad (2.1.8)$$

## 2.2 Seismic waves at teleseismic distances

Earthquakes (EQs) observed at epicentral distance up to about 700 km are called local EQs, from 700 km to about 2000 km are called regional EQs, and from >2000 km are called teleseismic EQs. The EQs observed at different distances expose different types and phases of the seismic waves.

Seismic waves arriving at distances from 10 to 30 degrees mainly propagate through the upper mantle and the lower mantle resulting in complicated short-period forms of P- and S-waves consisting of a sequence of successive onsets with different amplitudes. For the EQs with epicentral distances >30 degrees the P- and S-waves are followed by an increasing number of secondary waves, mainly phases, which have been reflected or converted at the surface of the Earth or at the

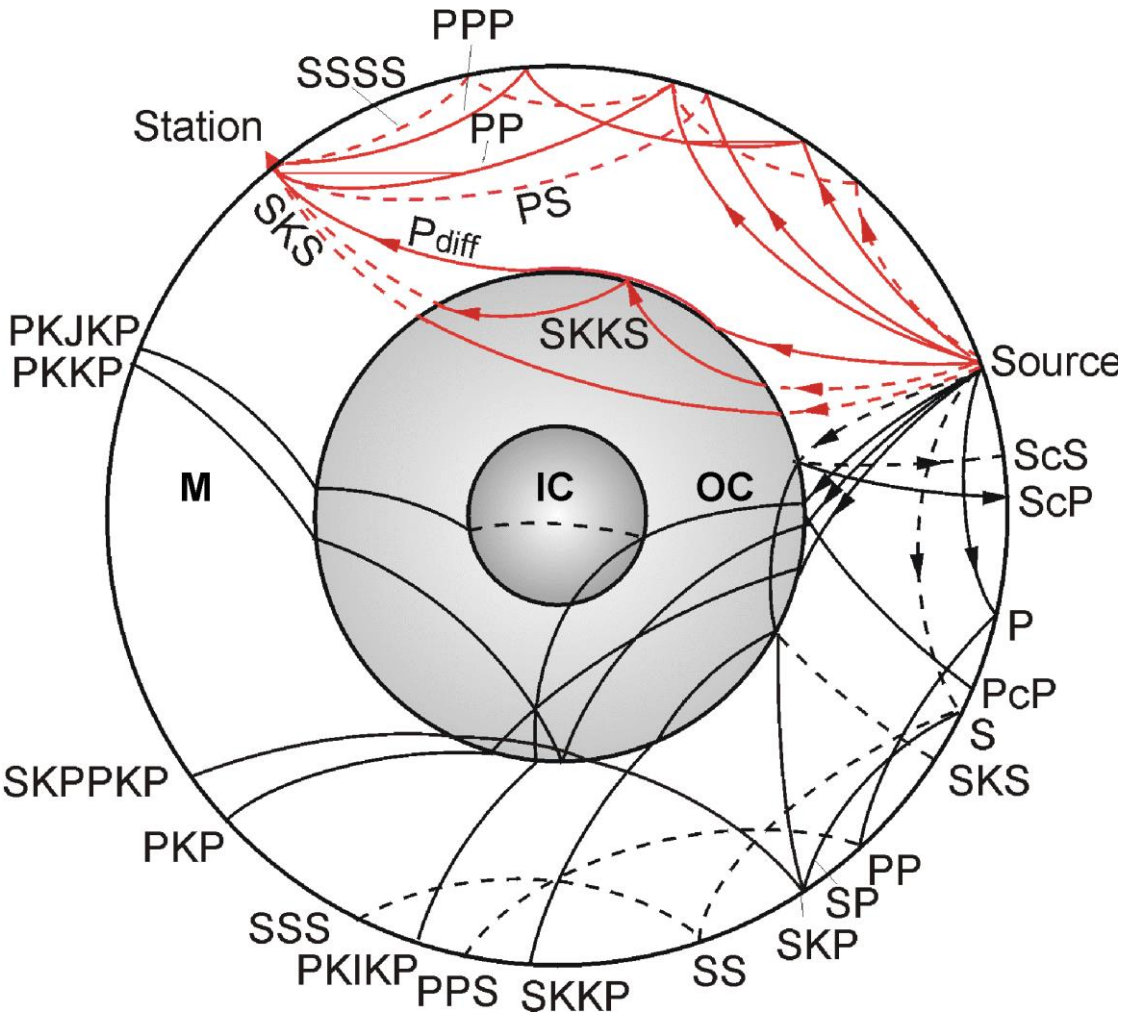


Fig. 2.5 Seismic raypaths through the mantle (M), outer core (OC) and inner core (IC) of the Earth with the respective phase symbols according to the international nomenclature. Solid lines indicate P-rays, and dashed lines indicate S-rays (after Bormann, 2002).

core-mantle boundary. In case of deep EQs a direct P-wave that leaves its source downwards will arrive at a teleseismic station first. For EQs with epicentral distances between 30 and 100 degrees the P- and S-waves propagate through the lower mantle, which is characterized by rather smooth positive velocity and density gradient, resulting relatively clearly structured P- and S-waveforms in

seismograms being the first prominent longitudinal and transverse wave arrivals. The first arrivals are followed by multiple surface and core-mantle boundary reflections or conversions of P- and S-waves such as PP, PS, SS and PcP, ScP, etc. (Fig. 2.5). At epicentral distances of >100 degrees only the P-waves which enter the outer core after strong downward refraction reach the surface.

The first discernible motion of a seismic phase in the record is called the arrival time and the measurement of it is termed picking of the arrival (Bormann, 2002).

## 2.3 Teleseismic tomography inversion

In teleseismic tomography one observes the teleseismic EQs to image the interior of the Earth. With an array of seismometers one can get detailed informations on the subsurface structure just below the array (Fig. 2.6). The calculations, based on certain model assumptions and parameter sets, are referred to as solution of a direct or forward problem, whereas the other way around, i.e. to draw inferences from the observed data itself on the effects and relevant parameters is termed as an inverse problem.

In teleseismic tomography some parameters must be defined before inversion. Usually the model is parameterized by a grid which contains a set of nodes where the values of seismic velocities of the reference model are defined, and during inversion the velocity perturbations are being calculated. An important parameter of the grid is the spacing between the grid nodes in both horizontal and vertical directions, which influence the resolution capabilities. For geophysical inverse problems, regularization methods, such as smoothing and damping are generally applied to condition the system. The smoothing constrains provide more stability to the system (Zhang and Thurber, 2007). The damping parameter determines how much noise present in the data is mapped in a resolved model. Underestimation of damping would result in noise fitting and overestimation would reduce lateral velocity variations. The optimal damping value should be selected by running a

series of inversions with a large range of damping values and plotting a trade-off curve between a model variance and a data variance. The trade-off curve is roughly hyperbolic. Below some certain damping value the modeling results start to wander away from this hyperbola, which indicates that the inversion is not behaving linearly, thus, the optimal damping value should be selected above that value, which is a good compromise between data misfit (too smooth model) and a large model variance (too complex, hence fitting the noise in the data) (Evans et al., 1994). Implementation of damping is important to handle a loss of information and reduce the instabilities which are inherent in many inversion problems.

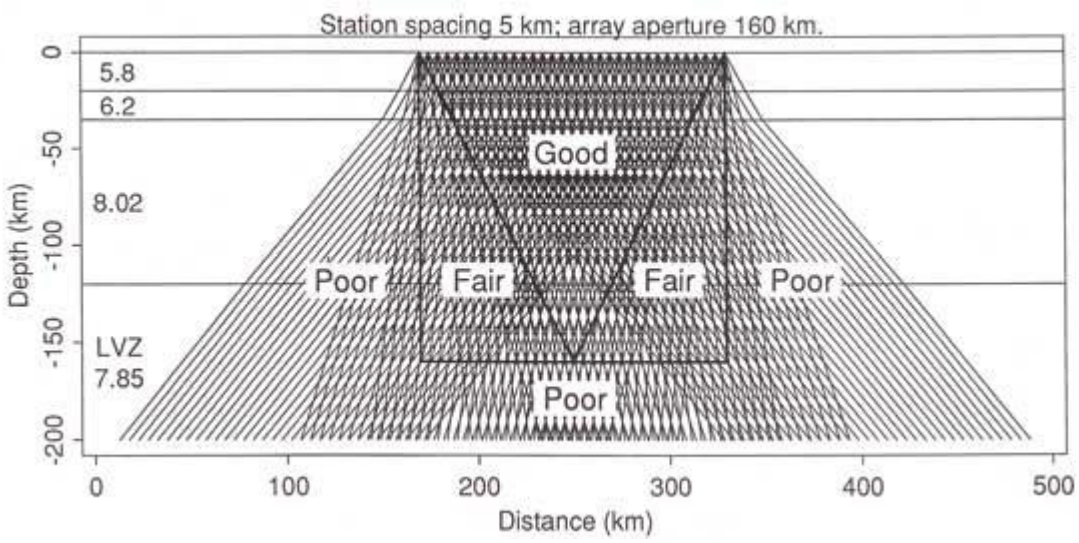


Fig. 2.6 Resolution characteristics in a teleseismic tomography inversion with an array of seismometers within area of 160 km (after Evans and Achauer, 1993). Solid lines indicate the raypaths of body-waves from teleseismic EQs to the seismic stations.

Most inverse problems are solved by comparing synthetic data with observed ones. The model parameters are then changed successively in an iterative process

until the differences between the observed and synthetic data reach a minimum (Tarantola, 1987; Menke, 1989).

Propagation of a seismic wave in a media depends on many parameters. If a propagating seismic wave meets heterogeneities along its way to a receiver point its travel time (TT) is increased or delayed. A structure of subsurface can be assessed by inverting the TT residuals calculated from the observed and predicted arrivals. According to Fermat's Principles, a seismic ray follows the minimum time path. A TT of a seismic ray is a function of raypath and velocity:

$$T = \int \frac{dl}{v(x)}, \tag{2.3.1}$$

where *T* is a TT, *dl* is an interval of raypath, and *v(x)* is a function of velocity. According to Aki et al. (1997) and Thurber (1983), non-linear Eq. 2.3.1 can be linearized:

$$d_i = \sum_{k=1}^{L} \mathbf{G}_{\mathrm{ik}} \mathbf{m}_{\mathrm{k}}, \tag{2.3.2}$$

where **G** is a matrix with TT calculated for every ray *i* through each cell, vector **m**=($m_1$, ..., $m_L$) defines perturbations of slowness of a reference velocity model with a number *L* of inverted nodes, and vector **d**=(1, ..., *N*) is a result of *N* TT residuals (number of rays). Eq. 2.3.2 for a least square solution can be rewritten:

$$\mathbf{m^{est}} = [\mathbf{G^T W G} + \mathbf{\Theta D}]^{-1} \mathbf{G^T W d}\,, \tag{2.3.3}$$

where $\mathbf{G^T}$ is a transpose matrix of **G**, **W** is a weighting matrix, **Θ** is a smoothing matrix, and **D** is a matrix of *a priori* constraints of a model (damping matrix) (Menke, 1984). The diagonal matrix **W** in Eq. 2.3.3 is composed of variances of **d**. The diagonal matrix **Θ** depends on parameterization of a reference velocity model. Eq. 2.3.3 can be solved using singular value decomposition (SVD) method. According to Koch (1985) and Thomson and Gubbins (1982) an equivalent nonlinear system is solved iteratively:

$$\mathbf{m_{final}} = \mathbf{m_0} + \mathbf{m_1} + \ldots + \mathbf{m_n}, \tag{2.3.4}$$

where $\mathbf{m_0}$ is one dimensional model. Each iteration involves a complete one-step inversion, including both ray tracing and model estimations. Iterations stop when

the model ceases to change significantly and a rout-mean-square (RMS) difference between the predicted and observed TT residuals is comparable to a data variance.

In teleseismic tomography ray tracing has a critical role. To resolve the forward problem in teleseismic tomography can be used different methods: ray approximation, which is the classical approach, and differential ray tracing. As in our study we use the first method, we disscuss it in more details. A raypath is determined through a model, i.e. which nodes the ray crosses and how much time it spends at each node. An algorithm produces the theoretical TT that are used in computing the relative residual arrival time data. A ray tracer affects both a matrix kernel **G** and a data vector **d** (Steck and Prothero, 1991). The procedure performs a simplex search for the fastest path of a planar wavefront to a point at the surface. In this procedure the departure point of a ray from the plane wave is not fixed, but determined by the algorithm itself. It assumes that the ray bending and distortions are caused by heterogeneities along their paths (Weiland et al., 1995; Sandoval, 2002).

The nonlinear teleseismic tomography inversion program TELINV (Weiland et al., 1995) was used in our study to perform inversions with the compiled dataset. The TELINV program can either 1) calculate propagation of the rays through a 3-D velocity model and output the TT, raypaths and synthetic relative TT for inversion testing, or 2) invert the P-wave TT residuals for a 3-D velocity structure.

## 2.4 Resolution estimates

The 3-D images obtained by tomography inversion depend on many factors such as quality of a dataset, parameterization of a reference velocity model, etc. Thus, it is important to estimate resolution in order to find the limits of precision of the inversion result. Resolution determines size of an object which can be resolved during an inversion. In teleseismic body-wave tomography the raypaths are

subvertical. Lateral resolution is higher than the vertical one, as the latter depends on a number of crossing rays at relatively high angles at various depths which is possible only with sufficient aperture of a seismic network. When calculating a TT of an observed phase through a model one must keep in mind that a wavefront can be affected not only by a cell which it crosses, but also by the neighbouring cells. An area around the propagating ray, which has the largest effect, is known as the first Fresnel zone. Resolution depends on a wavelength, and the smallest resolvable feature is larger than the width of the first Fresnel zone, which is defined as:

$$F = 2\sqrt{\frac{\lambda x(L-x)}{L}}, \tag{2.4.1}$$

where $\lambda$ is a wavelength, $x$ is a distance from feature to receiver, and $L$ is a total length of a raypath (Spetzler and Snieder, 2004). For a teleseismic P-wave phase of period of 1 s at a depth of 350 km an estimated radius of the first Fresnel zone is about 60 km.

One of the simple tools to estimate the ray coverage is to count the rays crossing a particular cell, i.e. how many rays hit the cell (Fig. 2.7). A hit matrix is used in this study to assess resolution as it is given as an ordinary output during inversion with the TELINV code. However, a hit matrix does not provide information neither of ray length in the cell nor its direction, thus, the method alone cannot fully define the resolution. For instance, the hit matrix usually indicates good resolution in the uppermost layers which is a misleading result while the rays travel through the uppermost part almost vertically and do not intersect.

Therefore, it is important to use other tools, such as the synthetic tests, in order to determine which parts of a study area can be reasonably resolved. The synthetic tests provide crucial information about model parameterization and spatial resolution capability. In tomography there are widely used synthetic velocity models of checkerboard and „spike“ types (Fig. 2.8). Purpose of the synthetic tests is to compile a synthetic dataset using a model with known distribution of the

velocity anomalies with the same station configuration as for a real data, and perform inversions which should resolve structure of the synthetic model. Having the same values of backazimuths and ray parameters in the synthetic dataset one can define the resolution capabilities in the study area.


Fig. 2.7 Ray distribution per inversion cell. Cell is well resolved when there are many rays with good crossing (left), and not crossing of many rays resolves a cell fairly well (middle), while too few rays with no crossing cannot properly resolve a cell (right).

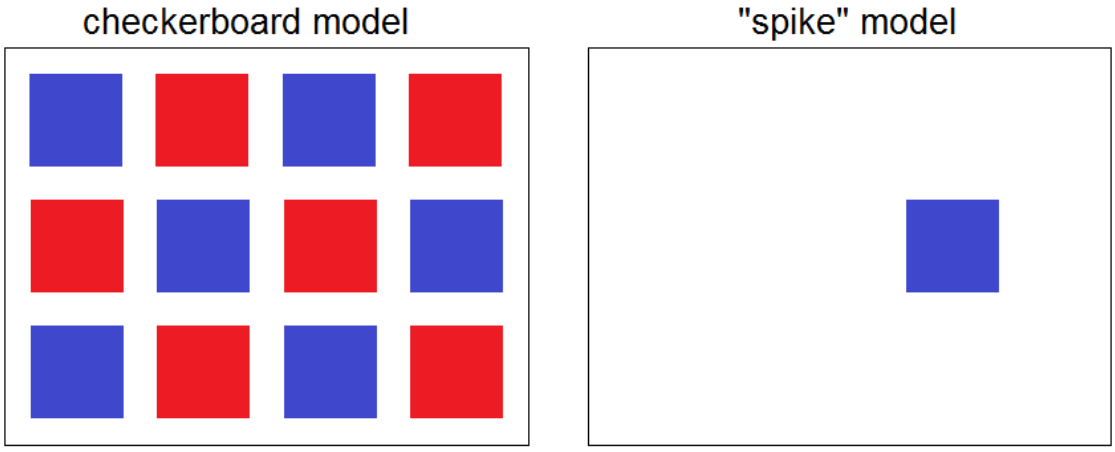


Fig. 2.8 Checkerboard (left) and „spike“ (right) synthetic models. Different colors show velocity anomalies with opposite values.

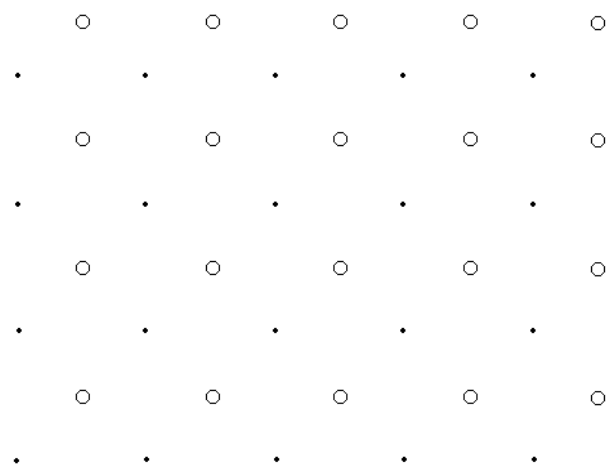

Fig. 2.9 Black dots and circles mark nodes of two grids, respectively, with the same origin of local coordinate system and grid spacing.

Model grid affects resolution as well. Once spacing between the grid nodes is determined the grid nodes themselves must be placed in exact locations. These locations are not a feature of the study area and can be chosen freely. However, a model grid is one of the parameters which must be defined prior an inversion, thus, one can test different grids. A virtual grid can be used to inspect stability of solution of an inversion. The virtual grid is usually compiled in such manner that an origin of a local coordinate system and grid spacing remains the same, but locations of the nodes (where the velocity perturbations are resolved) are shifted (or translated) by certain value horizontally (and/or vertically), i.e. if the primary coordinates of node *i* are $X_i$ and $Y_i$ then the coordinates of the same node in a virtual grid translated horizontally are $X_i+const_x$ and $Y_i+const_y$ (Fig. 2.9).

One of the ways to determine resolution is to inspect the diagonal elements of a kernel matrix **K**. The matrix **K** gives resolution length of each model parameter, thus, while plotting the diagonal elements on a map a difference in resolution is shown. The long resolution length means poorly resolved model parameter, while

the short resolution length means well resolved model parameter. The more rays cross the particular cell the better (the shorter) the resolution. Moreover, the more sophisticated SVD method provides information about a parameter-space of an inversion and shows a ratio of the total of the eigenvalues. This method requires large computational power.

## 2.5 Simulation filtering

Seismograms include information and effects caused by a seismic source, propagation medium, sensor and data processing. Understanding an influence of each of the effects reveal composition of a seismogram. A seismogram *u(t)* can be written as a result of convolution of three basic filters:

$$u(t) = s(t) * g(t) * i(t), \tag{2.5.1}$$

where *s(t)* is a signal from a seismic source, *g(t)* is a propagation filter, and *i(t)* is an overall instrument response (Bormann, 2002). When a seismometer records a seismic signal it always generates a component of distortion, which is defined as instrument response. Each type of seismometer has its own instrument response. Once one has a dataset recorded by different types of seismometers there is a need to have them displaying the same responses. In order to eliminate instrument response and to obtain uniform displacement signals in the seismograms one must perform a simulation filtering. During the procedure of simulation filtering a response of one type of seismometer is simulated as it was of another type of seismometer (Fig. 2.10). The procedure of simulation filtering is possible only when a transfer function of a recording instrument allows simulation of a desired one, and only if a recording system provides enough energy in all frequency ranges of a simulated instrument, thus, not all conversions can be performed. A process of conversion is expressed in equation (Scherbaum, 1996):

$$Y_{simulated}(z) = \frac{T_{simulated}(z)}{T_{recorded}(z)} Y_{recorded}(z) \tag{2.5.2}$$

where $Y_{simulated}$ is a transfer function of a desired instrument, $Y_{recorded}$ is a transfer function of an original instrument, $T_{simulated}$ is a z-transform of a desired instrument, and $T_{recorded}$ is a z-transform of an original instrument. A recording system is fully determined by its poles and zeroes and amplification factor (Sandoval, 2002).

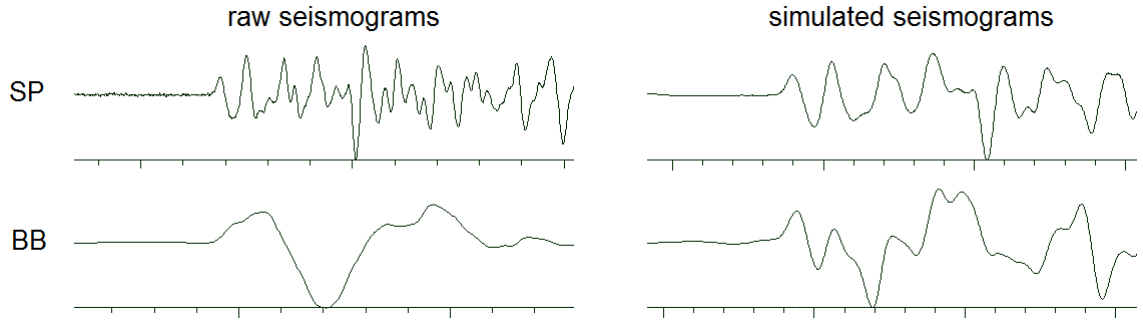


Fig. 2.10 Simulation filtering. Raw (left) and simulated (right) seismic signals of short-period (SP) and broadband (BB) sensors.

# Chapter 3

# DATASET

## 3.1 Data acquisition

In the study we used data of the PASsive Seismic Experiment PASSEQ 2006-2008 (Wilde-Piórko et al., 2008), which was carried out between 2006 and 2008 during international collaboration of 17 institutions from 10 countries:

1) University of Warsaw, Warsaw, Poland;
2) Alfred Wegener Institute for Polar and Marine Research, Bremerhaven, Germany;
3) Institute of Geophysics Czech Academy of Sciences, Prague, Czech Republic;
4) Vienna University of Technology, Vienna, Austria;
5) Geological Survey of Lithuania, Vilnius, Lithuania;
6) Institute of Geophysics Polish Academy of Sciences, Warsaw, Poland;
7) University of Leicester, Leicester, Great Britain;
8) Geological Survey of Denmark and Greenland, Copenhagen, Denmark;
9) GeoForschungsZentrum Potsdam, Potsdam, Germany;
10) Eötvös Loránd Geophysical Institute, Budapest, Hungary;
11) University of Oklahoma, Norman, USA;
12) Seismological Central Observatory, Erlangen, Germany;
13) Institute of Rock Structure and Mechanics Czech Academy of Sciences, Prague, Czech Republic;
14) University of Helsinki, Helsinki, Finland;
15) University of Oulu, Oulu, Finland;

16) University of Potsdam, Potsdam, Germany;

17) Vilnius University, Vilnius, Lithuania.

The PASSEQ 2006-2008 project aims to study lithosphere and asthenosphere around the TESZ. The PASSEQ project is linked with the TOR passive seismic experiment (Gregersen et al., 1999), which was realized during year 1996 to 1997 and was focused on the NW part of TESZ – the STZ between Sweden and Denmark – Germany, while the PASSEQ project is focused on the central part of the TESZ in Poland, mainly the TTZ, following the western margin of the EEC.

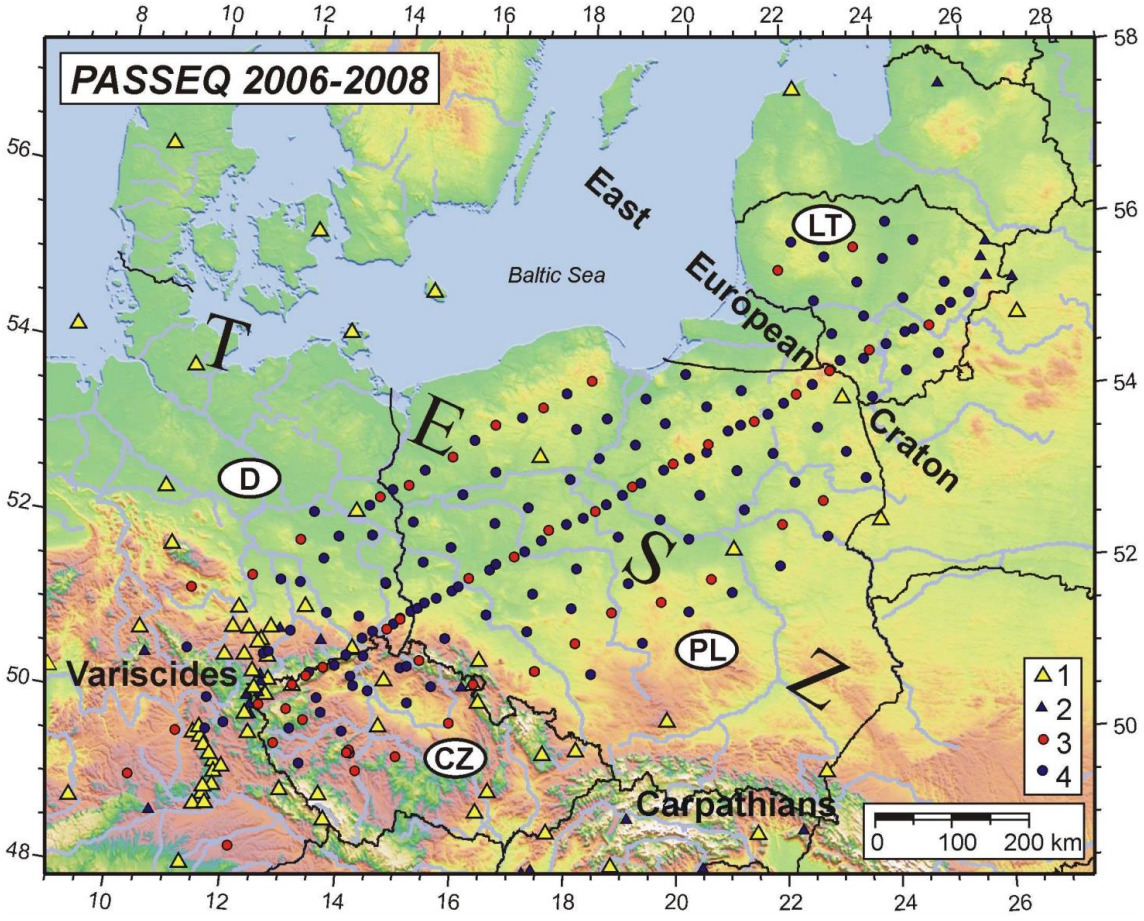


Fig. 3.1 Location of seismic stations operated in the region during the period of the PASSEQ 2006-2008 project (after Wilde-Piórko et al., 2008). 1, 2 – permanent broadband and short-period seismic stations; 3, 4 – temporary broadband and short-period seismic stations.

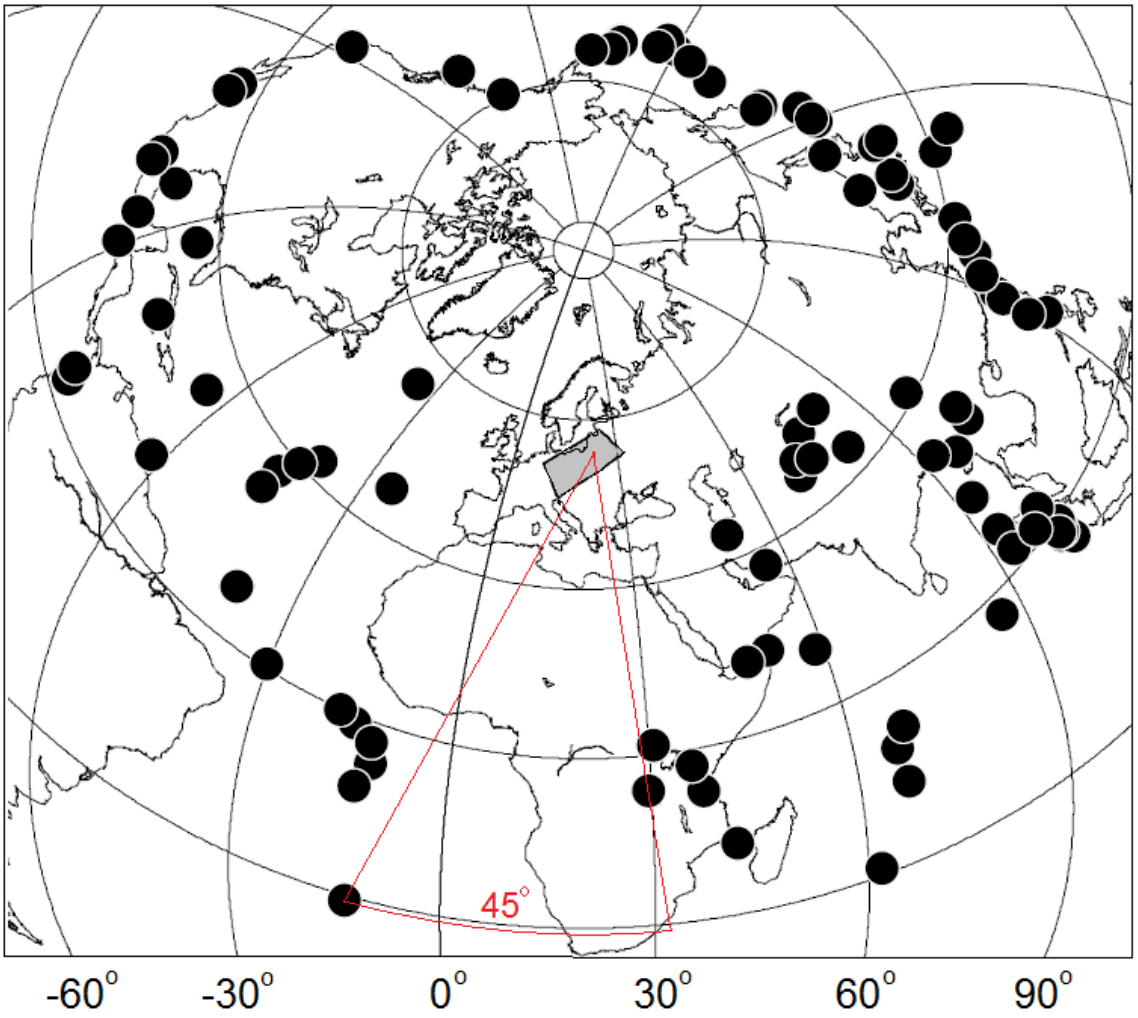


Fig. 3.2 Map of the epicenters of 101 EQs used in our study. Grey rectangle indicates the study area. The largest seismic gap is shown in red.

During the PASSEQ 2006-2008 project an array of temporary seismic stations was deployed along 1200 km long and 400 km wide area from Germany and the Czech Republic throughout Poland to Lithuania with an average spacing of 60 km between the stations while along a central transect the spacing was about 20 km (Fig. 3.1). The temporary array of 139 three-component short-period and 49 broadband seismic stations provided the continuous recordings from May 2006 to June 2008. The seismic stations were deployed at quiet sites such as forest houses,

castles, cloisters, small farms, etc., in the basements or on the ground in the buildings with concrete floor. The sampling frequencies were 20 Hz, 50 Hz or 100 Hz depending on the type of the data loggers.

The data of the PASSEQ temporary stations was combined with the data of the permanent stations, which operated in the region during the period of the PASSEQ project (Fig. 3.1), and the continuous database in miniSEED format (Ahern et al., 1993) was established in the GeoForschungsZentrum (GFZ), Potsdam, Germany. While the other copy of the data of a specific seismic station is stored in the participant country which served as a host during the PASSEQ project. Although the continuous database in the GFZ contains data of more than 200 seismic stations, due to some technical problems in our study in total we used data of 183 seismic stations. Information about the seismic stations used in our study is presented in Appendix 2. We used the one-event files created in the Institute of Geosciences Polish Academy of Sciences, Warsaw, Poland. The beginning of the file is several minutes before origin of an EQ, and the end of the file is several minutes after the seismic coda.

## 3.2 Earthquake data and picking of the P-wave arrivals

In teleseismic tomography it is important to use data of the EQs of particular parameters and geographical distribution. The EQs must have epicentral distances ranging from about 30 to 92 degrees (Sandoval, 2002). The lower limit ensures that seismic rays hit the target area from below steeply enough, and the upper limit ensures that the first observed arrival is a direct P-wave. It is important to have as good (and uniform) as possible the ray coverage in the study area in order to sample as many as possible the model cells, thus, one needs EQs from around the study area, which sometimes is impossible because the level of seismicity differs from region to region. Also, a magnitude of an EQ should be large enough in order to observe seismic signals of good quality, but not too high, because large

faults generate very complex seismic wave-trains which are difficult to study. Thus, using the seismological bulletins of the USGS (http://earthquake.usgs.gov/) and the ISC (http://www.isc.ac.uk/) we selected EQs with magnitude range from 5.5 to 7.2 and epicentral distance from 30 to 92 degrees from the Lithuanian–Polish border (23 ˚E and 54 ˚N) (Fig. 3.2). A majority of epicenters of the EQs is located to the east of the target area (i.e. in the regions of Sumatra, Japan and Kamchatka), while the largest seismic gap of about 45 degrees is for Africa–South Atlantic region (Fig. 3.2).

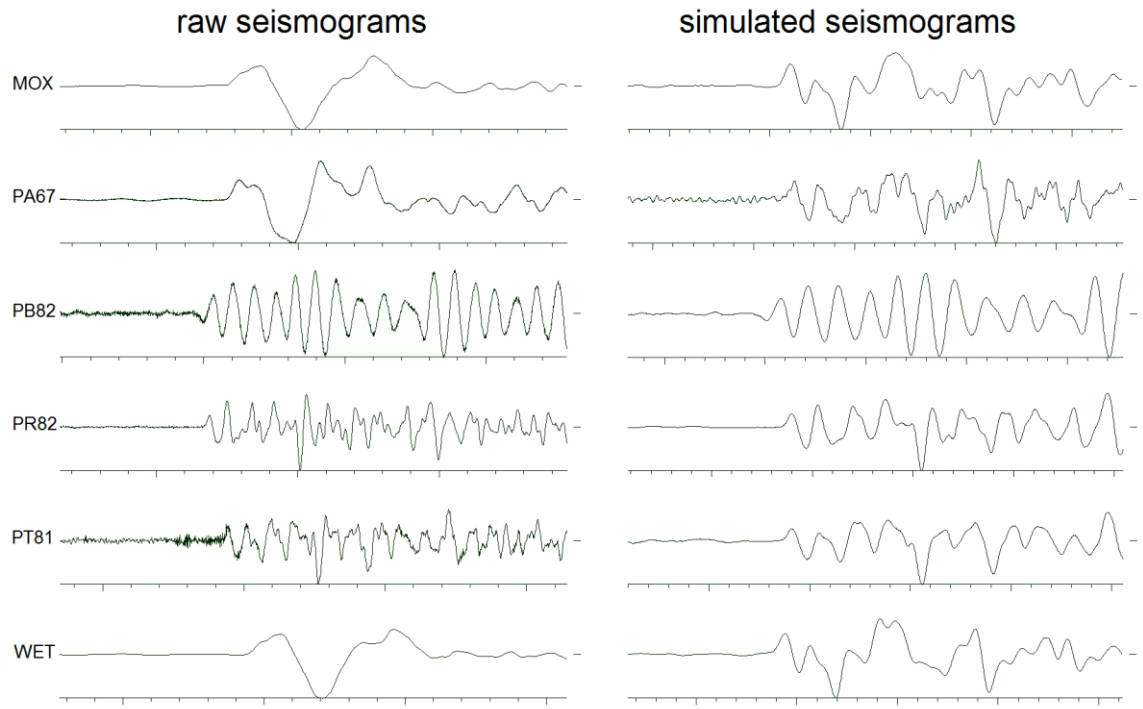


Fig. 3.3 Example of raw (left) and filtered with WWSS-SP filter (right) seismograms of EQ on 25.03.2007 at 00:41 UTC.

A procedure of picking of body-wave arrivals was performed using the Seismic Handler Motif (SHM) (http://www.seismic-handler.org/) program package. When an onset of a first arrival of a P-wave is too weak to be distinguised on all traces,

then some other part of a seismic signal is selected. The selected phase must be visible on most of the traces, and as close as possible to the first onset of the signal in order to avoid time errors due to dispersion and scattering of a propagating seismic ray (Evans and Achauer, 1993).

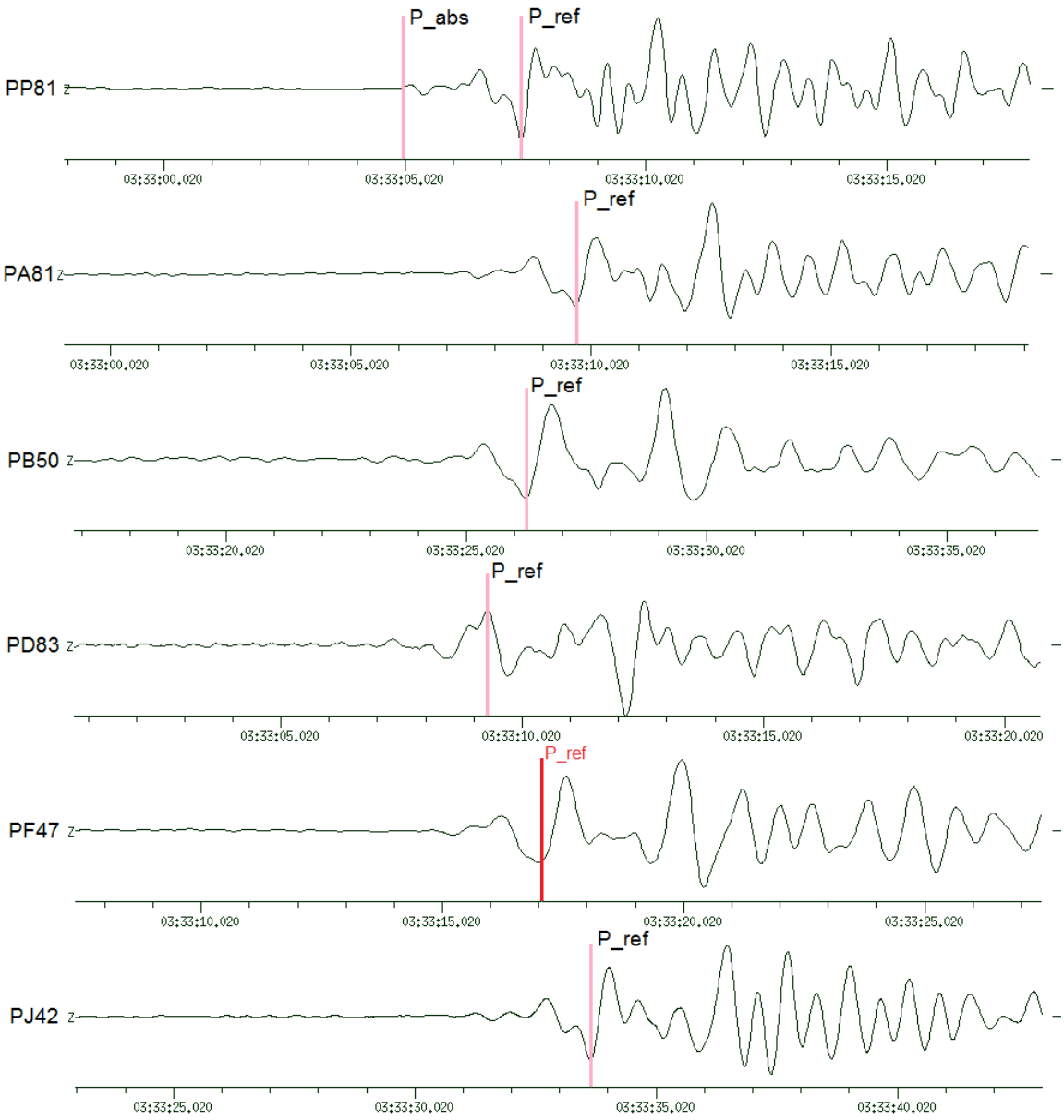


Fig. 3.4. Example of manual picking of the P-wave arrivals. Filtered seismograms of EQ on 02.08.2007 at 3:21 UTC. The uppermost trace is a reference trace with picked both the absolute (P_abs) and the relative (P_ref) arrivals.

As the seismic equipment deployed for the PASSEQ project varied in types of seismometers, dataloggers and digitizers (Wilde-Piórko et al., 2008), different response functions have been applied to the corresponding data. During the data review and analysis with SHM we used the World Wide Standardized Seismographic Network – Short Period (WWSS-SP) (Oliver and Murphy, 1971) transfer function, which includes both simulation filtering and instrument response. The procedure of simulation filtering (Chapter 2.5) enables picking of the same relative arrivals on the seismograms regardless of the types of seismic equipment (Fig.3.3). After simulation filtering we performed manual picking of the P-wave arrivals on seismograms of vertical components. As a signal-to-noise ratio (SNR) and data quality were not sufficient in the data of all seismic stations, it was impossible to pick the absolute P-wave arrivals. The problem was solved in the following way. From all traces of one event we picked a reference trace with relatively high SNR and picked an absolute P-wave arrival (i.e. onset of a signal) and a relative arrival of some well-expressed minimum or maximum of a signal. A correlation was performed by overlaying and aligning the wavelet of the reference signal over each trace, specifying the optimat fits, and picking the relative arrivals (Fig. 3.4). For some EQs we observed more than one type of waveforms, thus, we grouped the events with similar waveforms and picked absolute and relative P-wave arrivals in each group separately.

During the picking procedure we investigated quality of the data, which varies from station to station. During the data review we noticed three major types of problems related with the data:

1) wrong timing;
2) low signal-to-noise ratio (SNR);
3) inverted polarities.

During the data review with SHM we displayed the seismograms according to the epicentral distances, thus, the seismic stations with obvious timing problems were immediately identified (Fig. 3.5). However, if the timing error is very small, it is

hard to distinguish it, thus, a careful analysis of a dataset must be carried out. The data with wrong timing was not used in our study.

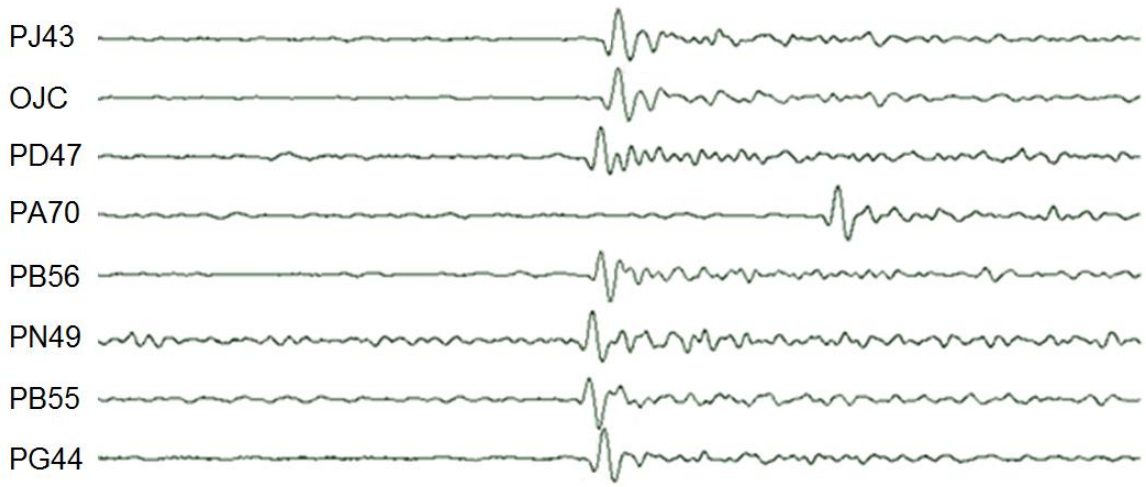


Fig. 3.5 The seismograms are distributed according to epicentral distances using location information from the seismological bulletins of the ISC. The obvious timing errors were immediately noticed (e.g. in station PA70).

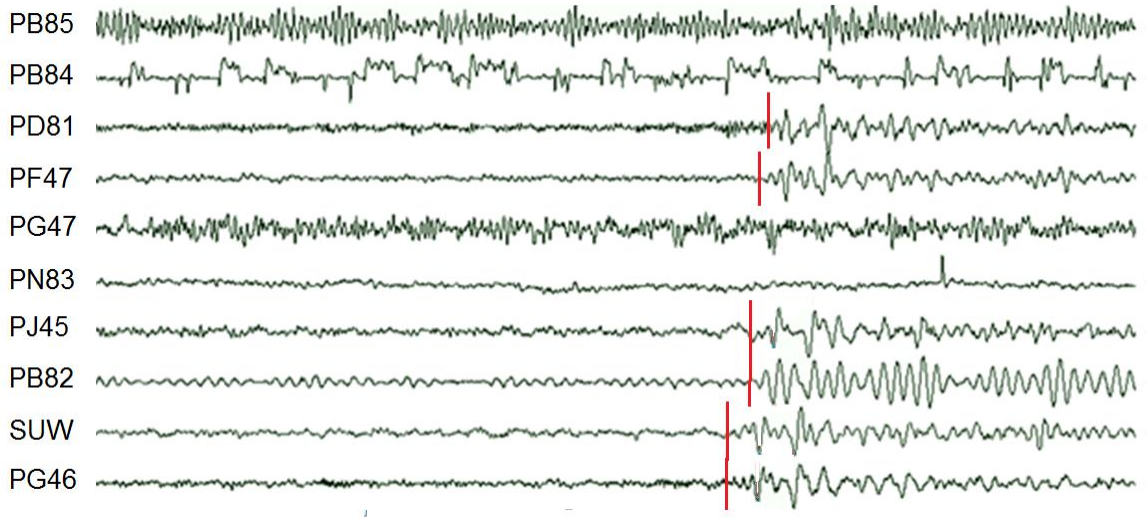


Fig. 3.6 Unfiltered seismograms with low SNR. Approximate onsets of the seismic signals are marked in red.

The SNR shows how weak the signals can be indicated on the traces regarding a noise level (Fig. 3.6). The low SNR means distorted seismic signals as well, thus, lower quality of a data.

Inverted polarities of the seismic signals may cause a lot of problems, because it is sometimes hard to distinguish whether the polarity is inverted or not, because for similar frequencies the wrong “ups” and “downs” of the signal can coincide quite well. During the data review signals with inverted polarities (compared to the majority of the seismic stations) were observed in data of PB82, PB85, PB88, PD81, PD82, PD83 and PN84 seismic stations (Fig. 3.7). For these stations the picking was performed either by distinguishing a group of traces with inverted polarities and picking different absolute and relative arrivals, or inverting a trace of a reference seismic station that the right „ups“ and „downs“ of a signal would coincide.

Regarding the data quality and picking error every pick was assigned with a quality (weighting) factor from 1 (best quality) to 3 (poor quality) (Fig. 3.8). In total, we manually picked 8308 P-wave arrivals recorded in 183 seismic stations (Table 3.1).

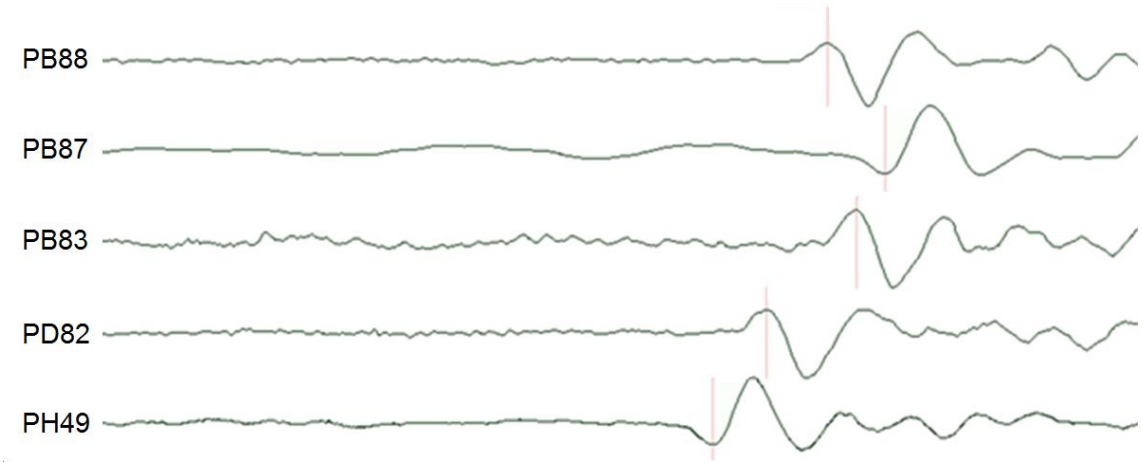


Fig. 3.7 Seismic signals with inverted polarities are observed on traces of PB88, PD83 and PD82 seismic stations, while majority of the seismic stations have the „right“ polarities, like PB87 and PH49 seismic stations.

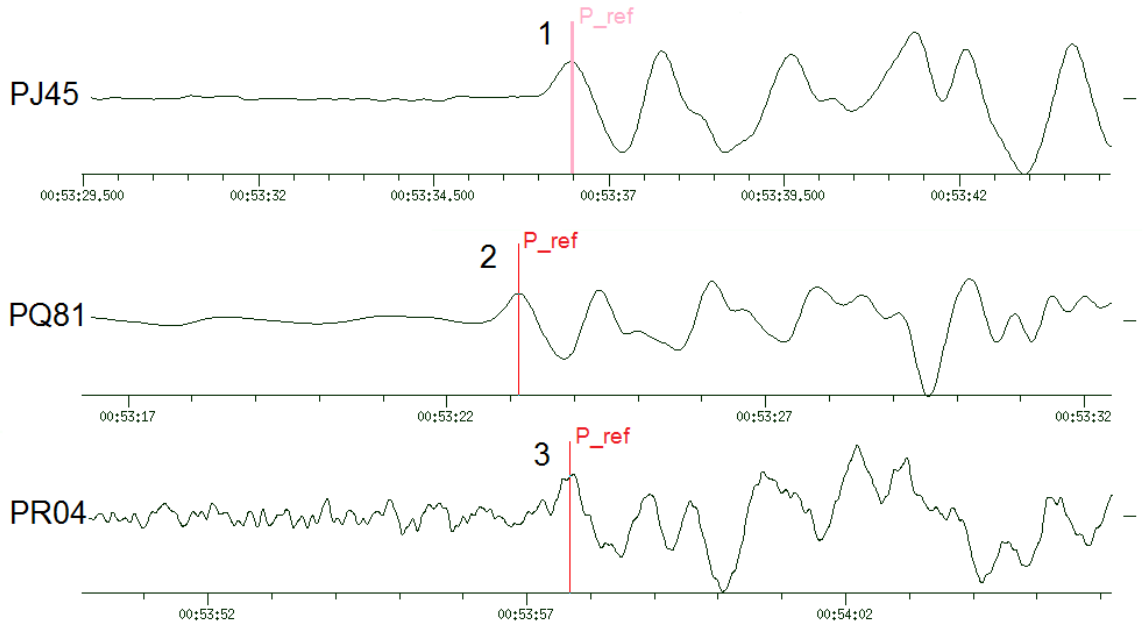


Fig. 3.8 Example of the picks with quality factors 1 (top), 2 (middle) and 3 (bottom) for EQ on 25.03.2007 at 00:41 UTC.

### 3.3 Compilation and analysis of dataset

Calculation of the theoretical travel times (TT) of the first arrivals of P-waves was performed using the location information of the EQs from the seismological bulletins of the ISC and Seismic Handler (SH) program package which uses the IASP91 velocity model. The TT residuals in every station were calculated by subtracting the theoretical TT from the observed one:

$$T_{picked} - T_{theoretical} = T_{residual}, \qquad (3.3.1)$$

where $T_{picked}$ is an observed TT, $T_{theoretical}$ is a theoretical TT calculated with SH, and $T_{residual}$ is a TT residual. When the dataset was compiled we performed careful analysis in order to identify and eliminate the bad quality data. We compiled the maps showing distribution of the TT residuals in different seismic stations for every EQ (Fig. 3.8), and plots showing distribution of the TT residuals for different EQs in individual seismic station (Fig. 3.9), which helped to identify the wrong data (even with slight timing errors) and highly improve quality and

reliability of our dataset. We assigned the misleading picks with quality factor >3, which was not used in our study (Table 3.1).

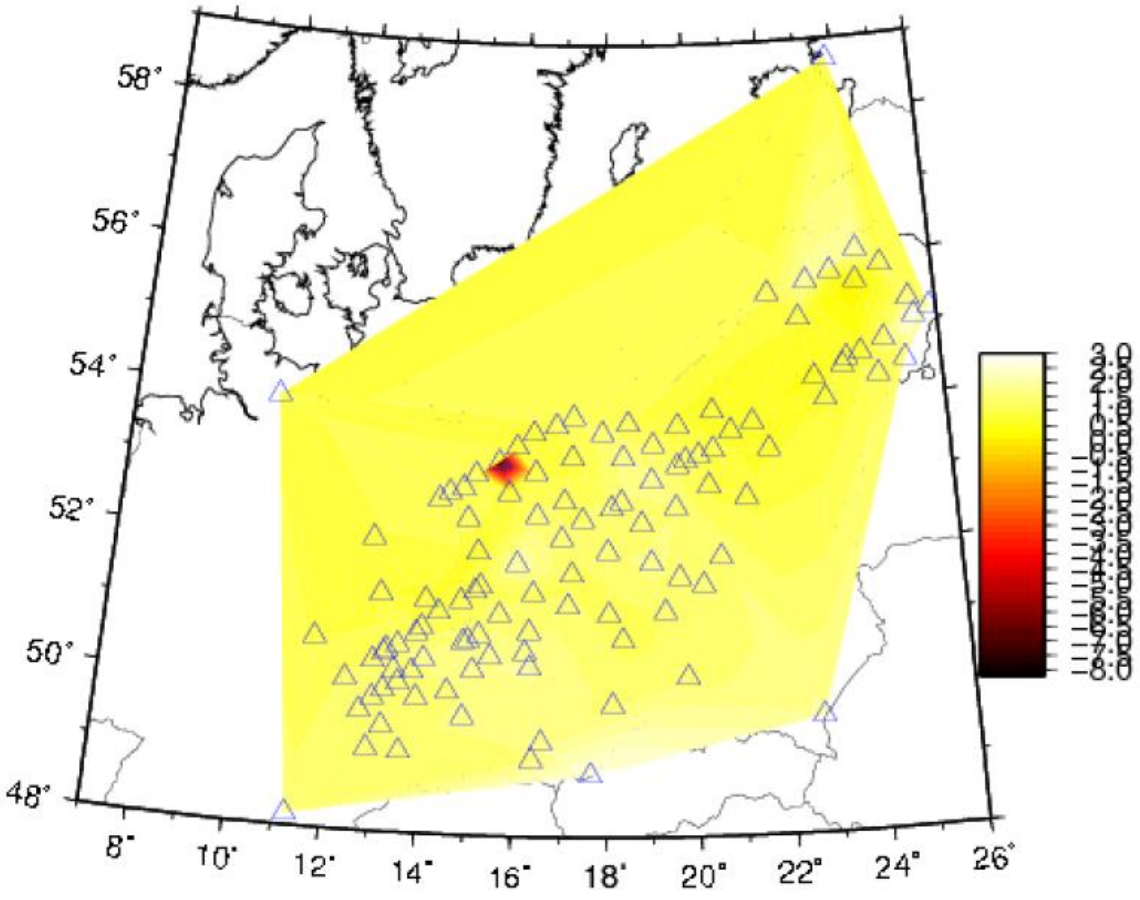


Fig. 3.8 Example of distribution of the observed TT residuals for EQs on 2007.07.16 at 14:17 UTC. Scale shows the TT residuals expressed in seconds.

As we plot the calculated TT residuals with quality factors 1 to 3 from the SW to NE parallel to a main transect of the study area (Fig. 3.10) we observe the larger values in stations located to the SW and the lower ones in the stations located to the NE of the study area. The area in between with the largest variations in the values coincides with the TESZ. The average values of the TT residuals calculated in individual seismic station of about 0.6-0.7 s are observed to the east, while the

larger ones of about 1.0-1.4 s are observed to the west from the TESZ, respectively (Fig. 3.11), which might be related to different tectonic settings. Analysis of the average values of the TT residuals for individual EQ show regional distribution (Fig. 3.12). The EQs with the smallest average TT values up to 0.6 s occurred in Kamchatka and the Aleutian region, while the highest ones from 1.5 to 2.3 s are observed for EQs from North and Central America and the North Atlantics. The intermediate values from 1 to 1.5 s are observed for the EQs in the Middle Atlantics, Africa, South and Southeast Asia.

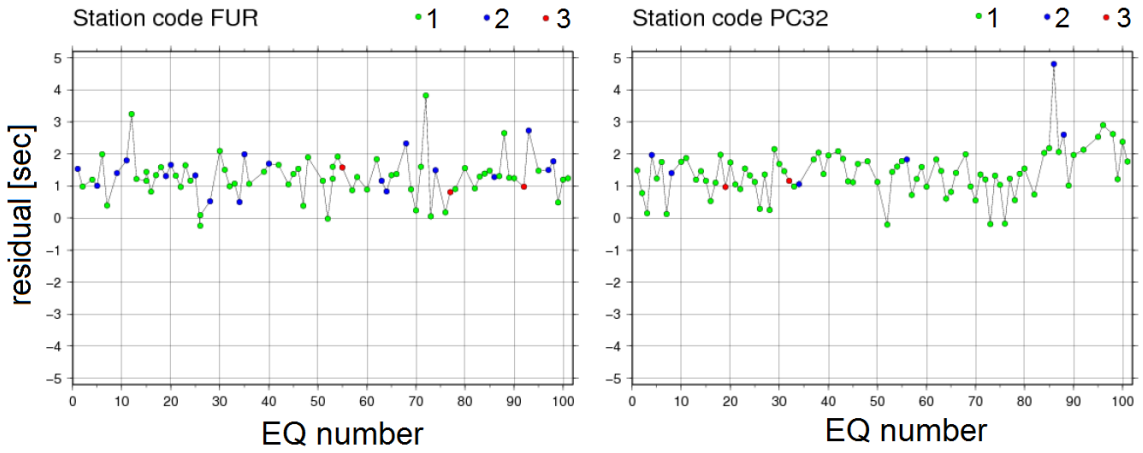


Fig. 3.9 Examples of distribution of the observed TT residuals for different EQs recorded in individual seismic station. Colors indicate quality factor of the picks.

Table 3.1 Complete dataset.

| **Weighting factor** | **Time error** | **Number of picks** |
|---|---|---|
| 1 | <0.2 s | 6008 |
| 2 | 0.2-0.3 s | 1557 |
| 3 | 0.3-0.4 s | 686 |
| >3 | wrong timing | 57 |
| **In total:** | | 8308 |

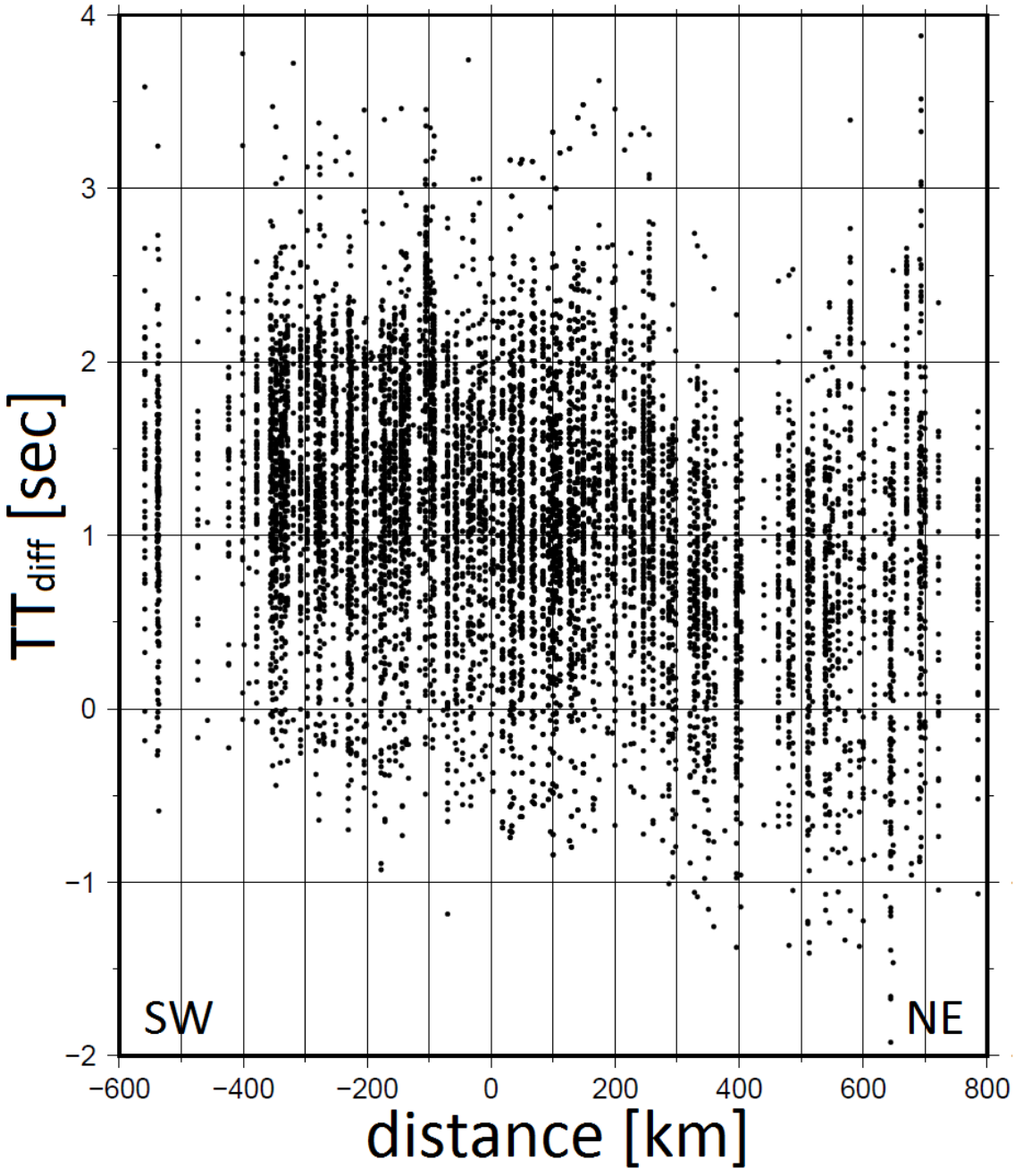


Fig. 3.10 Distribution of TT residuals observed in the seismic stations from the SW to the NE along the study area in the local Cartesian coordinate system.

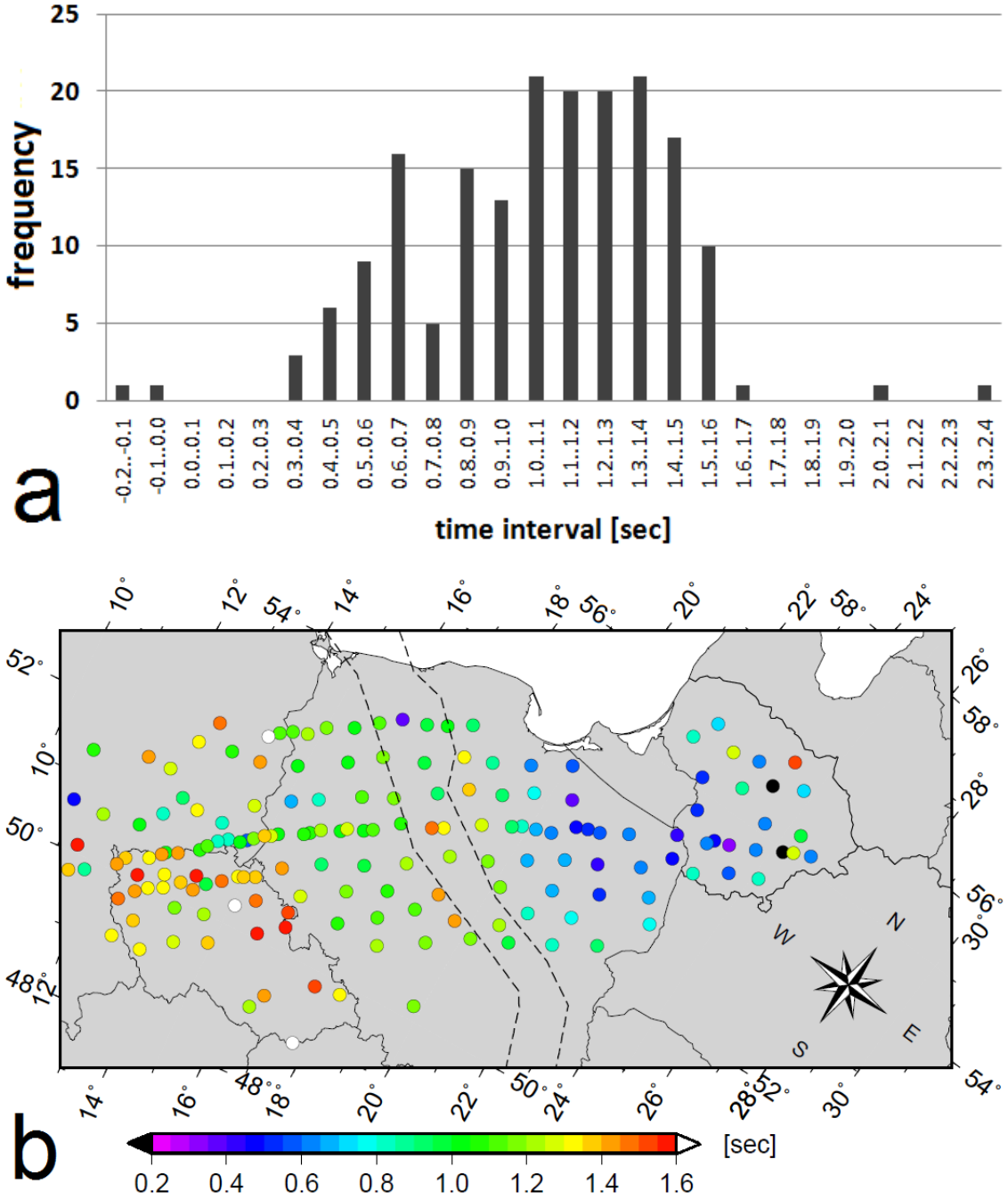


Fig. 3.11 (a) Distribution of average values of the TT residuals observed in the seismic stations. (b) Map of distribution of average values of the TT residuals observed in the seismic stations in the study area.

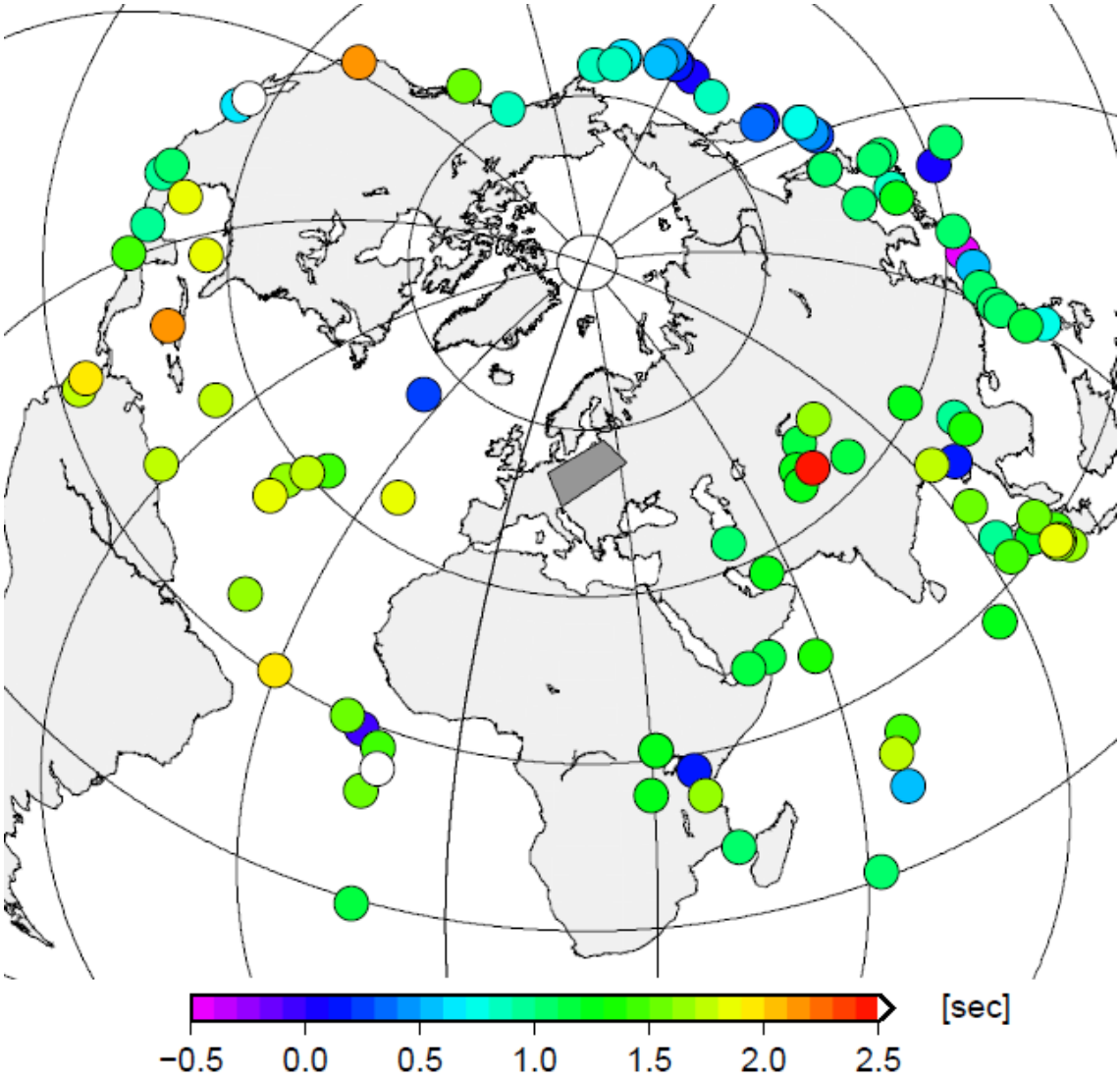


Fig. 3.12 Distribution of average values of the TT residuals for individual EQ.

# Chapter 4

## MODEL PARAMETERIZATION

The study area coincides with territory of the PASSEQ 2006-2008 project (Fig. 4.1). While parameterizing a model grid one must ensure that 1) a model can reproduce the data, and 2) that the data can resolve the values of model parameters. Size of model cells determines size of the structures which can be resolved during the data inversion. The smaller the cell the finer structures can be resolved, on the other hand, the more rays cross the cell the better the cell can be resolved, which would require a cell of large size. Thus, the size of a cell must be optimal to satisfy both conditions. The spacing between the grid nodes in our study was set to 50 km in horizontal directions (Fig. 4.1), which is reasonable taking into account the spacing between the seismic stations and frequency content of the observed seismic signals. The vertical spacing for the layers between 70 and 350 km depth varies from 20 to 50 km (Fig. 4.2).

The IASP91 velocity model (Kennett and Engdahl, 1991) was used as a reference velocity model in the teleseismic tomography inversion with the TELINV code. We compiled a 3-D velocity model with 16 layers of different thicknesses down to 700 km (Fig. 4.2). The inversions were performed assuming a constant slowness in each cell (Steck and Prothero, 1991) for ten layers between 70 and 350 km.

After careful analysis we set optimal parameters of smoothing **Θ**, damping **D** and number of iterations (Fig. 4.3). The smoothing was set to 50. The damping value was determined while running inversions with different values of damping and investigating trade-off between the data variance and model variance (Fig. 4.4). In the inversions we used two values of damping of 80 and 120 in order to obtain

some variations of smaller and larger scale, which showed up to 1.5 % difference in the amplitudes of the resolved P-wave velocity variations, while here we present results obtained using damping value of 120. We also found that three iterations are enough for inversion, because for higher number of iterations a model and a RMS error change insignificantly (Fig. 4.3).

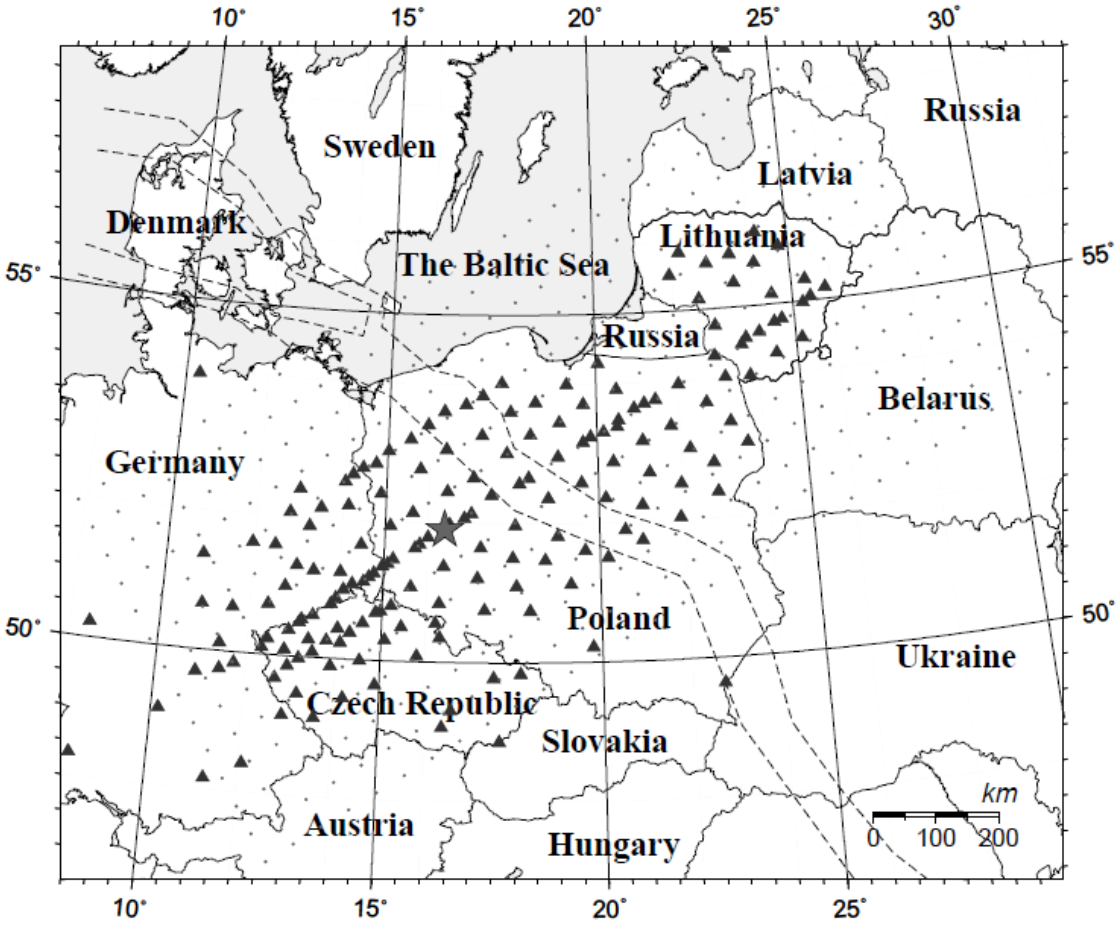


Fig. 4.1 Map of seismic stations used (triangles) and model nodes (dots) in our study area. Star indicates origin of the local Cartesian coordinate system. Dashed lines indicate the TESZ.

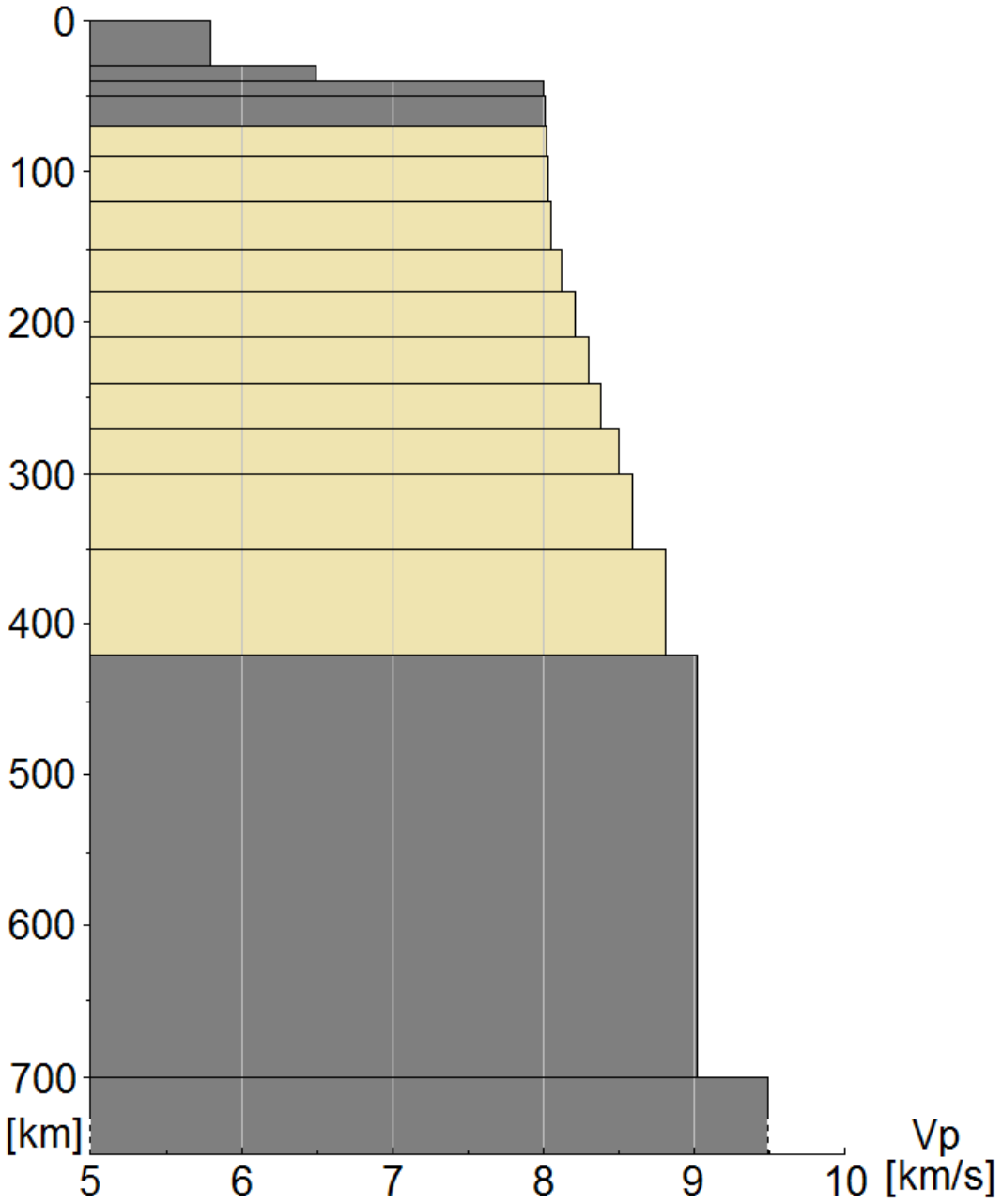


Fig. 4.2 Parameterization of the IASP9 velocity model by layers of different thicknesses. The 3-D reference velocity model has 16 layers with different depths indicated on vertical axis, while the values of seismic velocities are indicated on horizontal axis. Inversions were performed for ten layers from 70 to 350 km (light color).

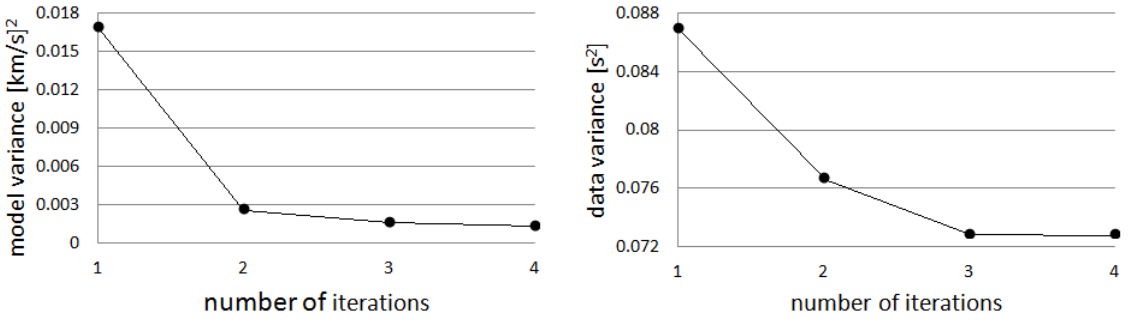


Fig. 4.3 Changes of the data variance (right) and model variance (left) after four iterations.

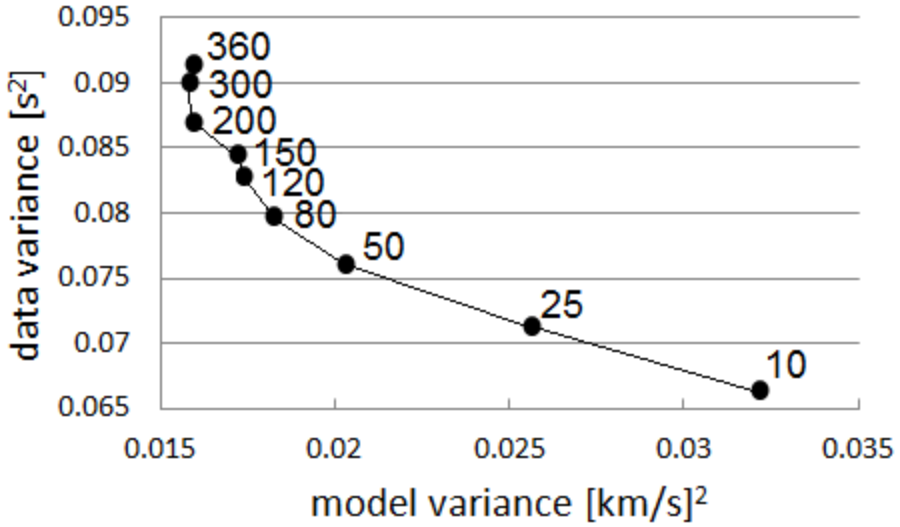


Fig. 4.4 Trade-off curve between data variance and model variance obtained during inversions after three iterations with different damping values from 10 to 360.

# Chapter 5

*"Per upelį žąsys skrido, į upelį plunksnos krito"*

*Lietuvių liaudies daina* [III]

## CRUSTAL TRAVEL TIME CORRECTIONS

The Earth's crust is more heterogeneous compared to its deeper layers. According to previous studies, the variations in the Moho depth (Fig. 5.1a) and thickness of the sedimentary cover are significant in the study area. In order to avoid the misleading results and to resolve heterogeneities in the upper mantle, it is important to eliminate from the data the effects which are created by the Earth's crust. For the small study areas sometimes 1-D crustal models is enough, but for the larger ones a precise 3-D model should be considered. In our study we used the 3-D crustal models. The crustal TT corrections for individual seismic stations were compiled in the following way:

$$TT_{model} - TT_{iasp} = TT_{diff}, \quad (5.1)$$

where $TT_{model}$ is a TT through a crustal model, $TT_{iasp}$ is a TT through the IASP91 velocity model, and $TT_{diff}$ is a TT difference.

To estimate the crustal TT corrections in the entire study area we used two crustal models: the EuCRUST-07 (Tesauro et al., 2008) 3-D model for Europe with

[III] *"Over a creek the geese flew, into the creek their feathers fell..." Lithuanian Folk song*

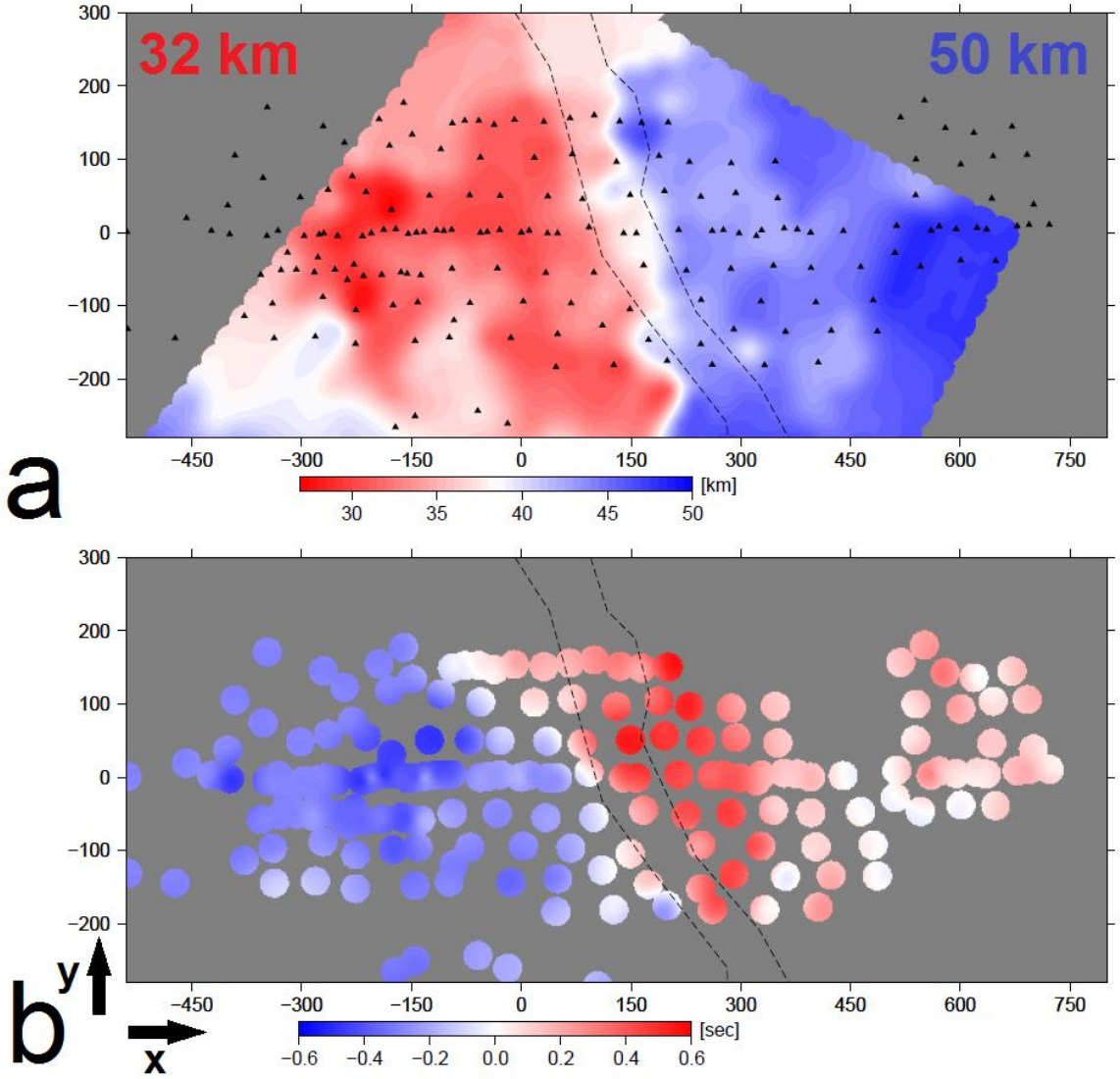


Fig. 5.1 (a) Moho map of the precise 3-D crustal model by Majdański (2012) which was used to estimate a part of the crustal TT corrections. The Moho depth for areas outside the model was defined using results of some DSS projects: the area to the east was assigned with 50 km and to the west with 32 km. (b) Estimated crustal TT corrections in the individual seismic stations. The values are expressed in seconds in respect to the IASP91 velocity model.

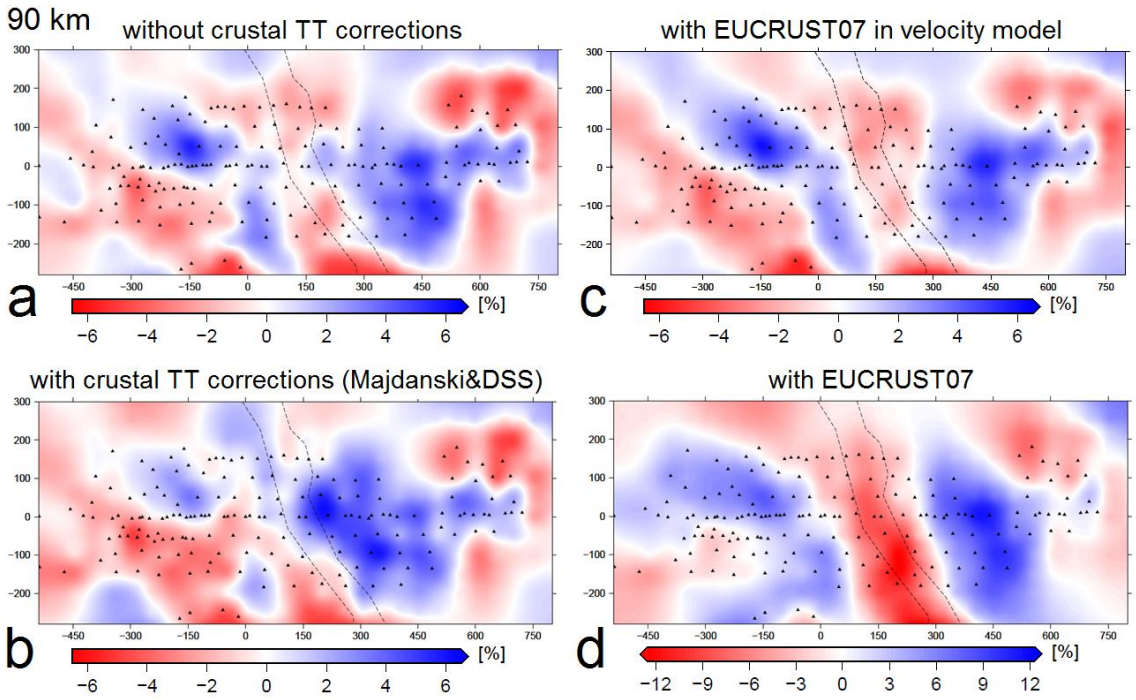


Fig. 5.2 Horizontal slices of the inversion results at the depth of 90 km (a) without crustal TT corrections, (b) with the set of crustal TT corrections compiled for individual seismic stations using crustal model by Majdański (2012) and results of some DSS projects, (c) with the EuCRUST-07 model introduced in the reference velocity model, and (d) with the set of crustal TT corrections calculated for individual seismic stations using the EuCRUST-07 model. Triangles indicate the seismic stations. Dashed lines indicate the TESZ. Results obtained with top quality data and damping value of 120.

model grid of 1˚×1˚, and a model based on a precise 3-D crustal model for Poland (Majdański, 2012) with model grid of 0.3˚ of latitude and 0.5˚ of longitude, and the 1-D approximations obtained during some DSS profiles for the territories which are not covered by model of Majdański (2012). In those territories the stations were assigned with constant values of the crustal corrections, which were estimated using the interpreted results (full velocity profiles) below shot point SP9

in the EUROBRIDGE'95 profile (Yliniemi et al., 2001) and shot point SP2 in the CELEBRATION09 profile (Guterch et al., 2003). The value obtained from the EUROBRIDGE'95 profile was used for stations deployed in Lithuania, and value obtained from the CELEBRATION09 profile was used for the stations deployed in Germany and the Czech Republic, while the depths of the Moho boundary of 50 km and 32 km were assigned, respectively (Fig. 5.1a). Both crustal models are described in details in Tesauro et al. (2008) and Majdański (2012).

In order to estimate an effect of the crustal TT corrections we performed inversion using the dataset with and without the crustal corrections (Fig. 5.2). First, we introduced the EuCRUST-07 crustal TT corrections into the input velocity model (in the uppermost non-inverted layers). The inversion results (Fig. 5.2c) show almost no difference compared to the results obtained without crustal TT corrections (Fig. 5.2a). Therefore, we concluded that this way of introducing the crustal TT corrections into the inversion is not sensitive enough. Then we calculated the crustal TT corrections for the individual seismic station assuming vertical propagation in the crust. The deficiency of this approach is that bending of the seismic rays in the Earth's crust is not taken into account, however, regarding the incidence angles in our dataset, the assumed vertical propagation in the crust causes <2 % shortening of the raypaths, thus, an effect in the inversion results on the calculated TT is negligible. The results obtained with the EuCRUST-07 model show artificially high amplitudes of velocity perturbations, especially around the TESZ where thickness of the sedimentary cover is significantly larger compared to that of the surroundings (Fig. 5.2d), thus, we concluded that the EuCRUST-07 model is not suitable for our dataset. The inversion results with the set of crustal TT corrections based on model by Majdański (2012) and results of some DSS projects (Fig. 5.2b) do not reproduce shape of the thick sedimentary cover in the TESZ (like in Fig. 5.2d), but shows two distinct structures on both sides of the TESZ. While comparing the results obtained with (Fig. 5.2b) and without (Fig. 5.2a) the crustal TT corrections we observe, as expected, some differences

beneath the TESZ. Moreover, the introduced crustal TT corrections slightly add up to the positive amplitudes of velocity variations observed beneath Poland to the east from the TESZ (most likely due to thick crust) and negative amplitudes beneath the Bohemian Massif, while slightly reduce the negative amplitudes beneath Western Lithuania (due to the Baltic sedimentary basin up to 2 km thick). The inversion results with the latter set of the crustal TT corrections (Fig. 5.1b) proved to be relevant, thus, the set was used in our study.

# Chapter 6

## RESOLUTION

Resolution assessment is important in order to evaluate precision of results of inversion. Resolution assessment includes calculation of spatial resolution and standard deviations of the model parameters. In general, resolution of an inversion is governed by spacing between the seismic stations, frequency content of the seismic signals and geometry of the seismic rays. The ray coverage of the cell blocks is also affected by horizontal and vertical grid spacing (Arlitt, 1999).

We had not enough computational power to perform inversions with the full dataset and the model grid of entire study area, thus, we selected the top quality data in order to perform inversions for the entire study area (Table 6.1). Moreover, we divided our dataset according to the distribution of the seismic stations and focused investigations on different parts of the study area (Table 6.1).

Table 6.1 Division of the compiled dataset: top quality dataset for the entire study area (PASSEQ), and datasets of quality factors 1 to 3 for the separate parts of the study area (TOWEST and EEC).

| | **PASSEQ** | **TOWEST** | **EEC** |
|---|---|---|---|
| **Nr. of picks** | 6008 | 6436 | 4195 |
| **Data quality** | 1 | 1, 2, 3 | 1, 2, 3 |
| **Nr. of seismic stations** | 183 | 138 | 94 |
| **Nr. of inverted nodes** | 3240 | 2040 | 2040 |
| **Grid nodes(x-y-z)** | 29-14-16 | 19-14-16 | 19-14-16 |

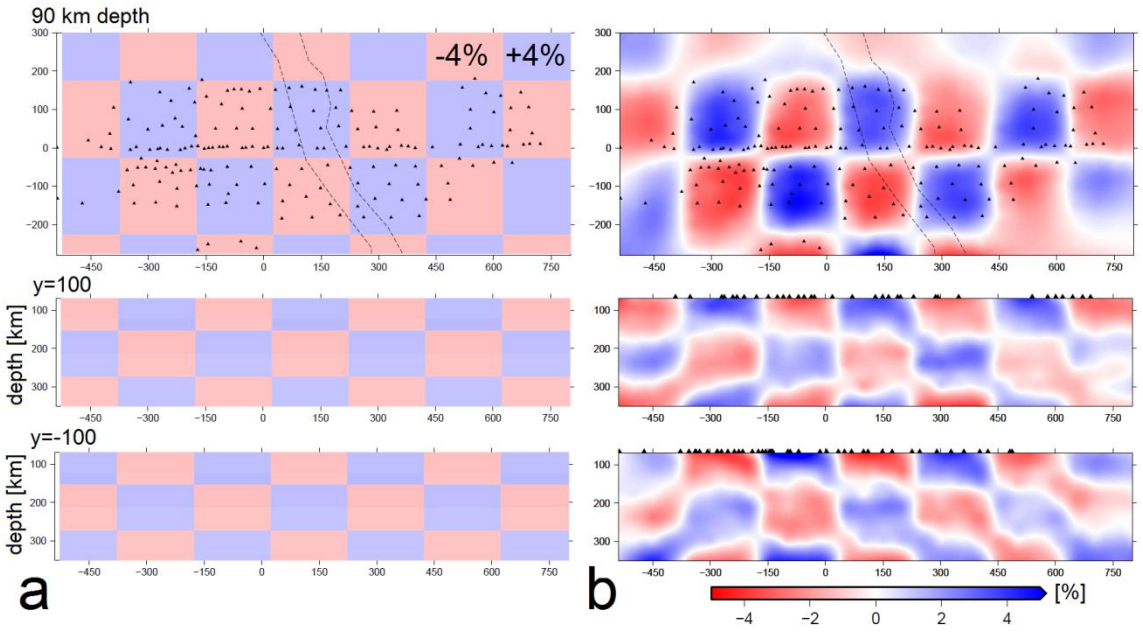


Fig. 6.1 Results of a checkerboard test using the top quality data of our dataset: horizontal slice at the depth of 90 km and two vertical slices of the study area. (a) Initial velocity model with synthetic blocks of 200 km in horizontal directions and ±4 % P-wave velocity difference compared to the IASP91 velocity model. (b) Inversion results with the synthetic dataset. Triangles mark the seismic stations. Dashed lines indicate the TESZ.

## 6.1 Resolution assessment for the top quality dataset

In our study we perform a synthetic test with velocity model of checkerboard type which shows what parts of the target area can be and cannot be resolved with the same station configuration as the real data. The compiled synthetic velocity model consists of alternating blocks with 4 % higher and lower velocity values compared to the IASP91 velocity model. The synthetic blocks extend 200 km in horizontal directions and embrace four layers (Fig. 6.1a). We also added small random perturbations to each synthetic TT. In the inversion results obtained with the synthetic dataset we observe reasonably resolved checkerboard-like structure (Fig.

6.1b). However, in the vertical slices we observe an eastward dipping vertical smearing which is most likely due to the majority of the seismic rays from the regions located to the east of the study area (Fig. 3.2). Moreover, the synthetic structure is resolved better in the western part than in the eastern part (Fig. 6.1b) due to the larger number of top quality picks in the data of the stations to the west from the TESZ.

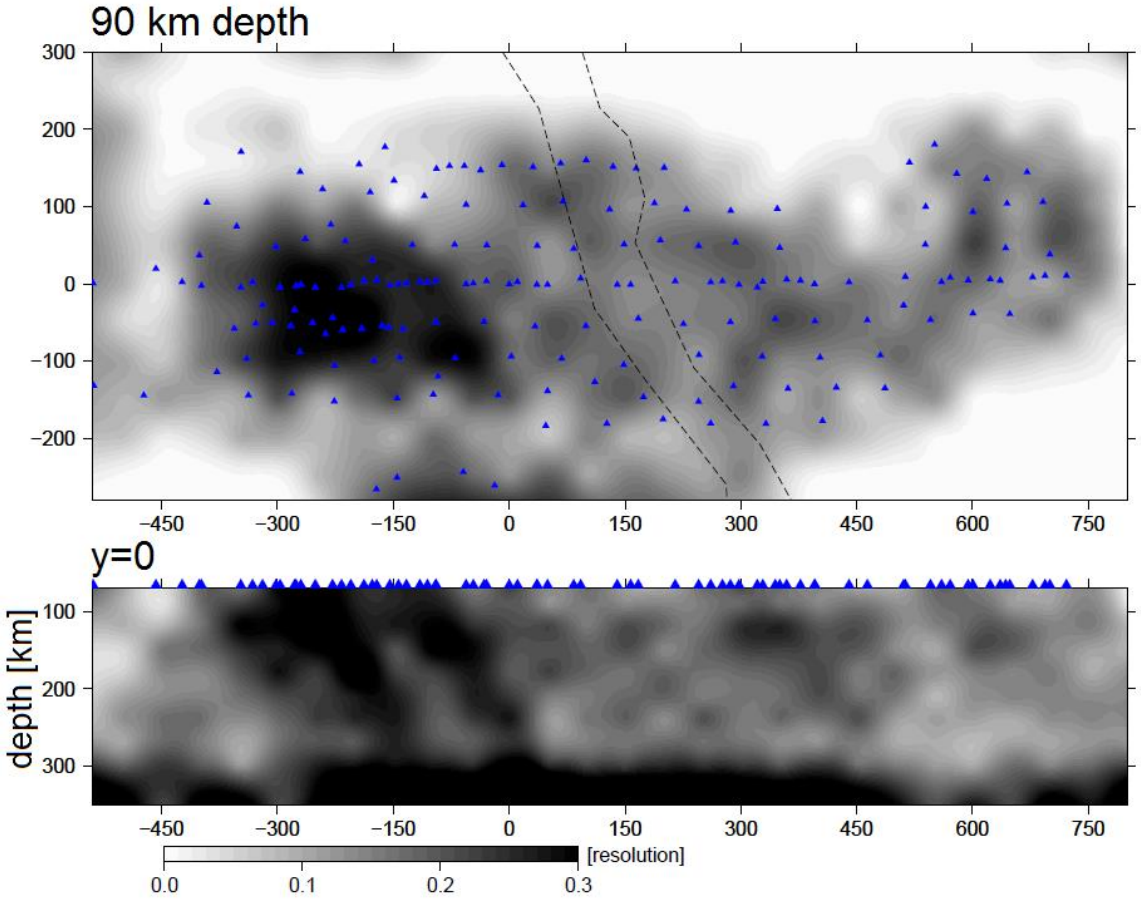


Fig. 6.2 Diagonal elements of the resolution matrix at the depth of 90 km and along the main transect. Low and high values show poorly and well resolved areas, respectively. Triangles mark the seismic stations. Dashed lines indicate the TESZ.

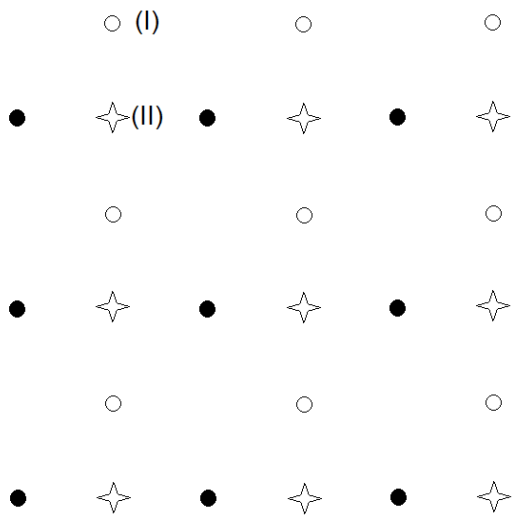


Fig. 6.3 Nodes of the virtual grids are translated at constant distances: compared to the primary grid (black dots), the virtual grid (I) is shifted 25 km along latitude and 25 km along longitude (white dots), and virtual grid (II) is shifted 25 km along longitude (stars), while origin of the local Cartesian coordinate system and spacing between the nodes remain unchanged.

A further estimate of resolution is derived from a resolution matrix. Fig. 6.2 shows the diagonal elements of a resolution matrix that provides a relative measure of resolution: low values mean poor resolution and high values mean good resolution. The horizontal slice at the depth of 90 km (Fig. 6.2) shows that areas directly below the seismic array are better resolved compared to the areas which are not underneath the array. The horizontal slice also indicates that in the SW part of the study area the higher values of resolution coincide with the highest station coverage and the larger number of the picks in our dataset. The vertical slice of the main transect (Fig. 6.2) shows the highest resolution in the SW part as well down to 300 km, while the high resolution observed at the bottom along the entire transect is an artifact from an inversion and should not be interpreted.

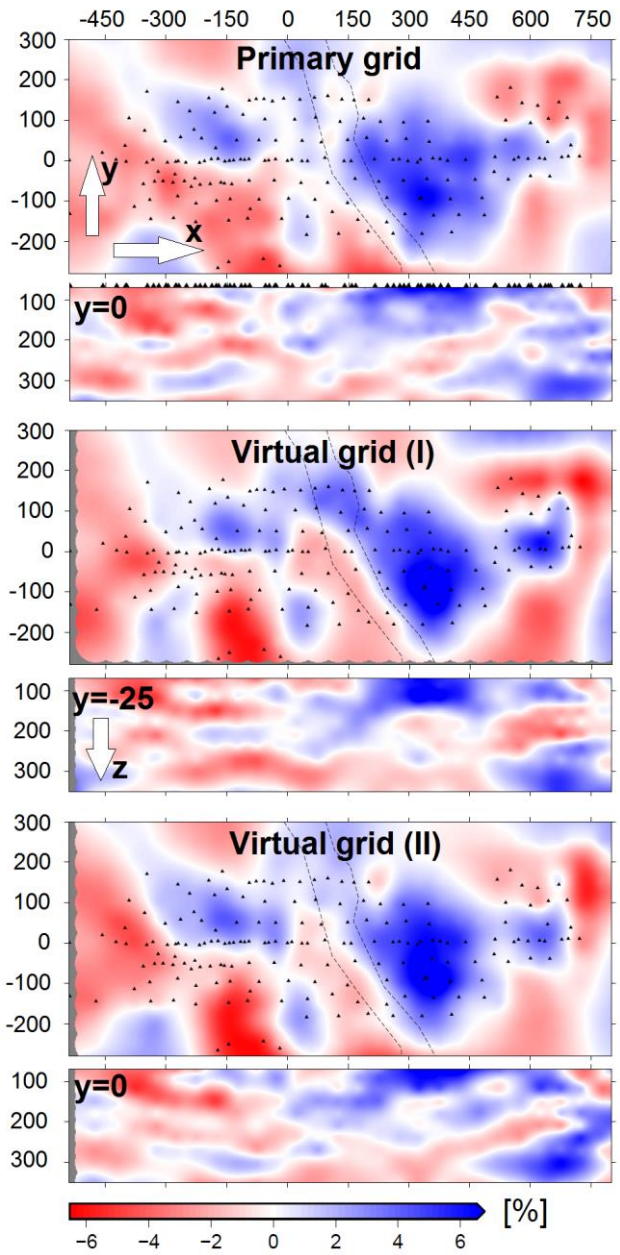


Fig. 6.4 Inversion results with primary grid (top) and two virtual grids (middle and bottom) (see Fig. 6.3). Results obtained with the top quality data and damping of 120. x, y and z indicate northing, easting and depth (km), respectively, in the local Cartesian coordinate system. Horizontal slices at 90 km are shown. Vertical slices are the same for the virtual grid (II), and shifted 25 km for the virtual grid (I) compared to the primary grid. Triangles mark the seismic stations. Dashed lines indicate the TESZ.

To check stability of an inversion result we performed inversions with two virtual grids (Fig. 6.3). The results obtained with the different grids (Fig. 6.4) show good consistency in the areas with good station coverage. Thus, we conclude that the model parameters are reasonable and inversion solution is stable.

## 6.2 Resolution assessment for datasets of different parts of the study area

We divided the entire study area according to geographical distribution into the so called EEC and TOWEST parts, which are equal in size and include the territories to the east and to the west from the TESZ, respectively, and both embracing the TESZ as an overlapping area (about 300 km of overlap) (Fig. 6.5). Model grids for the TOWEST and EEC parts have the same parameters, but amount of the seismic stations, thus, the number of picks varies (Table 6.1). Regarding both datasets with quality factors 1 to 3 in total we used 8251 picks.

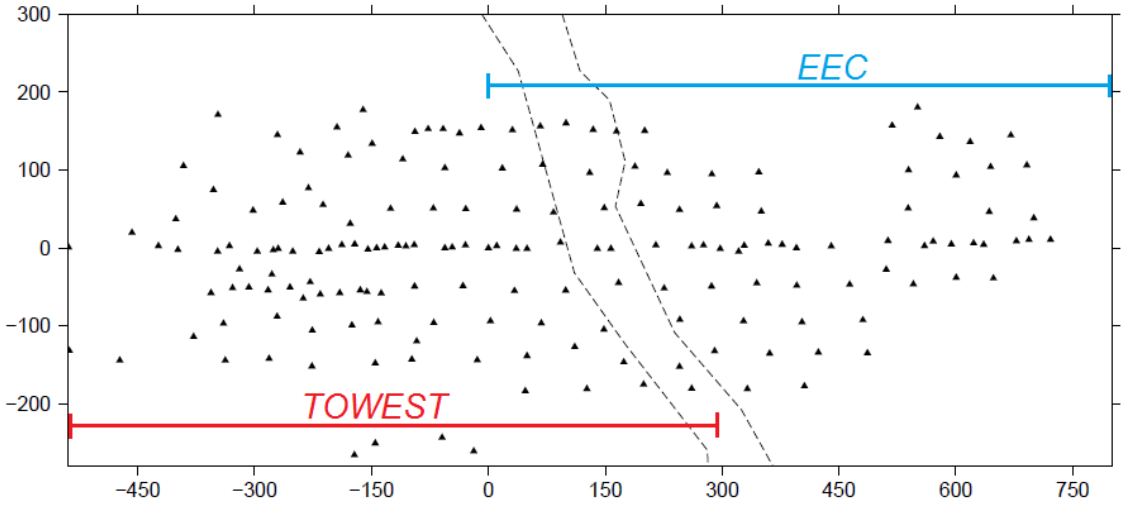


Fig. 6.5 Partition of the entire study area into two equal parts: the TOWEST part includes territories to the west from the TESZ and the TESZ, and the EEC part includes territories to the east from the TESZ and the TESZ. Dashed lines indicate the TESZ.

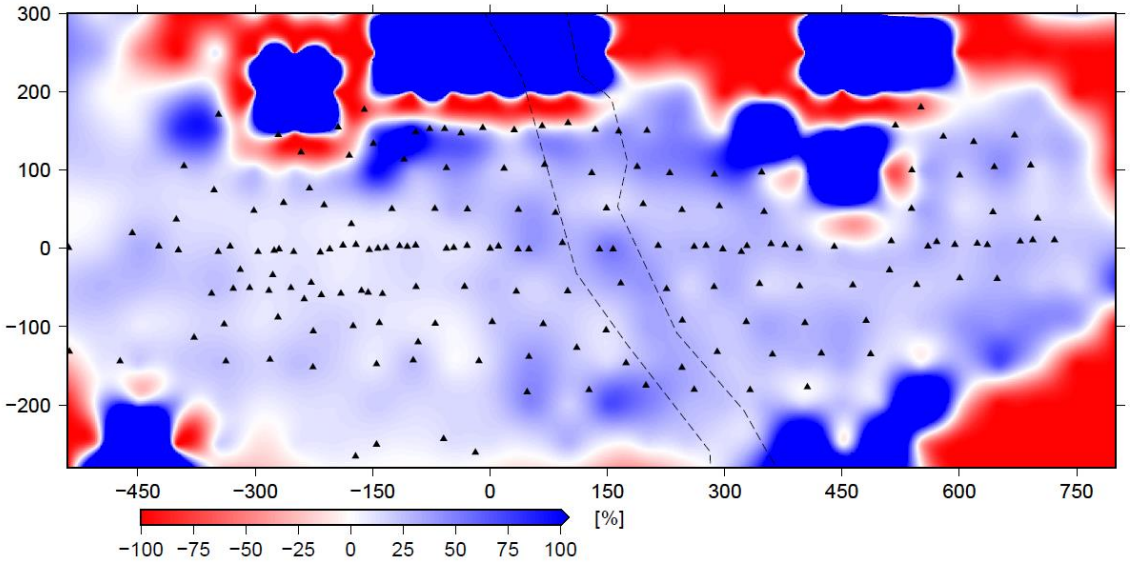


Fig. 6.6 Improvement in the hit matrix compared the results obtained with the top quality data and 1 to 3 quality data for the separated parts of the study area calculated according to Eq. 6.1. The horizontal slice at 90 km show increase in resolution up to 100 % for areas with good station coverage. Triangles mark the seismic stations. Dashed lines indicate the TESZ.

The inversion results obtained with the separated datasets show significant improvement in the hit matrixes. The hit matrixes of the separated TOWEST and EEC parts were merged along the middle line of the intersecting part in order to compare them with the hit matrix which was obtained using the top quality data only (Fig. 6.6). It is not truly correct to merge the results obtained during different inversions, because they may contain some regional components. The evaluation of the changes in the values was calculated as following:

$$\frac{r_s - r_e}{r_e} \times 100 = \Delta r\ [\%], \qquad (6.1)$$

where $r_e$ is a value of an element in the resolution matrix obtained for the entire study area, $r_s$ is a value of an element in the resolution matrix obtained for the separated parts of the study area, and $\Delta r$ is a difference expressed in percent.

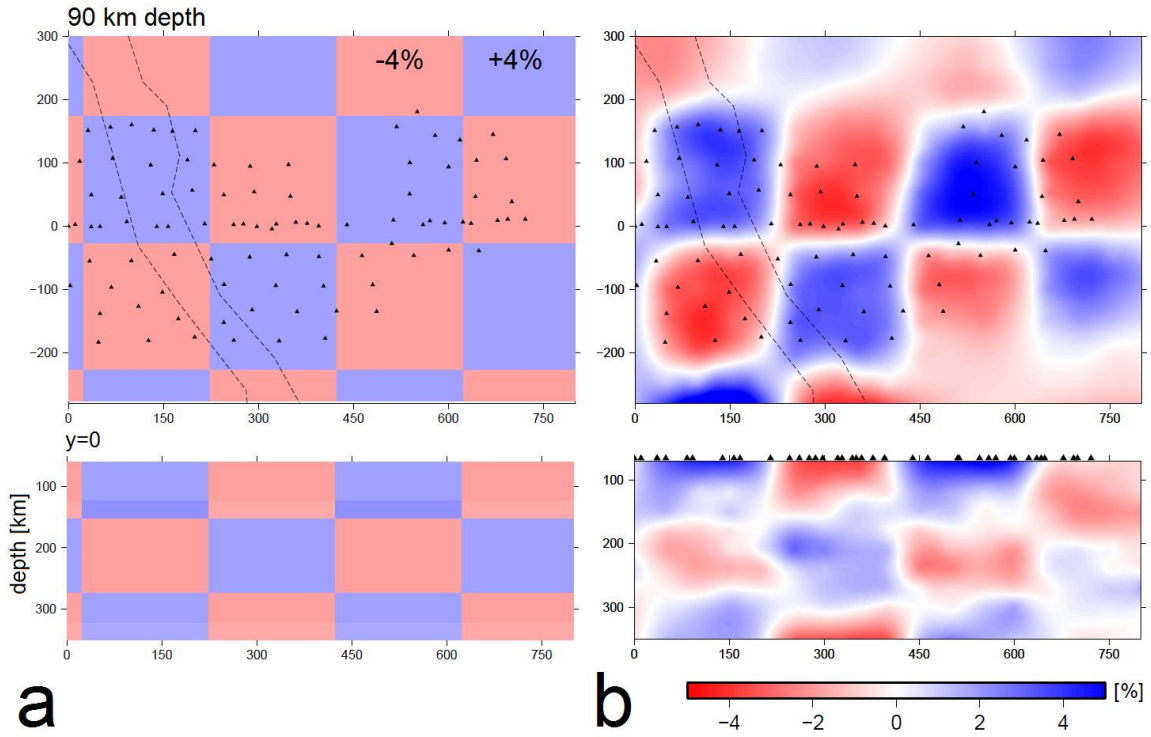


Fig. 6.7 Results of checkerboard test for the EEC part (damping of 120). (a) Initial velocity model with synthetic blocks of 200 km in horizontal directions and four layers thick with ±4 % P-wave velocity difference compared to the IASP91 velocity model. (b) Inversion results with the synthetic dataset. Triangles mark the seismic stations. Dashed lines indicate the TESZ.

In Fig. 6.6 we observe increase in the values of resolution in the areas with good stations coverage, while at the boundaries the noticeable reduction is observed due to the smaller amount of rays when separating the dataset. The resolution increased more in the EEC part compared to the TOWEST part, because in the EEC part we picked more P-wave arrivals of the lower quality.

For the EEC and TOWEST parts we performed the checkerboard tests. For the EEC part we applied the same synthetic model of checkerboard structure (Fig. 6.7) as for the entire study area (the eastern part) presented in Chapter 6.1.

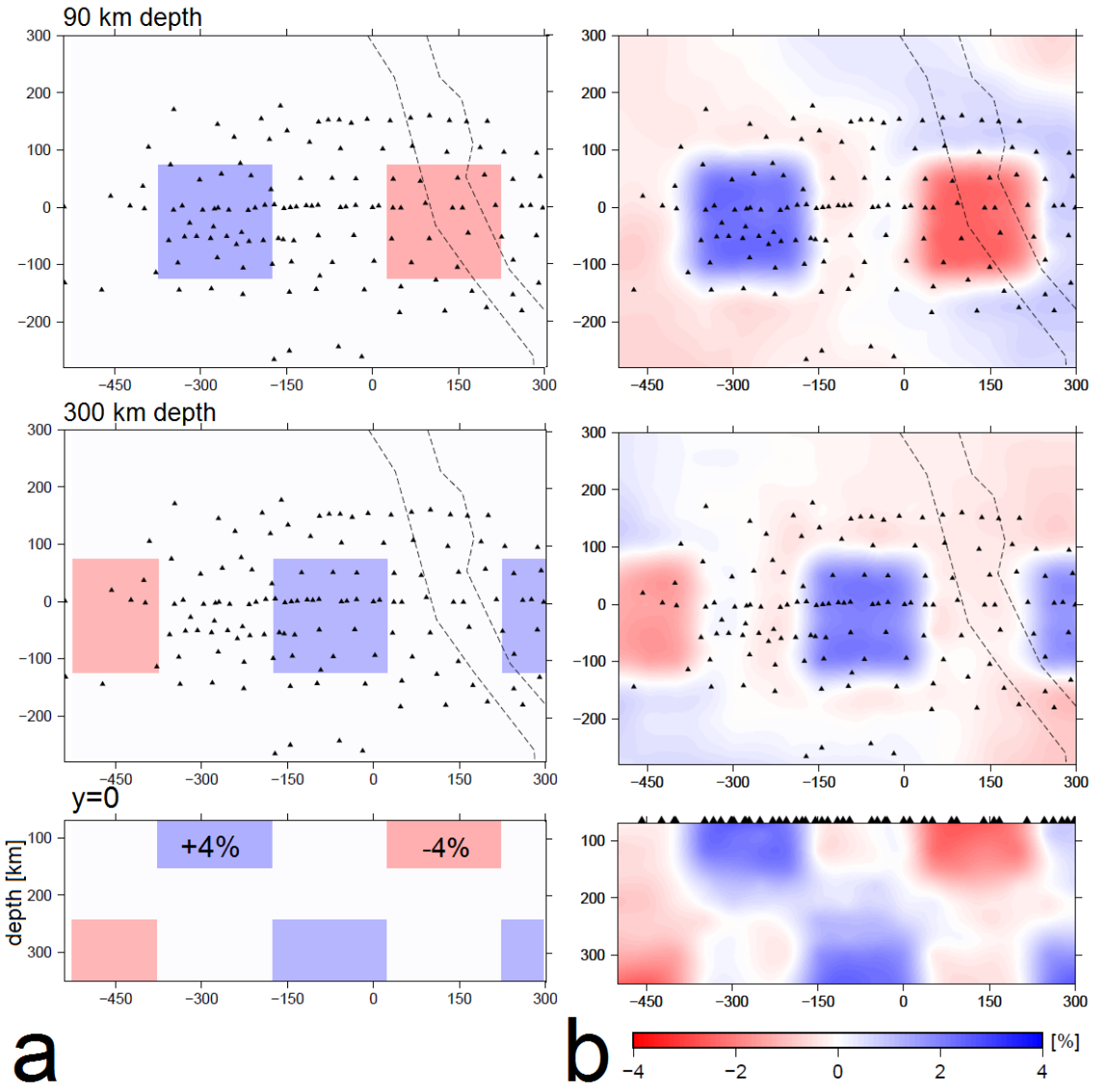


Fig. 6.8 Results of a semi-checkerboard test for the TOWEST part (damping of 120). (a) Initial velocity model with the synthetic blocks of 200 km in horizontal directions and ±4 % P-wave velocity difference compared to the IASP91 velocity model, and areas of seismic velocity values equal to those in the IASP91 velocity model in between the blocks. (b) Inversion results with the synthetic dataset. Triangles mark the seismic stations. Dashed lines indicate the TESZ.

For the TOWEST part we used different synthetic model, because the TELINV code did not fulfill the inversion with the previously described checkerboard type velocity model even with significantly increased boundaries of the model grid. Therefore, we used a synthetic velocity model of semi-checkerboard structure (Fig. 6.8). The synthetic model consists of blocks of 200 km in horizontal directions and four layers thick with ±4 % velocity difference compared to the IASP91 velocity model, but in between the blocks there are areas of velocity values equal to those in the IASP91 velocity model. We also added small random perturbations to each synthetic TT.

During analysis of the results of the checkerboard tests we find that in horizontal directions the structures can be resolved better compared to the vertical one. Moreover, we observe some vertical smearing dipping to the NE due to rays coming mostly from the NE-E-SE direction (Figs. 6.7b, 6.8b).

As the checkerboards do not provide complete resolution, we performed a synthetic test with geologically possible model in order to demonstrate that our dataset is able to resolve it. We compiled a synthetic 3-D "geological" model (Fig. 6.9) based on some geophysical and petrophysical studies (e.g. Wilde-Piórko et al., 2010; Griffin et al., 2003). The main features of the synthetic velocity model (Fig. 6.9) are: 1) the lower and the higher seismic velocity values to the west and to the east from the TESZ, respectively, 2) the shape of the LAB of a ramp type dipping to the NE direction, and 3) the deep cratonic roots for the EEC (in the NE part of the study area). We added small random perturbations to each synthetic TT and performed the inversion. The inversion results (Fig. 6.9) show resolved areas of the lower and the higher seismic velocity values to the west and to the east from the TESZ, respectively. In the results we also observe the clearly resolved ramp shape of the LAB and the deep cratonic roots in the NE part of the study area (Figs. 6.9).

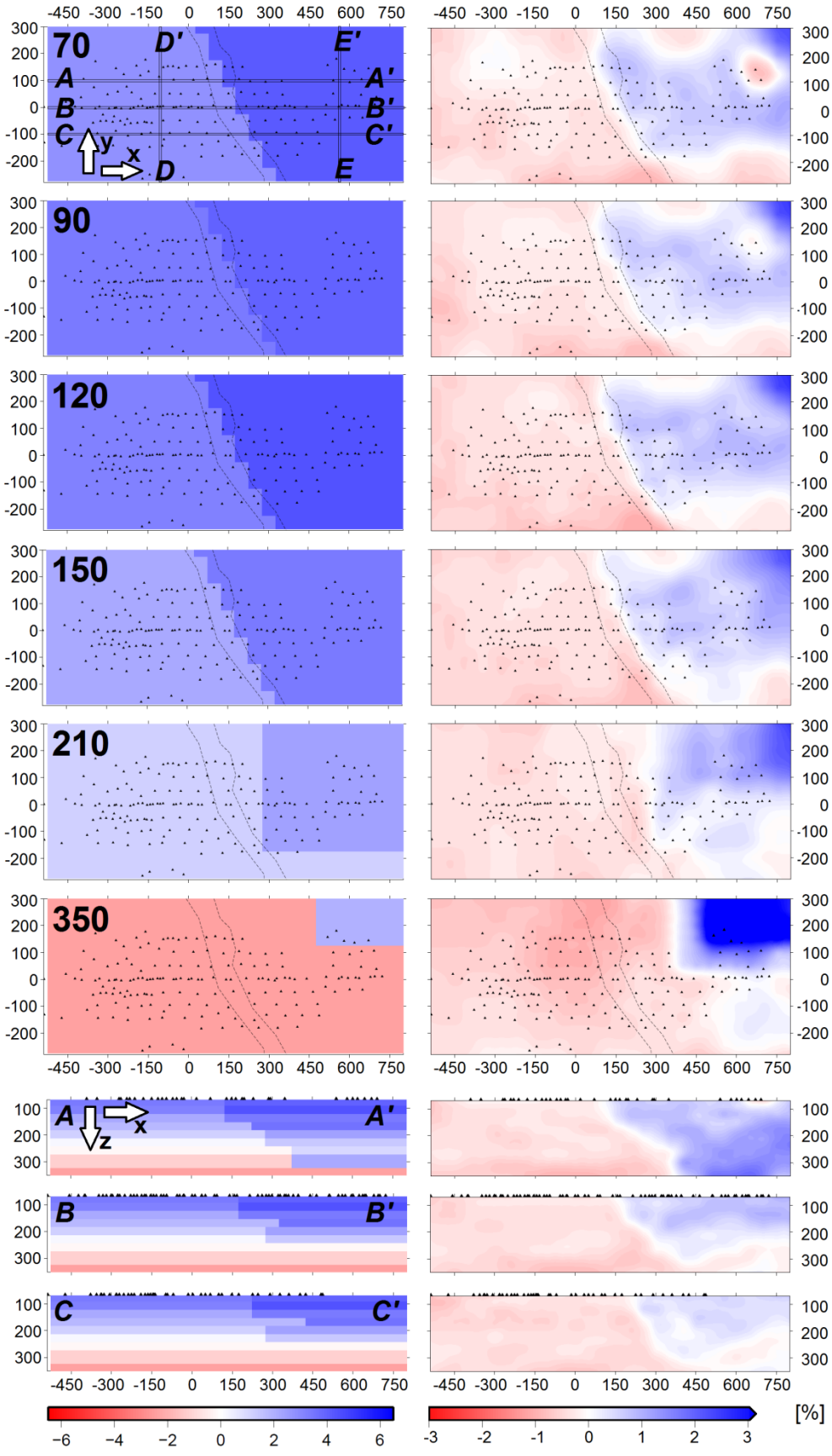
70
90
120
150
210
350
A
A'
B
B'
C
C'
D
D'
E
E'
x
y
z
-450 -300 -150 0 150 300 450 600 750
300 200 100 0 -100 -200
100 200 300
-6 -4 -2 0 2 4 6
-3 -2 -1 0 1 2 3
[%]

Fig. 6.9 P-wave velocity perturbations in horizontal slices at indicated depths (km) and vertical slices along the indicated transects obtained with the synthetic "geological" model: input velocity model (left), and inversion results (right). Triangles mark the seismic stations. x, y and z indicate northing, easting and depth (km), respectively, in the local Cartesian coordinate system. Dashed lines indicate the TESZ.

# Chapter 7

*„Žali ėgliai kaip kvietkai po dirvonus keri…“*

*Antanas Baranauskas* [IV]

## P-WAVE VELOCITY VARIATIONS OBTAINED FOR THE ENTIRE STUDY AREA

The study area has been investigated throughout many different studies discussed in Chapter 1.3, which provide some insight about possible structure of the upper mantle and the shape of the LAB, and help to speculate what we might expect to obtain in our results. All the discussed studies indicate the TESZ as a major tectonic boundary in Europe, and most of them report sharp P-wave velocity variations around the TESZ. Moreover, the studies indicate the higher seismic velocities to the east of the TESZ and the lower ones to the west of the TESZ, while they show more prominent seismic LAB beneath the younger part of Europe compared to the EEC.

Fig. 4.4 indicates that the optimal damping value for the real dataset is 80. However, we performed inversions with damping values of 80 and 120, and the results with damping value of 80 shows the higher velocity variations (about 1 %) of smaller scale compared to the results obtained using damping value of 120. As

[IV] *“The green junipers grow spread throughout the unbroken soil as blooming plants…” Antanas Baranauskas*

we aim to resolve regional (larger) scale variations, we present the results obtained with damping value of 120.

For the entire study area we performed inversions with the real data from 70 km down to 350 km (Figs. 7.1, 7.2, 7.3). Using 1 to 3 quality data for the separated parts (Table 6.1) we obtain the better ray coverage compared the results obtained with the top quality data only, thus, increase in resolution. A comparison between the results obtained with different datasets show similar distribution of the P-wave velocity variations (Fig. 7.3). The checkerboard tests (Figs. 6.7, 6.8) show that we can trust the results down to the bottom of the inverted layers, however, at the bottom we observe some differences beneath the TESZ area because of different ray coverage (Fig. 7.3).

The results obtained with the real and the synthetic "geological" datasets are compared (Fig. 6.9, 7.1, 7.2, 7.3), while the discussion is carried out in Chapter 9.

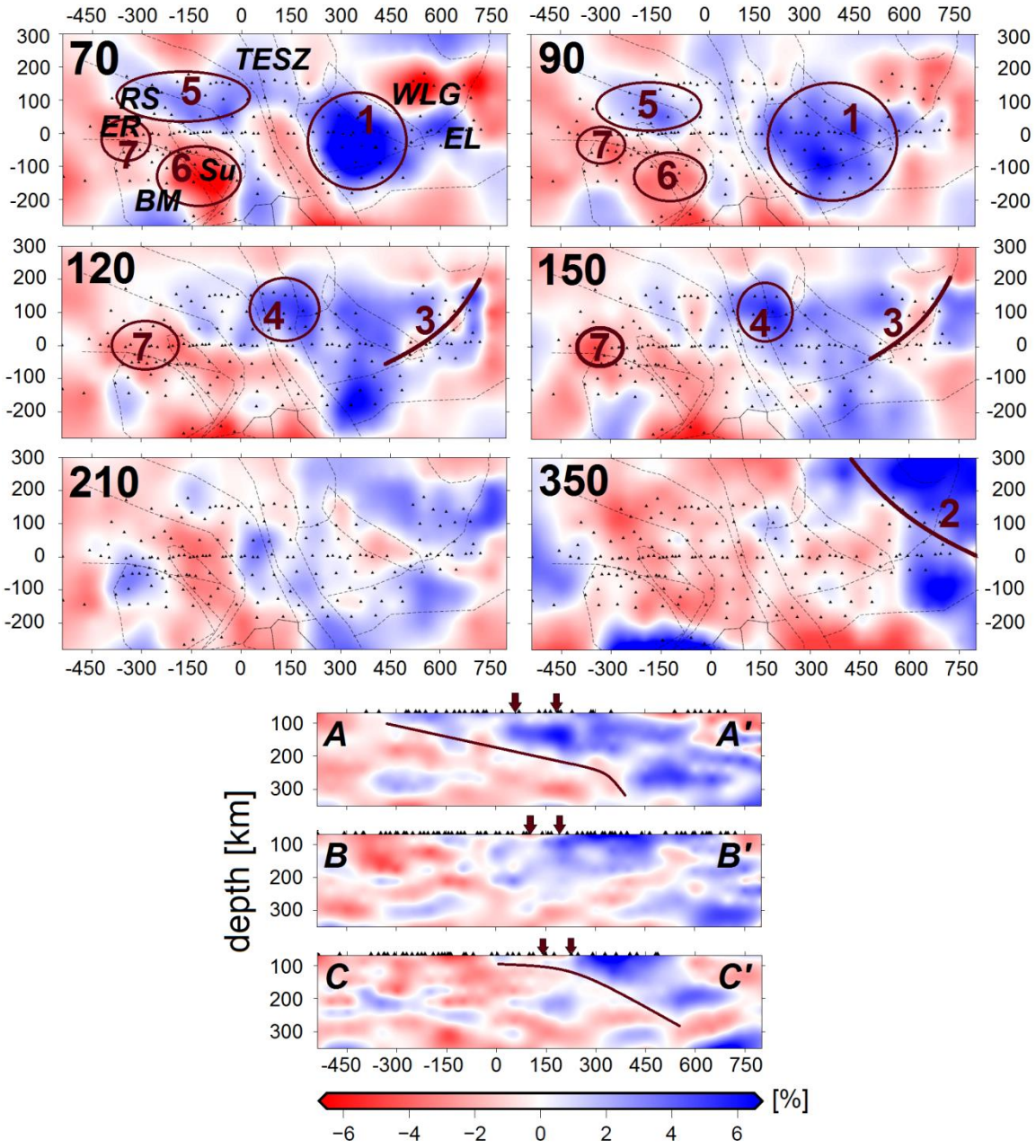


Fig. 7.1 P-wave velocity perturbations in horizontal slices at indicated depths (km) and vertical slices along the indicated transects obtained with the real dataset. Triangles mark the seismic stations. Dashed lines on horizontal slices indicate boundaries of the tectonic units (see Fig. 1.2b). Numbered areas mark the discussed structures: 1 – high velocity area beneath Poland (craton); 2 – deep cratonic roots extending to at least 300 km or more beneath Lithuania; 3 –

palaeosubduction boundary between the WLG and the EL; 4 – high velocity area beneath Northern Poland; 5 – higher velocity area along the Rheic Suture; 6 – lower velocity area beneath the Sudetes Mountains and the Bohemian Massif; and 7 – low velocity area beneath the Eger Rift. Solid lines on vertical slices show the interpreted seismic LAB; and brown arrows indicate the TESZ. For more explanations see Fig. 6.9.

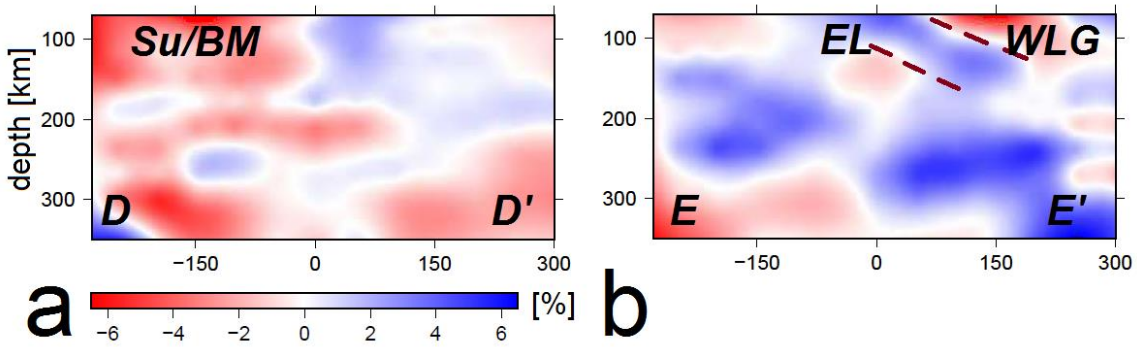


Fig. 7.2 P wave velocity perturbations in vertical slices DD' and EE' transverse to the main transect (see Fig. 6.9). (a) Low velocities are observed in the western part of the Bohemian Massif (BM) and the Sudetes Mountains (Su) from the depth of 70 km. (b) Dashed lines indicate possible palaeosubduction slab under Lithuania between the WLG and the EL.

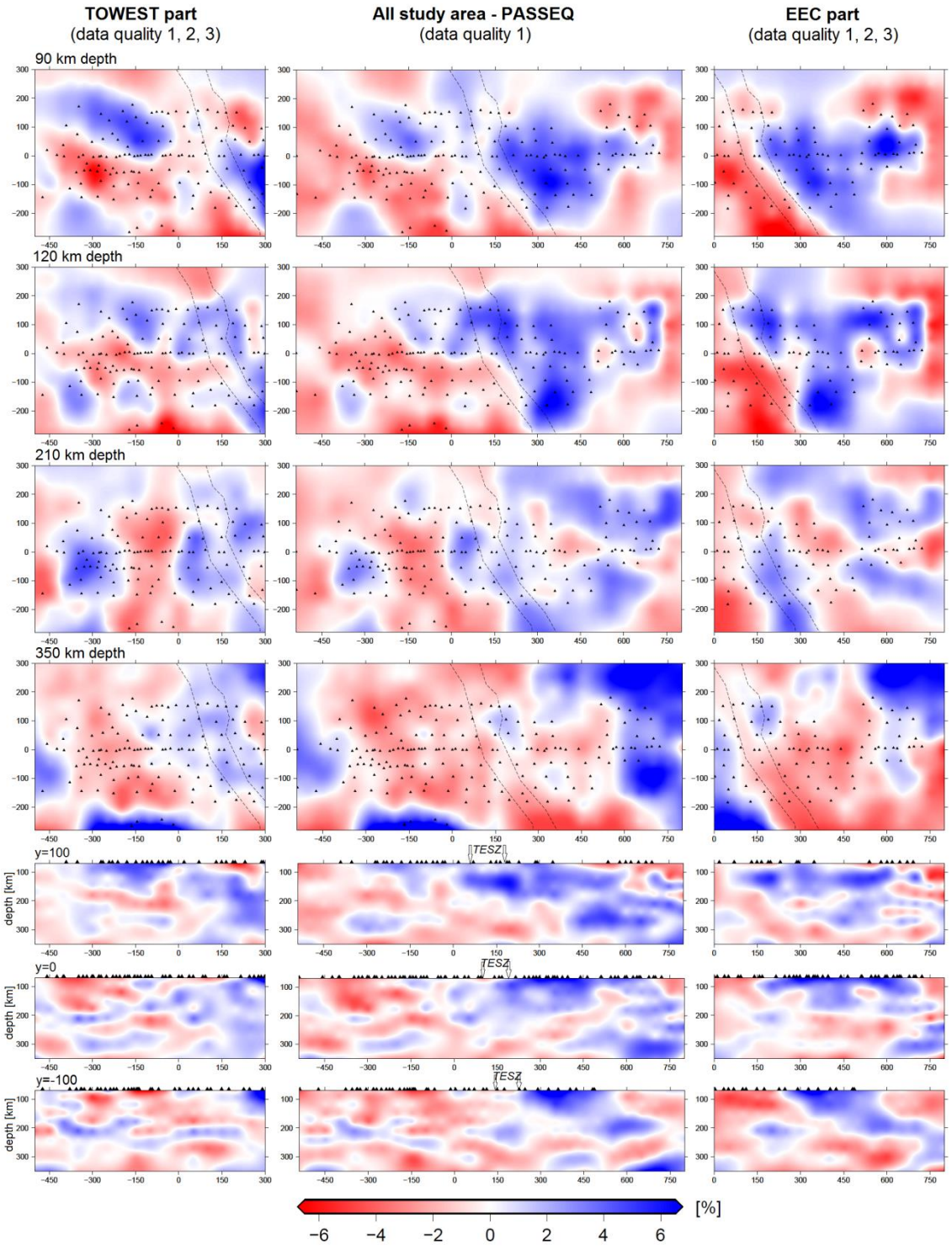


Fig. 7.3 Comparison of the results obtained with the top quality data for the entire study area (middle) and with 1 to 3 quality data for the TOWEST (left) and EEC (right) parts.

# Chapter 8

## DETAILED STUDY OF THE CRATONIC PART OF THE STUDY AREA: P-WAVE VELOCITY VARIATIONS

The special study is focused on the SW part of the EEC and aims to find correlation between the crustal units and the upper mantle, and to resolve local to regional structures in the upper mantle and to determine thickness of the lithosphere. Compared to the inversions for the entire study area we use data of quality factor 1 to 3, but different set of the crustal TT corrections and damping value, and the inversions are performed for layers between 60 and 350 km.

Table 8.1 Dataset used in the study focused on the SW part of the EEC.

| **Weighting factor** | **Time error** | **Number of picks** |
|---|---|---|
| 1 | <0.2 s | 2808 |
| 2 | 0.2-0.3 s | 958 |
| 3 | 0.3-0.4 s | 429 |
| **In total:** | | 4195 |

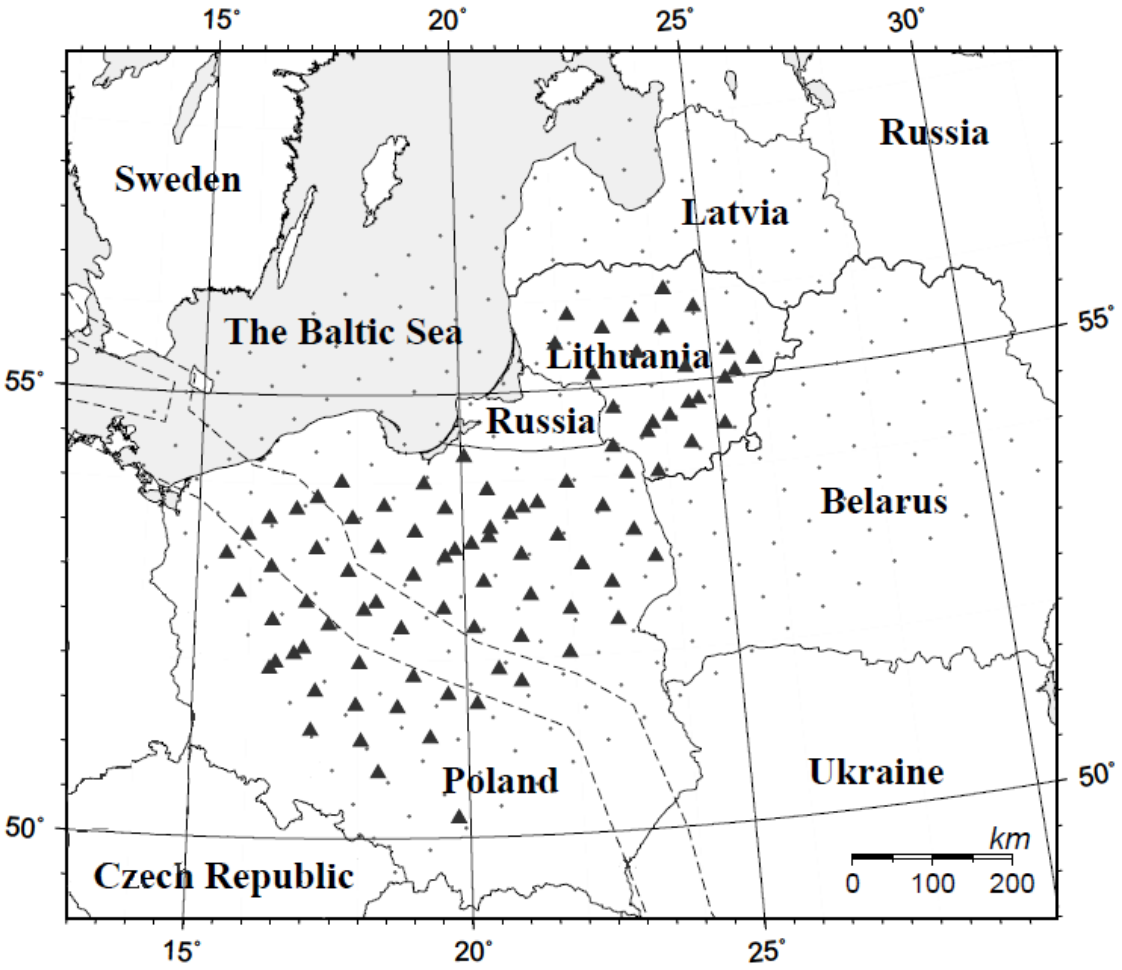


Fig. 8.1 Map of the seismic stations (triangles) used, and locations of nodes of a model grid (dots). Dashed lines indicate the TESZ.

## 8.1 Dataset and model parameterization

In this special study we use data from the seismic stations deployed in the TESZ and to the NE from it (Fig. 8.1). The dataset contains 4195 picks of the P-wave arrivals of quality factor 1 to 3 recorded at 94 seismic stations from 101 teleseismic EQs (Table 8.1). The model grid used in this study was parameterized using the same criteria as for the entire study area (see Chapter 4). The reference velocity model used is shown in Fig. 4.2, but in this study the uppermost inverted layer starts at the depth of 60 km. Spacing between the grid nodes in horizontal

directions was set to 50 km (Fig. 8.1). Information about model parameterization is the same as for the EEC part presented in Table 6.1.

We performed a number of inversions with different values of smoothing **Θ** and damping **D** in order to assess optimal parameters of the inversion. The smoothing value was set to 50, while the optimal damping value of 80 was determined investigating the trade-off curve between the data variance and model variance (Fig. 8.2).

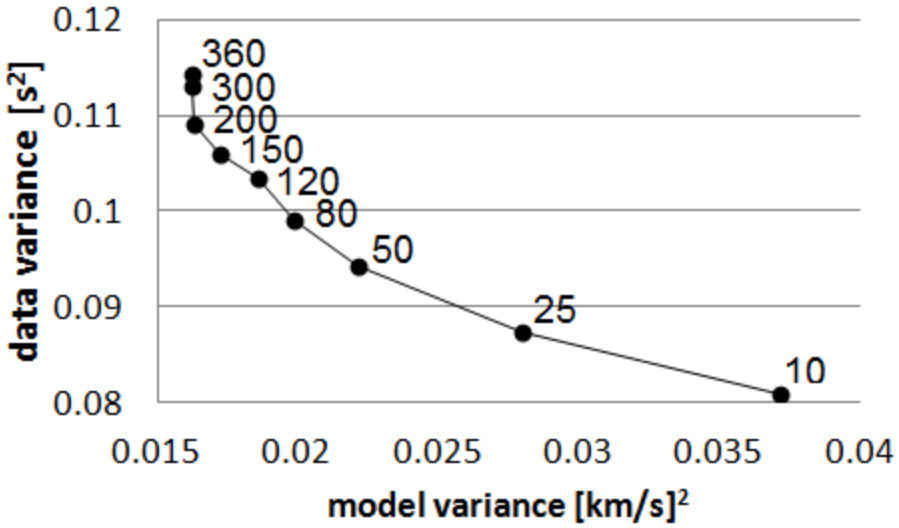


Fig. 8.2 Trade-off between model variance and data variance after three iterations obtained during inversions with damping values from 10 to 360.

## 8.2 Crustal travel time corrections

In order to estimate the crustal TT corrections we use two precise 3-D crustal models by Majdański (2012) for Poland and by M. Budraitis (unpublished) for Lithuania (Fig. 8.3a). Both crustal models were compiled using results of all available DSS projects, e.g. EUROBRIDGE, CELEBRATION, POLONAISE, BABEL (BABEL Working Group, 1993), etc., carried out around Poland and

Lithuania. A detailed description of the crustal model used to estimate the crustal TT corrections for the stations deployed in Poland is presented by Majdański (2012), while M. Budraitis's unpublished crustal model is showed in Fig. 8.4. The crustal model contains different crustal layers with assigned constant seismic velocities: 2.6 km/s in the sedimentary cover, 5.8 km/s in the upper crust, 6.4 km/s in the middle crust, 6.8 km/s in the lower crust which is terminated by the Moho boundary with assigned velocity value of 8.0 km/s.

We used Eq. 5.1 to estimate the crustal TT corrections regarding the vertical velocity structure beneath the stations (Fig. 8.3b). The estimated corrections were introduced into the inversion as described in Chapter 5. While comparing the inversion results obtained without (Fig. 8.5a) and with (Fig. 8.5b) the applied crustal TT corrections, one may observe a significant difference. Although the distribution of velocity variations is quite similar, the amplitudes of velocity perturbations are much higher in the results obtained without the crustal TT corrections. The largest differences (Fig. 8.5) are observed in places which coincide either with the thick sedimentary cover or the deep Moho: on the NE edge of the TESZ beneath the Polish Basin, beneath Western Lithuania and beneath Poland to the east of the TESZ.

## 8.3 Resolution

To estimate resolution we use a hit matrix and a synthetic checkerboard test. The hit matrix (Fig. 8.6a) shows good ray coverage beneath the seismic array. We also plot the reconstructed raypaths of some random EQs (Fig. 8.6b) which indicate dominating raypaths from the E-SE direction because of most of the EQs located to the east of our study area (Fig. 3.2). Moreover, we plot the kernel values in each layer (Fig. 8.7) which show the values ranging from -0.04 to 0.09, while the values closer to 0 are observed mostly in areas with the poorest station coverage.

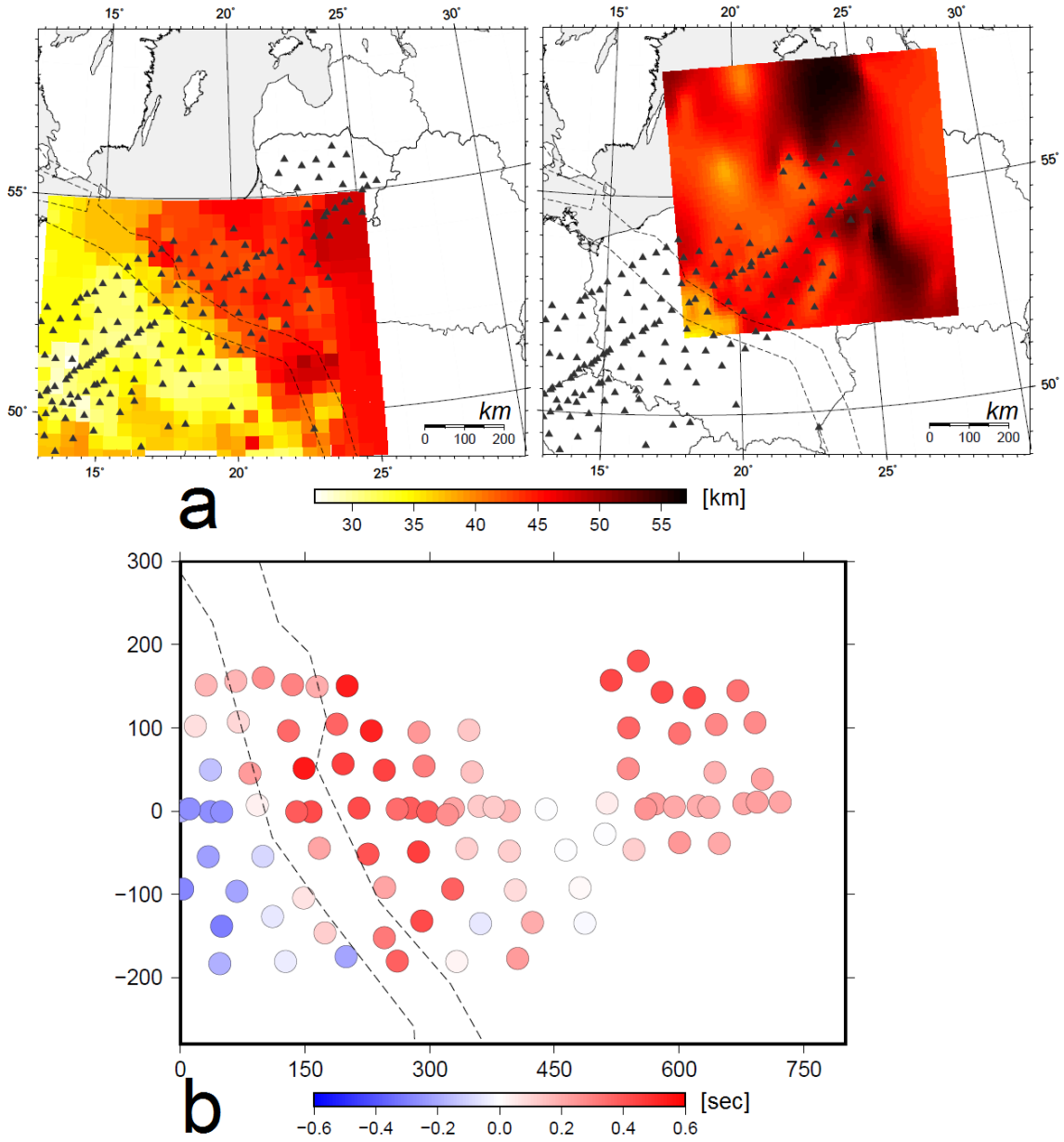


Fig. 8.3 a) Moho maps of the crustal models by Majdański (2012) (left) and M. Budraitis (unpublished) (right) which were used to estimate the crustal TT corrections. The Moho depths in the depicted area vary from 27 to 57 km. b) Estimated crustal TT corrections for individual seismic stations expressed in seconds compared to the IASP91 velocity model.

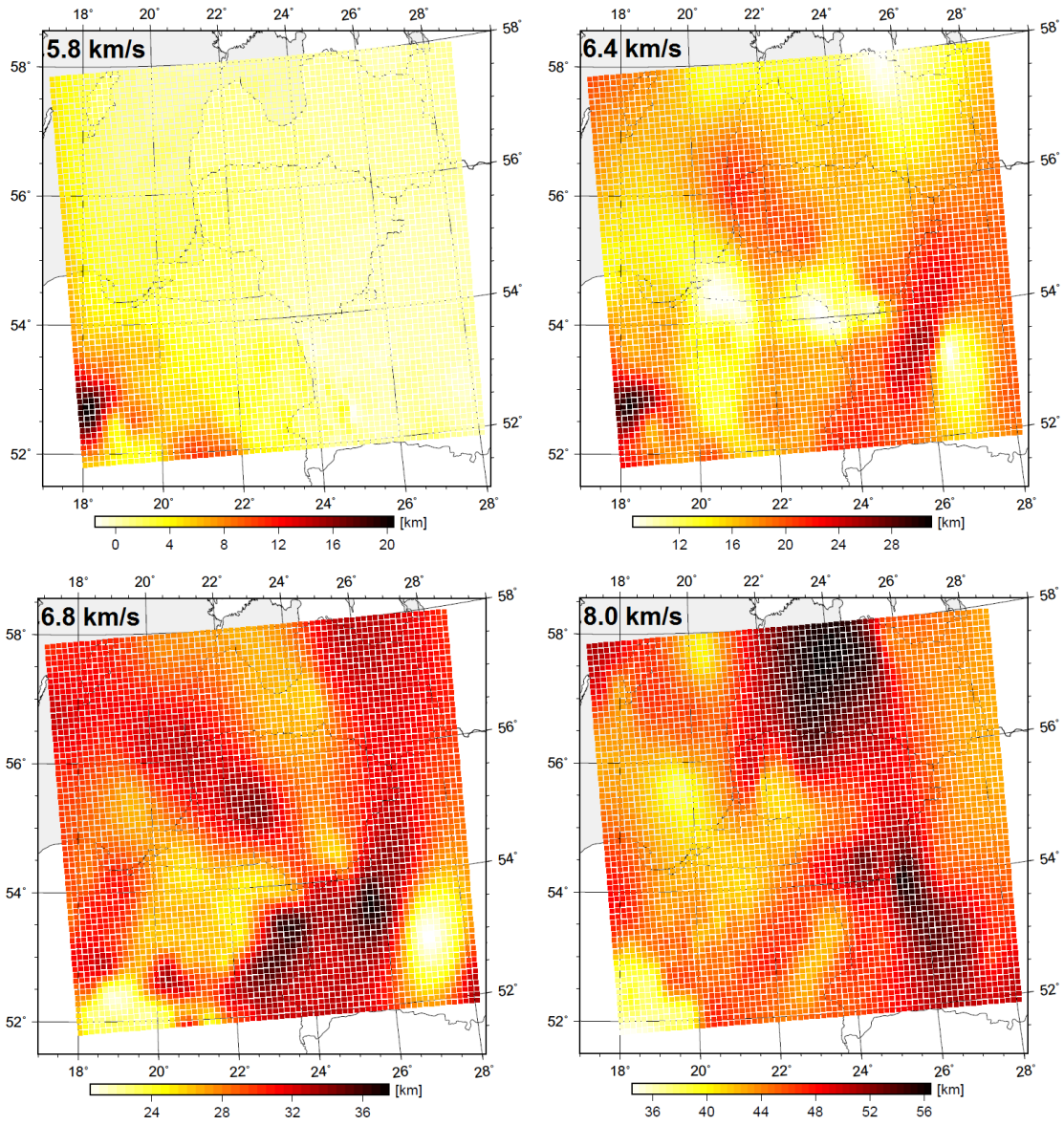


Fig. 8.4 Crustal model by M. Budraitis (unpublished). Maps show depth of the top of each layer with the defined constant seismic velocity. In the sedimentary cover, which extends from the surface down to the layer with seismic velocity of 5.8 km/s, was assumed seismic velocity of 2.6 km/s. The layer with seismic velocity of 8.0 km/s coincides with a depth of the Moho boundary.

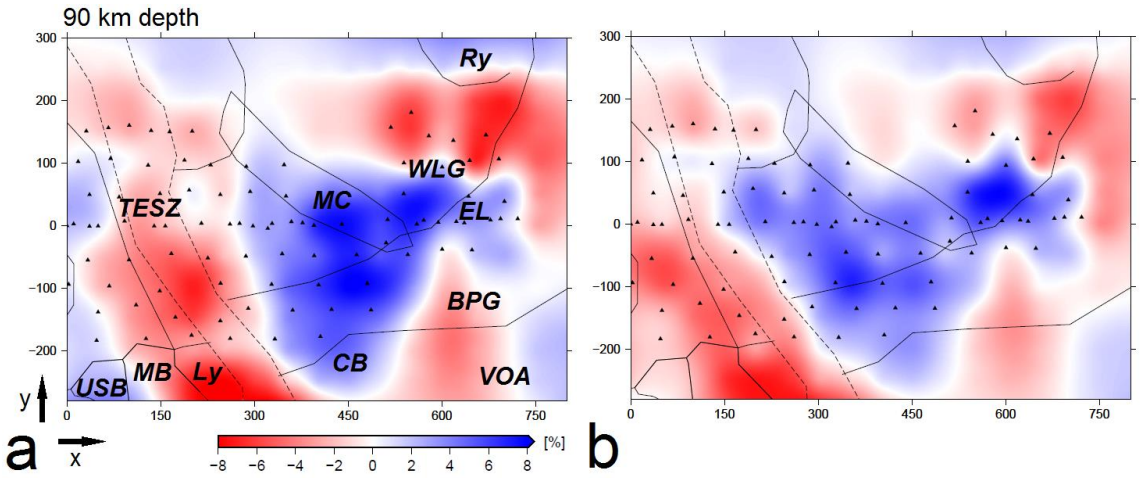


Fig. 8.5 P-wave velocity variations obtained with the real dataset a) without crustal TT corrections, and b) with crustal TT corrections. Lines indicate boundaries of the tectonic units: BPG, Belarus–Podlasie Granulite Belt; CB, Central Belarus Belt; EL, East Lithuanian Domain Ly, Lysogory; MB, Malopolska Block; MC, Mazury Complex; Ry, Riga granitoid pluton; TESZ, Trans-European Suture Zone; USB, Upper Silesian Coal Basin; VOA, Volyn–Orsha Aulacogen; WLG, West Lithuanian Granulite Domain.

For the checkerboard test we used the same synthetic velocity model as described in Chapter 6.2 (Fig. 8.8a). The inversion results show that the synthetic velocity structure is reasonably resolved in the areas with good station coverage (Fig. 8.8b). However, in horizontal directions the synthetic structure can be resolved better while in the vertical slices we observe a significant vertical smearing dipping to the NE-N-SE direction due to the rays coming mostly from the regions to the east of the study area.

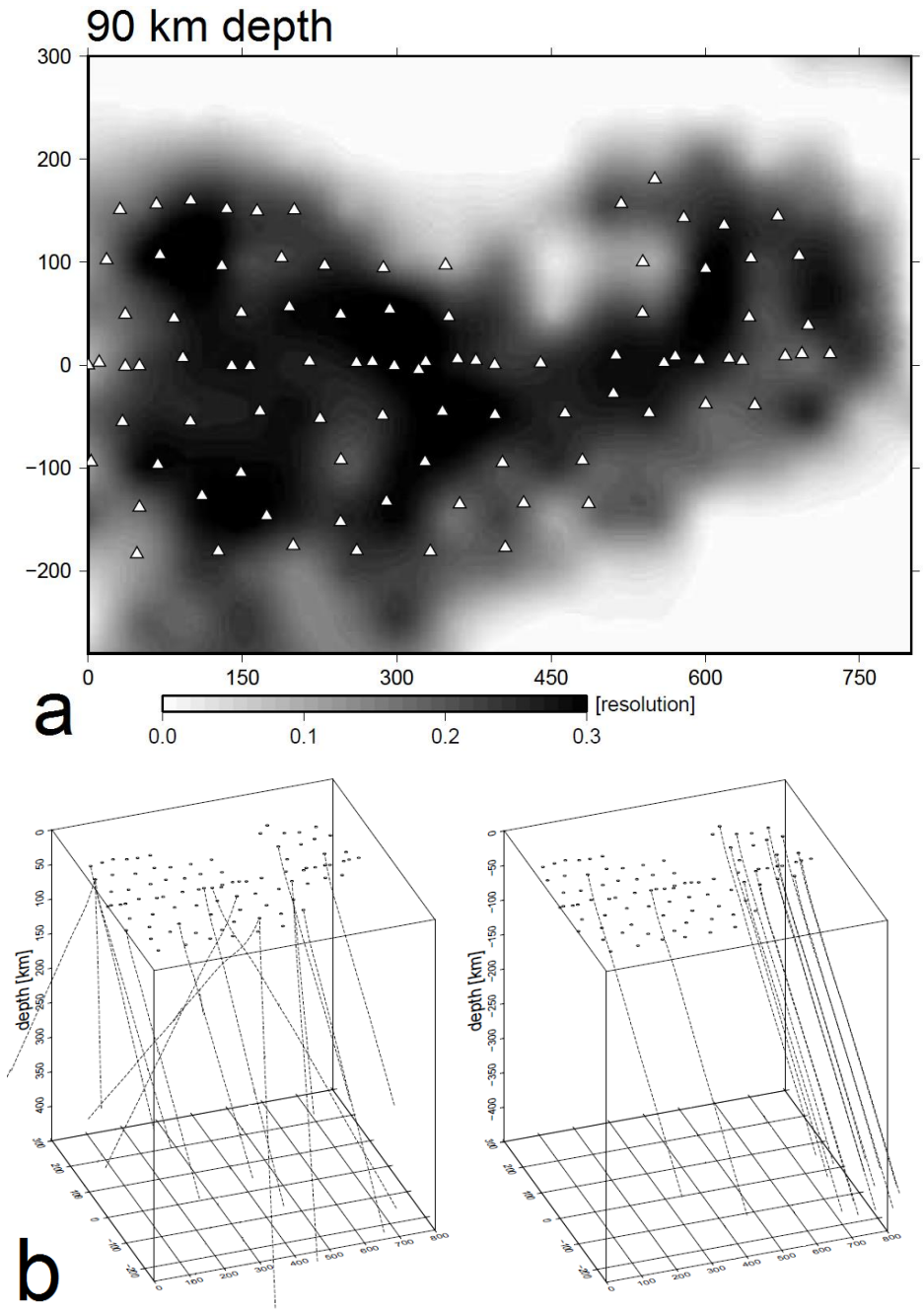


Fig. 8.6 (a) Hit matrix in horizontal slice at the depth of 90 km obtained with the real dataset. Triangles mark the seismic stations. Scale shows relative amount of a number of rays which transverse a particular cell: low and high values show poorly and well resolved areas, respectively. (b) Constructed synthetic raypaths (dashed lines) for several EQs (left), and for one EQ (right). Dots indicate the seismic stations.

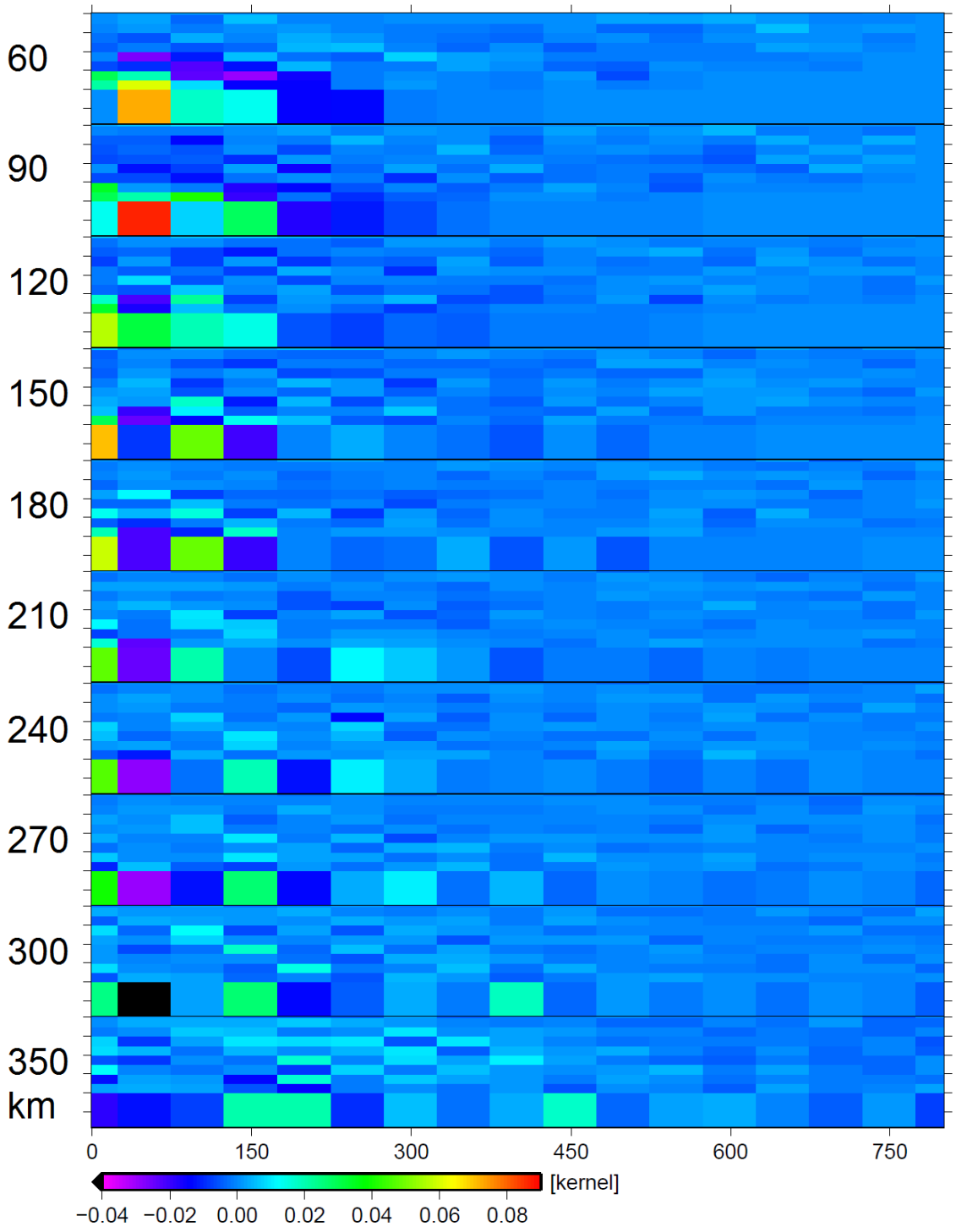


Fig. 8.7 Values of kernel matrix in every inverted layer.

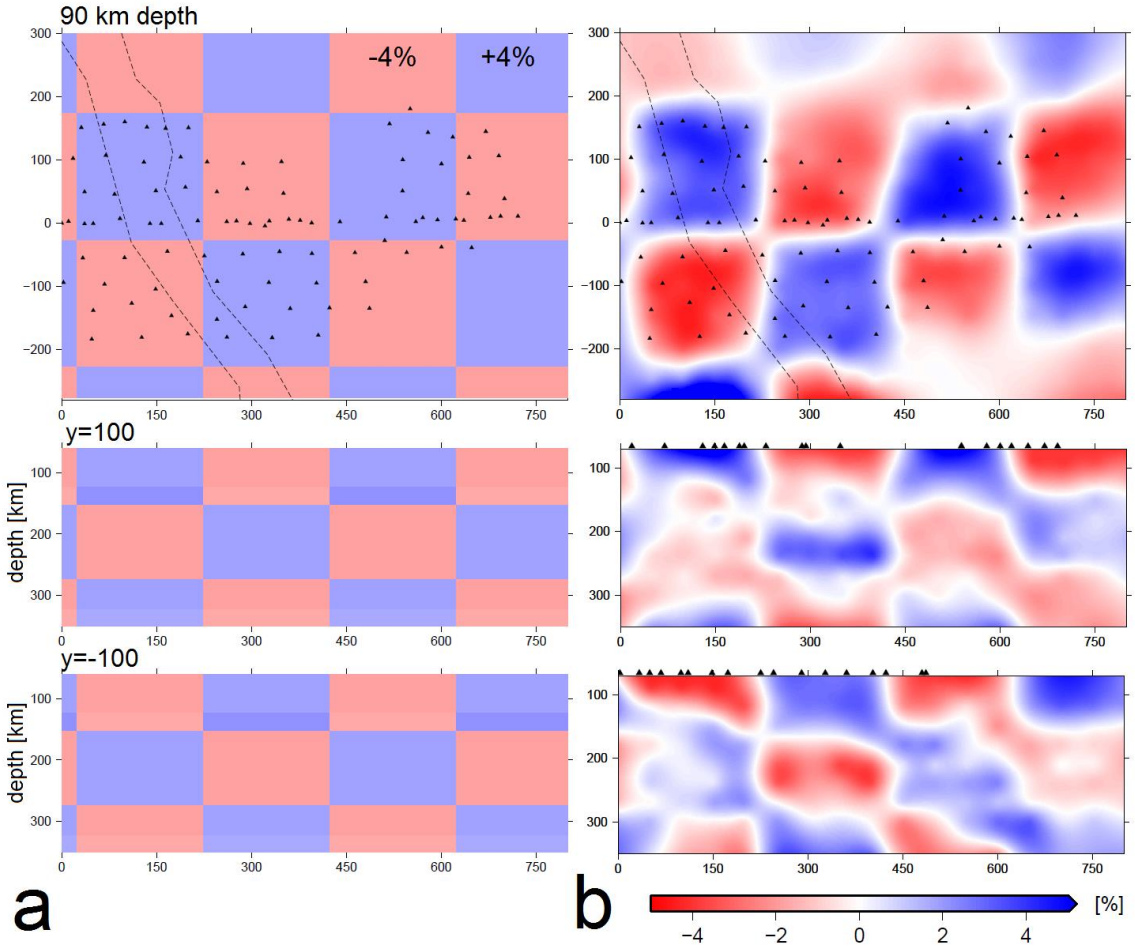


Fig. 8.8 Results of a synthetic checkerboard test (damping of 80). Horizontal slice at the depth of 90 km and two vertical slices parallel to the main transect of the target area. (a) Synthetic velocity model with blocks of 200 km in horizontal directions and ±4 % velocity difference compared to the IASP91 velocity model. (b) Inversion results with the synthetic dataset. Dashed lines indicate the TESZ. Triangles indicate the seismic stations.

We also performed a synthetic "spike" test in order to evaluate the effects of vertical smearing. We compiled a synthetic "spike" velocity model (Fig. 8.9a) with only one 4 % higher velocity block compared to the IASP91 velocity model in the study area. The synthetic block of 200 km in horizontal directions and three layers thick was set beneath Lithuania. The place was selected taking into account

the significant velocity anomalies (e.g. Fig. 7.1, 7.2) observed beneath Lithuania and due to my personal interest to this specific part of the study area. A synthetic dataset for the "spike" test was compiled adding slight random perturbations to each synthetic TT. The obtained results (Fig. 8.9b) show resolved high velocity anomaly, but also show quite significant vertical smearing, which implies that in our results with the real data the resolved structures are vertically smeared. Moreover, the "spike" test demonstrates that the magnitude of inversion artefacts is quite small (about 1 %), thus, in our results we should not interpret perturbations smaller than 1 %.

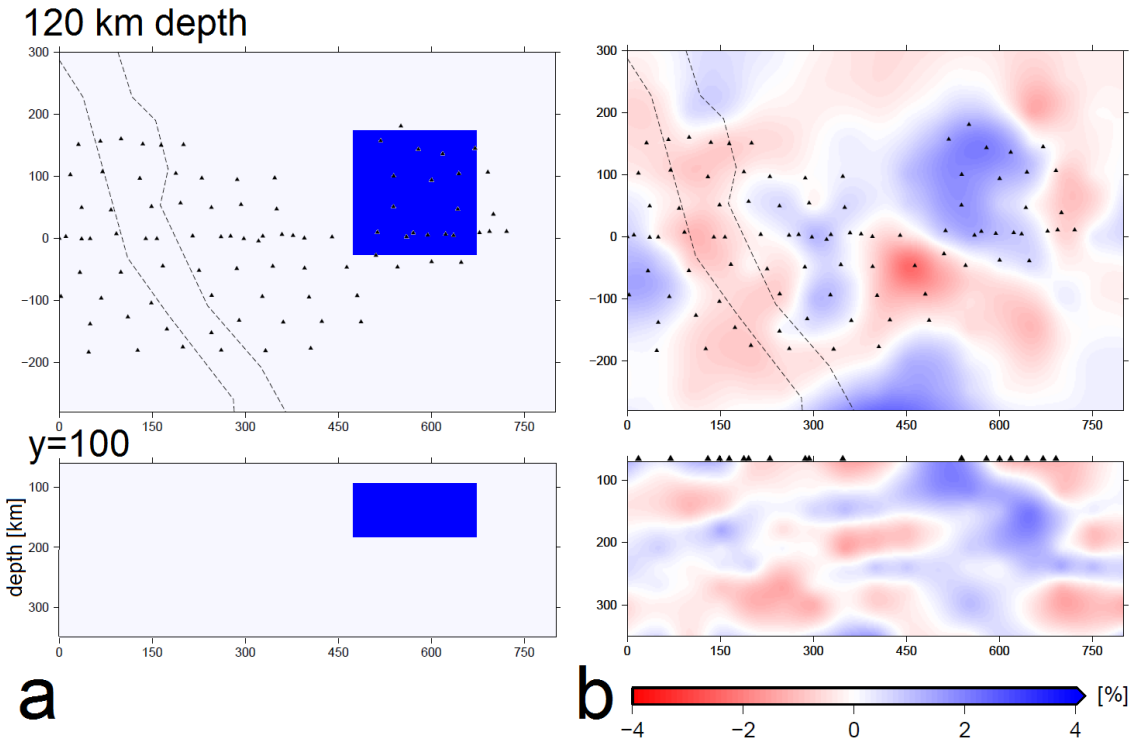


Fig. 8.9 Results of a synthetic "spike" test. Horizontal slice at the depth of 120 km and vertical slice parallel to the main transect. (a) Synthetic velocity model with one high velocity block of 200 km in the horizontal directions and three layers thick. In the block the P-wave velocity value is 4 % higher compared to the IASP91 velocity model. (b) Inversion results with the synthetic dataset. Dashed lines indicate the TESZ. Triangles indicate the seismic stations.

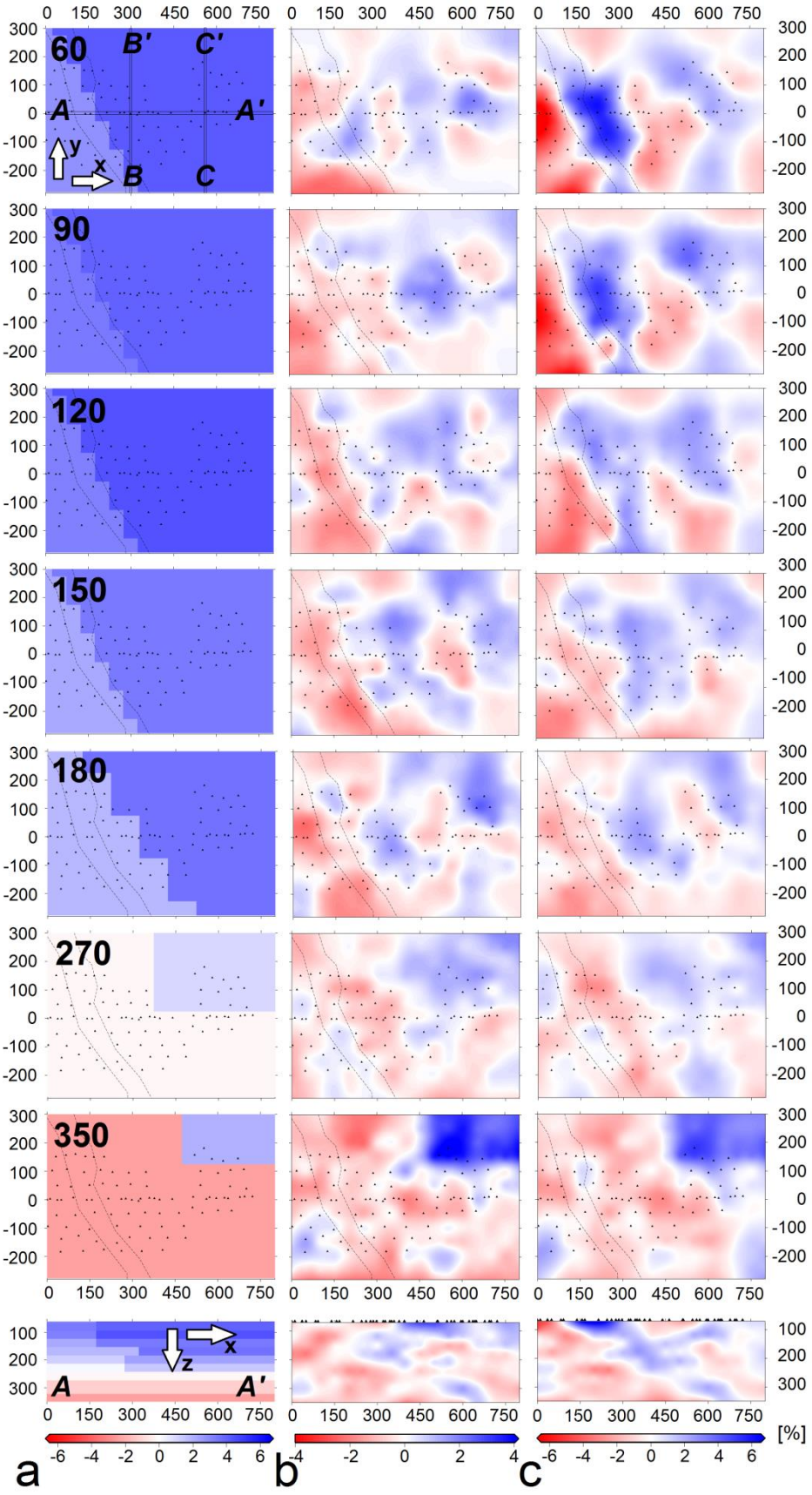
60
90
120
150
180
270
350
A
A'
B
B'
C
C'
x
y
z
0 150 300 450 600 750
300 200 100 0 -100 -200
100 200 300
-6 -4 -2 0 2 4 6
-4 -2 0 2 4
[%]
a
b
c

Fig. 8.10 Synthetic "geological" test. P-wave velocity perturbations in horizontal slices at indicated depths (km) and vertical slice along the main transect *AA'*. x, y and z indicate northing, easting and depth (km), respectively, in the local Cartesian coordinate system. The initial synthetic "geological" velocity model (a), the inversion results with the synthetic dataset without (b) and with the crustal TT corrections (c). Thin dashed lines on the horizontal slices indicate the TESZ. Thin double lines indicate locations of the vertical transects. Triangles indicate the seismic stations.

As previously, we want to demonstrate that our dataset is able to resolve not only the checkerboard type structures, but also some geologically possible models. Thus, based on some geophysical and petrological studies (e.g. Wilde-Piórko et al., 2010; Griffin et al., 2003) we compiled a synthetic "geological" 3-D velocity model. In the synthetic velocity model (Fig. 8.10a) we introduced the seismic velocity values 2 to 6 % higher compared to the IASP91 velocity model at different depths beneath the craton. In the TESZ area we introduced the LAB of shape of a ramp dipping to the NE direction with seismic velocity values close to those of the craton but up to 2 % smaller down to about 180 km. At the depths between 270 and 350 km we introduced velocities 2 to 4 % lower compared to the IASP91 velocity model beneath the study area except in the NE part where we introduced about 4 % higher velocity area compared to the IASP91 velocity model, which implies that we expect the deeper cratonic lithosphere in this part. With the synthetic dataset, which was compiled adding small random perturbations to each synthetic TT, we performed inversions without (Fig. 8.10b) and with the crustal TT corrections (Fig. 8.10c) as used with the real data. The crustal corrections were applied in order to obtain similar raypaths in the upper layers, and to estimate the effects of the crustal corrections to the amplitudes of

velocity variations and the depth to which this effect is significant. The inversion results with the crustal TT corrections (Fig. 8.10c) show in total about 2.5 % higher amplitudes of velocity variations (both positive and negative) compared with the results obtained without crustal corrections (Fig. 8.10b). Such a high value of amplitudes of velocity variations is because the synthetic dataset was compiled using the theoretical TT, while the crustal corrections used with the real data reduce the amplitudes of velocity variations (Fig. 8.5). Moreover, we indicate that the effect due to the applied crustal TT corrections is significant (up to 0.5 %) down to about 120 km, while going deeper the effect is negligible (Figs. 8.10b,c). Both results obtained using the synthetic dataset with and without crustal TT corrections (Figs. 8.10b,c) show the reasonably resolved LAB of a ramp-type and deep cratonic lithosphere going down to 350 km in the NE part of the study area.

## 8.4 Distribution of P-wave velocity variations

Using the real data we obtained a distribution of P-wave velocity variations in the upper mantle from 60 km down to 350 km in the SW part of the EEC (Figs. 8.11, 8.12). The results obtained during different inversions are discussed in Chapter 9.

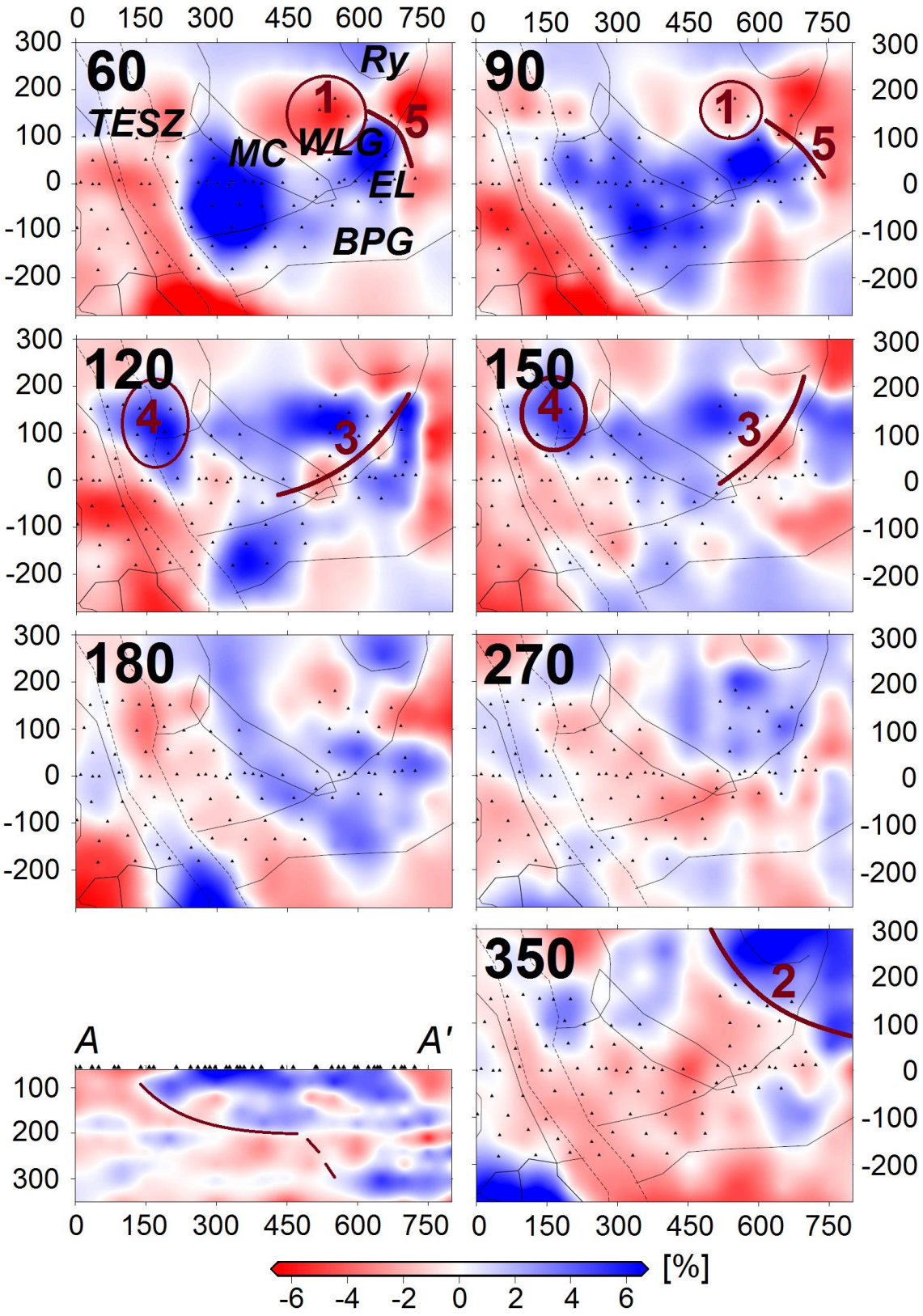
60
TESZ
MC
WLG
Ry
EL
BPG
1
5
90
1
5
120
4
3
150
4
3
180
270
350
2
A
A'
0 150 300 450 600 750
300 200 100 0 -100 -200
-6 -4 -2 0 2 4 6
[%]

Fig. 8.11 P-wave velocity perturbations in horizontal slices at indicated depths (km) and vertical slice along the main transect *AA'* (see Fig. 8.10a) obtained with the real dataset with applied crustal TT corrections. Bluish and reddish areas show, respectively, the higher and lower P-wave velocity values compared to the IASP91 velocity model. Triangles indicate the seismic stations. Solid thin lines on the horizontal slices indicate boundaries of the tectonic units (see Fig. 8.5). Numbered areas on horizontal slices indicate the discussed velocity anomalies: 1 – upper mantle dome; 2 – thick cratonic lithosphere; 3 – possible palaeosubduction boundary between the WLG and the EL; 4 – higher velocity anomaly beneath the northern part of the TESZ; 5 – possible termination of the EL (and maybe the WLG) crustal unit in northern Lithuania. Solid and dashed line on the vertical slice marks the interpreted seismic LAB.

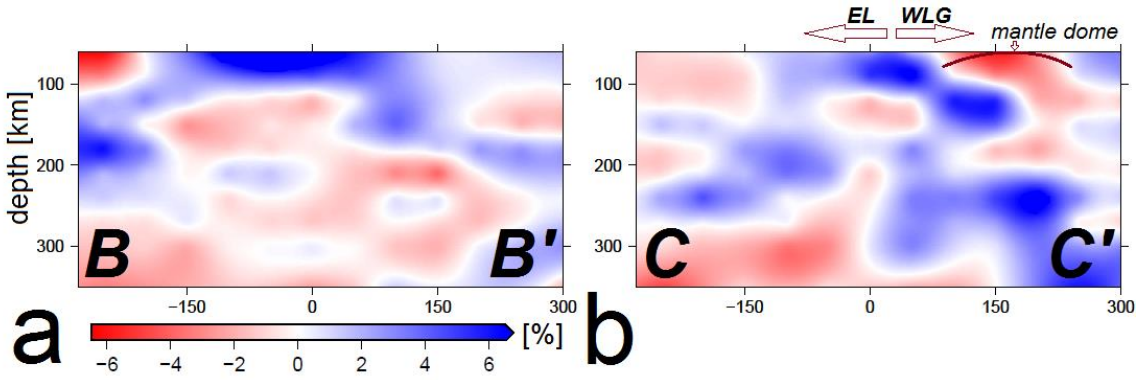


Fig. 8.12 Vertical slices (see Fig. 8.10a) (a) along the *BB'* transect close to the eastern edge of the TESZ, and (b) along the *CC'* transect about 350 km to the NE from the TESZ. Thick lines indicate the possible structures: the palaeosubduction boundary between the EL and the WLG, and the upper mantle dome beneath the WLG.

# Chapter 9

*"Tupi žvirblis kamine su lapine kepure:*

*-Tu, žvirbleli, pulsi, visas susikulsi…"*

*Lietuvių liaudis* [v]

## DISCUSSION

As shown by numerous seismic studies (e.g. Knapmeyer-Endrun et al., 2013b), the LAB in Precambrian cratonic areas is not easily detected by the seismic methods and can be misinterpreted with the so-called Mid-Lithospheric Boundary. The nature of the latter is still not completely understood. However, the seismic LAB can be detected beneath the younger areas and traced across boundaries of the cratons in the passive seismic experiments that sample both cratonic and non-cratonic lithospheres. In our study we used data of such a passive seismic experiment and performed inversions with a compiled dataset of P-wave residuals, and resolved structure of the upper mantle from 60 km for the EEC and from 70 km for the entire study area down to 350 km. The obtained model of P-wave velocity variations can be used to estimate the LAB and the lithosphere thickness around the TESZ.

---

[v] *"The sparrow with a leafy hat is sitting in a chimney:*
*- You sparrow will fall and hurt yourself badly…"*
*Lithuanian Folk*

## 9.1 Amplitudes of velocity variations

In the results we observe the amplitudes of velocity variations up to ±6.5 (Figs. 7.1, 8.11), which are too large to be explained by geological factors only. In teleseismic tomography many factors, such as disturbances in the real data, model parameters, inversion method, etc., have influence to the observed amplitudes of velocity variations.

The effects on amplitudes of velocity variations could be due to:

**Raypaths.** In teleseimic tomography some discrepancies in the results may occur as not full raypaths from source to receiver are inverted, thus, the unknown velocity heterogeneities outside the model are mapped into the final result.

**„Flat-Earth" transformation**. The „flat-Earth" transformation has an effect on the apparent velocities (see Chapter 2.1). The entire study area continues about 1300 km, thus, the "spherical Earth" model should be considered. However, the TELINV code used in our study implements the „flat-Earth" transformation and we did not correct our dataset for the spherical model. As our model extends to the depth of 700 km, the horizontal stretch at the bottom is about 11 %. The majority (70 %) of the angles of incidence in our dataset are between 15 and 20 degrees, thus, neglecting the sphericity would cause about 1.5 % of the observed velocity contrast.

**Damping**. Too high damping value would increase velocity contrast while too low value would result in a reduction of lateral variations. In our study we performed careful analysis in order to estimate the optimal damping values for our datasets, which were used in the inversions.

**Crustal TT corrections.** As precise as possible the crustal TT corrections are essential in order to eliminate the crustal effects from the inversion results. In fact, the crustal effects are never truly eliminated, only reduced, because every crustal model used to estimate the correction has its own limit of precision. In our results we indicate that the crustal TT corrections have effects on the result down to about 120 km, while in the deeper layers their effect diminishes (Figs. 8.10b,c). The

effect due to the applied crustal TT corrections could be about 1 % of the observed velocity contrast. Moreover, the way we implement the crustal TT corrections assumes vertical ray propagation through the crust, which causes shortening of <2 % in the raypaths in the crust, however, this effect on the amplitudes of velocity variations is negligible.

**Anisotropy**. Some studies of anisotropy in Europe (e.g. Babuška et al., 2008; Plomerova et al., 2008; Wüstefeld et al., 2010; Sroda et al., 2014) show the larger anisotropy for Western Europe and the TESZ compared to the EEC. Thus, the effect on the amplitudes of velocity variations due to anisotropy could be more important in the study for the entire area.

Thus, taking into account all the causes listed above we should consider the amplitudes of velocity perturbations not ±6.5 %, but most likely close to about ±3 %.

## 9.2 Structure of lithosphere in the study area

The inversion results with the real dataset show the higher P-wave velocity values compared to the IASP91 velocity model beneath the EEC and the lower ones beneath Western Europe, while the TESZ is resolved as a transitional complex structure with significant velocity perturbations in longitudinal and transversal directions (Fig. 7.1). This general finding coincides with results by Koulakov et al. (2009) who reported on a sharp transition occurring along the TESZ from the negative, characterizing the young tectonic features of Central-Western Europe, to positive beneath the old EEC. Moreover, we indicate that the seismic LAB is more distinct beneath the Phanerozoic part of Europe than beneath its Precambrian part, which coincides with the results by Plomerova et al. (2010) and Knapmeyer-Endrun et al. (2013b).

The previous studies indicate existence of the seismic anisotropy in the upper mantle in the study area (e.g. Babuška et al., 2008; Plomerova et al., 2008;

Wüstefeld et al., 2010; Sroda et al., 2014). The anisotropy may be due to the variations in temperature and rock composition.

To the east of the TESZ a pronounced high velocity area in the upper mantle is observed beneath Poland (Figs. 7.1, 8.11). The high velocity anomaly is observed down to at least 180 km. The velocity perturbations down to about 120 km could up to about 2 to 3 % higher compared to the IASP91 velocity model, but in the deeper layers they are slightly smaller, which indicates most likely effects due to the crustal TT corrections. The depth of the observed higher velocity area coincides well with the results by Wilde-Piórko et al. (2010), Majorowicz et al. (2003) and Koulakov et al. (2009) who report on the positive anomalies in this area down to about 200 km. Legendre et al. (2012) find the highest velocities in the mantle lithosphere of the EEC at about 150 km depth. Moreover, the results obtained with the synthetic dataset (Fig. 8.10b) show that the P-wave velocity values beneath the craton down to 180 km could be about 2 to 3 % higher compared to the IASP91 velocity model.

An important finding is a higher velocity area in the lithospheric mantle from 120 km down to about 150 km in the northern part of the TESZ (northern Poland) (Figs. 7.1, 8.11). This area is spatially coincident with studies of Knapmeyer-Endrun et al. (2013a) who observe an increase in TT of Ps-conversions across the mantle transition zone, which could be caused either by a temperature reduction or an increase in water content in this region. In general, in the upper mantle beneath the northern TESZ the seismic velocity values are close to those beneath the craton, while going to the south the seismic velocity values are smaller.

Further to the NE from the TESZ the high velocity structure goes deeper, and beneath the territory of Lithuania we find the thickest lithosphere of about 300 km or more (Figs. 7.1, 8.11). Due to vertical smearing (Figs. 6.1, 6.7, 6.8, 8.8), which is intrinsic to most of the tomography inversions, the observed higher velocity area could be extended deeper than it really is, however, our result is in a good agreement with other observations. The obtained value of the lithospheric

thickness is about 50 km larger compared to the global tomography results obtained by Artemieva et al. (2006), but coincides well with results obtained from P- and S-wave tomography by Koulakov et al. (2009) who find the P-wave velocities up to 2 % higher extending to at least 300 km beneath Lithuania. Thick lithosphere extending to at least 250 km depth was also found beneath central part of the Fennoscandian Shield (Sandoval et al., 2004), but there was found no clear low-velocity zone that could be attributed to the seismic LAB anywhere within the depth range of 300 km (Bruneton et al., 2004; Geissler et al., 2010; Legendre et al., 2012). Our study does not show the seismic LAB beneath the EEC either. The study of the S-receiver functions by Knapmeyer-Endrun et al. (2013b) indicate a negative conversion that could be related to a velocity decrease at 190 km to 230 km depth which is in agreement with the depth estimates for the cratonic LAB, however, the conversions were observed not in all analyzed seismic stations in the EEC, thus, the authors suggest that the stations might imply spatial variations in the sharpness of the corresponding velocity change. Moreover, there is a good correlation between our results obtained with the real and the synthetic datasets (Figs. 6.9, 8.10), which imply that the lithosphere thickness increases going from the TESZ towards the NE and could be larger than 300 km beneath the EEC.

The velocity model by Wilde-Piórko et al. (2010) propose the higher P-wave velocity values compared to the IASP91 velocity model in the territory of Poland below 250 km. Our results with the real and the synthetic datasets (Fig. 8.10, 8.11) indicate that the seismic velocities at these depths could be 1 to 3 % smaller or equal to the velocity values in the IASP91 velocity model.

Beneath Lithuania at the depth of 120-150 km we find a lower velocity area which follows the MLSZ (Figs. 7.1, 8.11) – the predicted paleosubduction zone between the WLG and the EL (Motuza, 2004; Motuza, 2005; Motuza and Staškus, 2009). Our results (Fig. 7.2b) also indicate a slope of higher velocities dipping to the north which coincides with the model proposed by Motuza and Staškus (2009) that the EL subducted under the WLG. We think that this feature may indicate the

slab of „frozen“ palaeosubduction. The lower velocity area observed below the slab along the predicted palaeosubduction edge could be related to temperature increase.

Beneath Western Lithuania down to 90 km we observe a lower velocity anomaly (Fig. 8.11) which could be possibly related with the upper mantle dome. Motuza et al. (2000) proposed that the mantle dome could have been formed due to delamination processes, because beneath the WLG the heat flow, which is significantly higher compared to that of the surroundings, was observed (Kepezinskas et al., 1996; Rasteniene et al., 1998) and the reflectors in the upper mantle were found (Giese, 1998; Motuza et al. 2000). The observed the reflectors can potentially represent the delaminated slices of the crust which sank into the mantle (e.g. Defant and Kepezhinskas, 2002). The results by Motuza et al. (2000) are based on the DSS results where the reflected seismic waves were observed, but in our study we do not deal with the reflected waves and cannot observe similar reflectors. However, as delamination processes occur locally, the local lower velocity area observed in our results beneath the WLG could be related to the local upper mantle dome. The delamination processes could have been possibly caused by the proposed subduction between the WLG and the EL (discussed previously), as such events may cause delamination (e.g. Oxburgh, 1972; Bird, 1978; Bird, 1979).

The higher velocity values to the west of the TESZ are observed beneath Northern Poland-Germany along the Rheic Suture down to about 90-100 km, while closer to the TESZ the LAB is observed at the depth of about 120 km (Figs. 7.1, 8.11). The result is consistent with results by Knapmeyer-Endrun et al. (2013b) and Wilde-Piorko et al. (2010), who indicated the average seismic lithosphere thickness of about 90 km and associated the upwelling of the LAB beneath Western Europe and the TESZ with partial melting of the upper mantle. Moreover, the studies of Shomali et al. (2006) and Gregersen et al. (2010), which have been focused on the STZ from the TOR data, indicate lithosphere thickness

of about 100 km in Northern Germany. In the NW part of our study area, which is very close to the latter territory, we obtain similar results to those obtained from the TOR data. The depth of the LAB of about 100 km is a common characteristic to the Phanerozoic regions (Plomerova et al., 2002b).

Our results show dominating lower velocity values compared to the IASP91 velocity model to the west of the TESZ (Fig. 7.1) which coincides with results by Koulakov et al. (2009) who reported the negative anomalies up to 4 % for this area. In our results we find a large lower velocity area of about -2 to -3 % compared to the IASP91 velocity model beneath the Bohemian Massif, the Sudetes Mountains and the rift systems in Central Europe from depth of at least 70 km (Figs. 7.1, 7.2a). The lithosphere thinning of 80-90 km beneath the Armorican terrains of the Saxothuringian, the Tepla-Barrandian and the Moldanubian has been reported in studies by Babuška and Plomerova (2001). Karousova et al. (2013) find an extensive low-velocity heterogeneity in the upper mantle beneath the Bohemian Massif, while Koulakov et al. (2009) report on a broad negative zone (−1 to −3 %) beneath the Central Rift System and the Bohemian Massif at the depth from 100 km to 200 km. Moreover, our results indicate a lower velocity anomaly under the Eger Rift, which is on the NW edge of the Bohemian Massif (Fig. 7.1). Although the Eger Rift is relatively small structure, our dataset is sufficient to resolve it, thus, we indicate that the lower velocity area beneath the rift extends down to at least 180 km. This result is in a good agreement with the results obtained by Karousova et al. (2013) who indicate the most distinct low-velocity perturbations along the Eger Rift down to about 200 km, and Koulakov et al. (2009) who observe a low velocity zone (−2 %) in the uppermost mantle between depths of about 80 and 250 km. Plomerova et al. (2007) related the broad low-velocity anomaly beneath the Eger Rift to an uplift of the LAB.

The asthenosphere on the western edge and on the eastern edge of the TESZ is at the depth of about 150 km and 180 km, respectively. Moreover, the structure of the TESZ varies significantly going from NW to SE (Fig. 7.1). In the studies of

Legendre et al. (2012) it is found that the lithospheric mantle beneath the TESZ shows moderately high velocities and is of intermediate character between that of the cratonic lithosphere and the thin lithosphere of Central Europe. The studies carried out around the TESZ indicated a sharp discontinuity along the TESZ, but provided no strong evidence on a shape of the LAB beneath it due to lack of resolution (discussed in Knapmeyer-Endrun et al. (2013a)). In our study we use a dense network of the seismic stations (Fig. 4.1), thus, we are able to resolve the shape of the LAB with higher precision. In the results (Fig. 7.1) we indicate that in the northern part of the study area the higher velocity anomaly (which is associated with the seismic LAB) is observed deeper going to the NE direction, which shows a ramp-shape of the LAB. An angle of deepening of the LAB is about 30 degrees (Fig. 7.1). In the northern part of the TESZ we do not recognize any separate structures or clear contact which could be related to the different tectonic settings of Phanerozoic and Proterozoic Europe (because we study the lithosphere while the contact is more significant in the crust), but further to the south we may refer to a sharp and steep contact slightly dipping to the NE direction on the eastern edge of the TESZ (Fig. 7.1). In our „geological“ synthetic model we introduced and reasonably resolved the ramp type LAB dipping to the NE direction (Fig. 6.9a,b) which is somehow similar to the results obtained with the real data (Fig. 7.1). Gregersen et al. (2010) compared results of different studies performed using data of the TOR project and concluded that the transition between the two tectonic settings on both sides of the STZ, is sharp and steep with a weak tendency to the NE slope. Going further to the south the LAB is shallower and its shape changes most probably due to younger tectonic processes in the region (Fig. 7.1).

## 9.3 Traces of crustal units in the SW part of the EEC

In the SW part of the EEC at the depth of 60 km (Figs. 8.11, 8.12) we indicate some correlation between the observed amplitudes of velocity perturbations and the Moho depth. The larger positive amplitudes are significant beneath Poland and Eastern Lithuania where the Moho boundary is deeper, while the negative amplitudes are observed beneath the TESZ and Western Lithuania where the crust is thinner. This could be related either to the imperfect crustal TT corrections used or with different geological conditions.

Beneath Lithuania we may infer a possibly resolved boundary between two crustal units – the EL and the WLG – which is significant at the depths of 120-150 km, which is discussed previously in Chapter 9.2.

In Northern Lithuania we observe a significant transition between areas of positive and negative amplitudes of velocity variations down to 90 km (Fig. 8.11). We indicate that this area of strong contrast marks a possible termination of the EL and the WLG by Svecofennian orogenic belt extending to the SE-NW direction, and shows that these crustal units do not continue into the territory of Latvia. Bogdanova et al. (2001) (Fig. 1.3) show that the EL and the BPG crustal units terminate in Northern Lithuania and Northern Belarus, respectively, but the WLG continues to Latvia where it contains the Riga batholith of AMCG-type. A number of studies (e.g. Bruneton et al., 2004; Beller et al., 2013) showed that the upper mantle beneath the anorogenic granitoid massifs inside the cratonic crust is different from that of the surrounding cratonic mantle. In our results we may relate the possible effects from the batholiths with the observed negative velocity perturbations, however, the resolution is quite poor in this part of the study area (Fig. 8.6a), thus, we cannot assert its effects on the results. There are no stations in Belarus, thus, we cannot interpret the BPG termination there.

# Chapter 10

*"Žarsto baltą smėlį Širvinta nurimus..."*

*Salomėja Nėris* [VI]

## INTERPRETATION AND CONCLUSIONS

From the results discussed before we indicate that the structure of the upper mantle is complex, however, development of the tectonic model is not a scope of our study. Thus, we compiled a possible model of the velocity perturbations in the upper mantle (Fig. 10.1). The model extends from the depth of 70 km to 350 km. As teleseismic tomography inversion depends on many factors the interpretation of its results must be very careful. Thus, the sketch of our tectonic model is very robust and shows only large-scale resolved structures. In the model we use only three colors: blue color is associated with the cratonic lithosphere, while grey and pink colors indicate similar and lower values of the seismic velocities compared to the IASP91 velocity model. Our model demonstrates the shape of the LAB and contact between the EEC and Western Europe. In our model large emphasis lies upon the shape and depth of the seismic LAB and the lithosphere thickness, as well as on some distinguished lower velocity anomalies in the study area. We

[VI] *"The eased Širvinta spreads loose its white sand..." Salomėja Nėris*

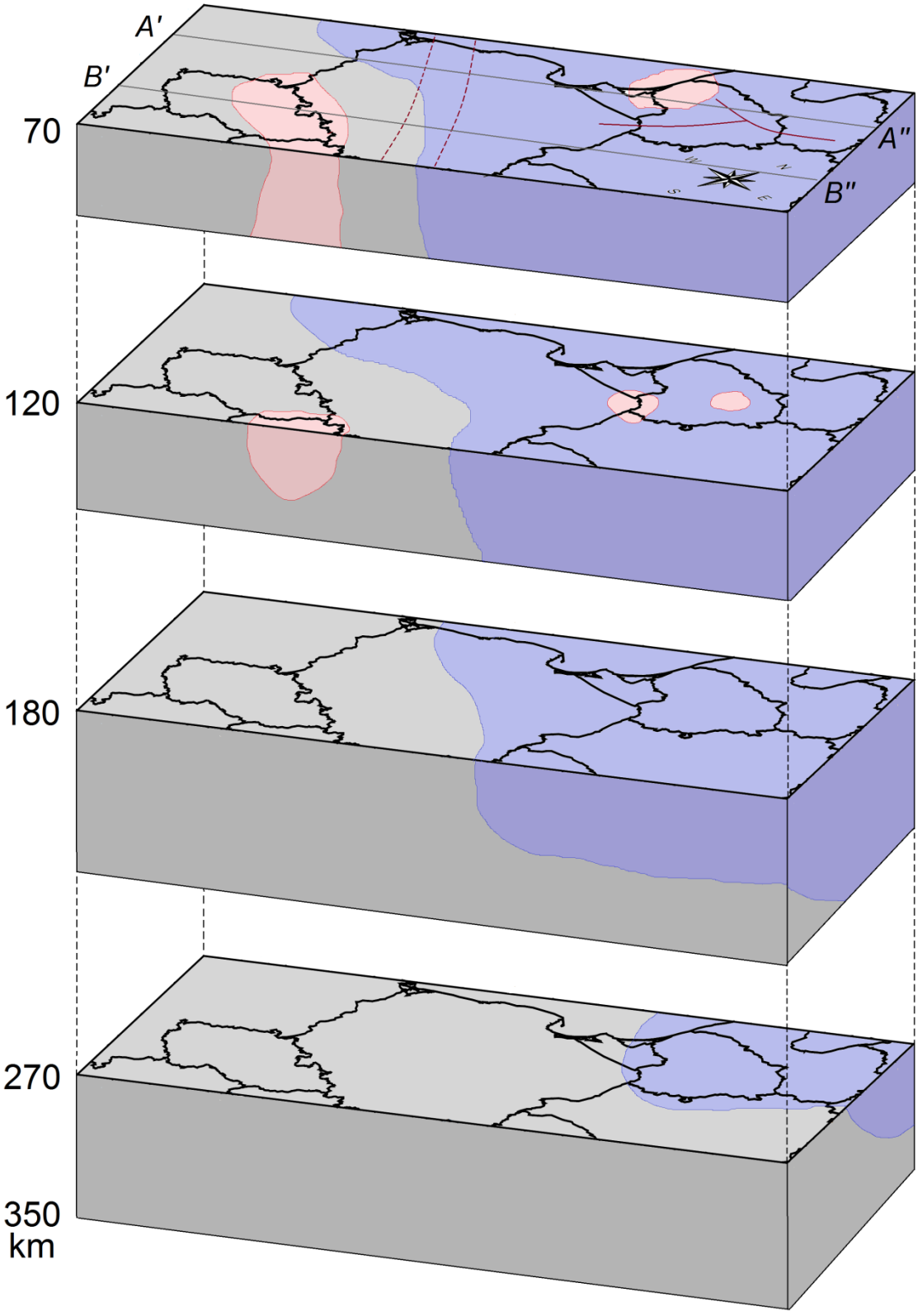
A′
B′
A″
B″
70
120
180
270
350
km

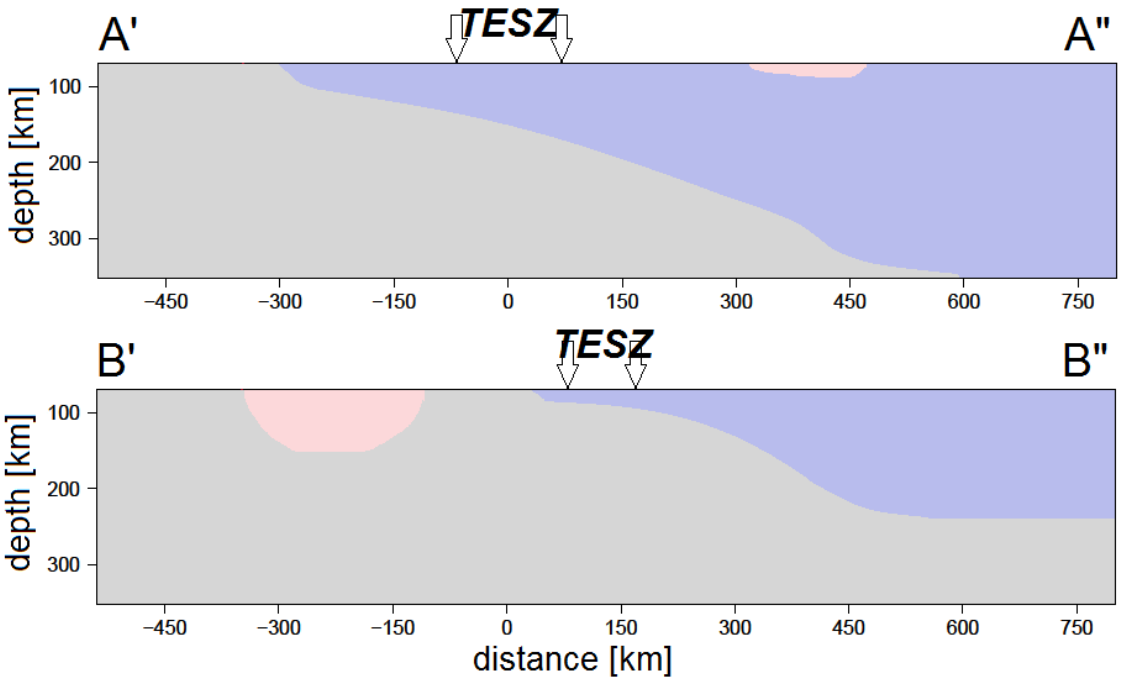


Fig. 10.1 Sketch of interpreted model of velocity variation in the upper mantle in the study area from 70 km to 350 km. Solid black lines – political boundaries; dashed brown lines – the TESZ; solid brown lines – possibly resolved crustal boundaries; solid grey lines show depicted vertical transects *A'A"* and *B'B"*. Colors: grey – areas with seismic velocities close or equal to those in the IASP91 velocity model; pink – areas of lower seismic velocities compared to the IASP91 velocity model; light blue – cratonic lithosphere.

assume that going deeper the values of seismic velocities are close to those in the IASP91 velocity model.

The aim of the interpretation and sketched model is to generalize the results obtained during the teleseismic tomography study using data of the stations deployed in Western-Central and Eastern Europe during the period of the PASSEQ 2006-2008 project. The obtained model demonstrates the shape of the LAB and contact between the EEC and Western Europe, and we hope that it will

help to improve understanding of the structure of the upper mantle beneath the study area and will provide some deeper understanding about evolution of the tectonic structures, and will be useful for developing research in the future.

**General conclusions:**

- The seismic velocity values in the study area vary up to about ±3 % compared to the IASP91 velocity model.

- The higher velocity values compared to the IASP91 velocity model to the east of the TESZ correspond to the older EEC and the lower ones to the west of the TESZ correspond to younger Central-Western Europe. The TESZ is a well expressed tectonic boundary with complex structure and intermediate characteristics between those of the EEC and Western Europe.

- The seismic LAB is more distinct beneath the Phanerozoic part of Europe than beneath its Precambrian part. The lower velocity values from 70 km are observed under the Bohemian Massif, the Sudetes Mountains and the Eger Rift, while further north beneath the Variscides the depth of the LAB is about 100-120 km. Our study does not show the seismic LAB beneath the EEC, but beneath Lithuania we find the thickest lithosphere of about 300 km or more. In the TESZ the asthenosphere is at a depth of 150-180 km which is an intermediate value between that of the EEC and Western Europe.

- In the northern part of the TESZ the upper mantle is more of cratonic type. We infer that the seismic LAB in the northern part of the study area is of a ramp type dipping to the NE direction at an angle of about 30 degrees.

Under the nothern part of the TESZ we do not recognize any contact between the Phanerozoic and the Proterozoic parts of Europe, but further to the south we may refer to a sharp and steep contact slightly dipping to the NE direction on the eastern edge of the TESZ. Going to the south the shape of the LAB beneath the TESZ is changing and its depth is shallower most likely due to younger tectonic processes.

- The lower velocity area beneath Western Lithuania may be possibly related to the upper mantle dome. We also find an indication of „frozen“ palaeosubduction boundary between the EL and the WLG beneath Lithuania. Subduction processes may have possibly caused delamination and formation of the upper mantle dome above the subducting slab.

- From the results we imply that the EL and maybe the WLG crustal units terminate in Northern Lithuania, and do not continue to the territory of Latvia.

# AKNOWLEDGEMENTS

My study is a part of the PASSEQ 2006-2008 project (Wilde-Piórko et al., 2008).
The study was partly funded by NordQuake project.
The cutted one-event files used for data analysis were created in Institute of Geophysics Polish Academy of Sciences, Warsaw, Poland. Many thanks to someone who produced them!
Figures were produced using the GMT (Wessel and Smith, 1991), Microsoft Exel and Microsoft Paint software.
For the seismological data review, picking of the P-wave arrivals and calculations of the theoretical P-wave arrivals we used SH program package (and its SHM version as well) (http://www.seismic-handler.org/).

---

I am very grateful to my Prof. Dr. Gediminas Motuza (Department of Geology and Mineralogy, Faculty of Natural Sciences, Vilnius University, Vilnius, Lithuania), who in practice is my unofficial supervisor. I thank Him for introducing me to the right people, for sincere support, advices and help during my studies, and taking care of the big part of the bureaucracy while organizing the defense of my theses (as I was not a "very permanent" resident in Lithuania any more…). I admire His enthusiasm and curiosity about exploring new things related not only with geology, but also with science in general, and His wide point of view to various aspects.
I appreciate the support and guidance of my official supervisor Dr. Elena Kozlovskaya (Sodankylä Geophysical Observatory / Oulu Unit, University of Oulu, Oulu, Finland). She has been guiding me through the fields of seismology since my Master degree and provided to me a great deal of knowledge and insight into it. Her precise, consistent and fine way of "doing the science" always encouraged me to do my work better and better. I am also thankful for introducing me to other colleagues and expanding my list of important contacts.

Many thanks to Prof. Dr. Mariusz Majdański (Institute of Geophysics Polish Academy of Sciences, Warsaw, Poland) for helping me with a lot of technical issues, like Linux scripts, compilation of the crustal TT corrections, for sincere support and advices while writing and reviewing our papers. I am grateful for His patience while explaining me the things with which I was not familiar before. I very much appreciate His help and company during my visits in Oulu, Finland, for a wonderful phrase „Ilma, tea break?!" during the long working hours there, for introducing to me the "almighty" **awk** command (in Linux) and the optimistic point of view.

Thanks to Dr. Peter H. Voss (Geological Survey of Denmark and Greenland – GEUS, Copenhagen, Denmark) for help with the TELINV code, for preparations of the dataset used in our study, for His help during the paper writing and some constructive and useful advises.

Special thanks to Hanna Silvennoinen (the PhD student in Sodankylä Geophysical Observatory/Oulu Unit, University of Oulu, Oulu, Finland) for helping me with the TELINV code, especially for providing a GMT script which plots the smoothed tomography maps, for useful discussions and good company during my visits in Oulu, Finland. I am grateful (and always will be) for Her good will picking me up from the airport around midnight, and generosity providing me with some household things and a remarkable white cup with a black dog among them.

I appreciate a good will of the Lithuanian Geological Survey – my previous (and the first!) employee – for a possibility to adjust my work and my studies, for sending me to some useful conferences, training courses and meetings.

I thank NORSAR – my current employee – for understanding the importance of my studies and giving me some time to finish it. I thank my colleagues very much for sincere support and interest to my activities.

I appreciate a very useful discussion with Prof. Dr. Ulrich Achauer from the University of Strasbourg at my poster presentation during the EGU conference in

Vienna (Austria) in 2014. It developed my understanding of the tomography results and encouraged to look deeper and more careful into the technical details of the process of inversion and interpretation of the results.

I thank to the all the reviewers and referees of the papers related to my theses, because their comments and suggestions helped to improve the quality, precision and language of our papers, as well as the quality of my theses.

I am grateful to my family and some friends for immeasurable versatile support during my studies. I apologize them for being somehow unsocial for the last few months.

---

I have always regarded myself as a physicist since I got the diploma of Bachelor in Physics, even after I have started to work in the field of seismology about 6 years ago. But after my theses I think I should change my attitude and understanding of myself and obtain my new status of seismologist.

# REFERENCES

Ahern, T., Casey, R., Barnes, D., Benson, R., and Knight, T.: SEED Reference Manual – Standard for the Exchange of Earthquake Data. IRIS, pp 244, 2006.

Aki, K., A. Christoffersson, and Husebye, E. S.: Determination of the three-dimensional seismic structure of the lithosphere, J. Geophys. Res., 82, 277-296, 1977.

Aksamentova, N. V., and Naydenkov, I. V.: Explanatory note of the geological map of the crystalline basement of Belorussia and the Adjoining Areas. Academy of Sciences of the Belorussian SSR, Minsk, 1991.

Arlitt, R.: Teleseismic body wave tomography across the Trans-European Suture Zone between Sweden and Denmark. PhD theses, ETH, Swiss Federal Institute of Technology Zürich, Swiss, 1999.

Artemieva, I. M., Thybo, H., and Kaban, M. K.: Deep Europe today: Geophysical synthesis of the upper mantle structure and lithospheric processes over 3.5 Ga. In: Gee, D., and Stephenson, R. (eds.), European Lithosphere Dynamics. Geological Society London, Special Publication, 32, 11-41, 2006.

BABEL Working Group: Deep seimic reflection/refraction interpretation of crustal structure along BABEL profiles A and B in the southern Baltic Sea. Geophys. J. Int., 112, 325-343, 1993.

Babuška V., and Plomerova J.: Subcrustal Lithosphere Around the Saxothuringian-Moldanubian Suture Zone – a model derived from anisotropy of seismic wave velocities. Tectonophysics, 332, 185-199, 2001.

Babuška, V., Plomerova, J., and Fischer, T.: Intraplate Seismicity in the Western Bohemian Massif (Central Europe): A possible correlation with a paleoplate junction. J. Geophysics, 44, 149–159, 2007.

Babuška, V., Plomerova, J., and Vecsey. L.: Mantle fabric of western Bohemian Massif (central Europe) constrained by 3D seismic P and S anisotropy. Tectonophysics, 462, 1–4, 149–163, 2008.

Banka, D., Pharao, T. C., Williamson, J. P., and the TESZ Project Potential Field Core Group: Potential field imaging of Paleozoic orogenic structure in northern and central Europe. Tectonophysics, 360, 23–45, 2002.

Belka, Z., Ahrendt, H., Franke, W., Wemmer, K.: The Baltica-Gondwana suture in central Europe: evidence from K–Ar ages of detrital muscovites and biogeographical data. In: Franke, W., Haak, V., Oncken, O., Tanner, D. (Eds.), Orogenic Processes: Quantification and Modelling of the Variscan Belt. Geological Society, London, 87–102, 2000.

Beller, S., Kozlovskaya, E., Achauer, U., and Tiberi, Ch.: Joint inversion of teleseismic and gravity data beneath the Fennoscandian Shield. EGU General Assembly 2013, Geophysical Research Abstracts, 15, EGU 2013-4771-2, 2013.

Bird, P.: Initiation of intracontinental subduction in himalaya. J. Geophys. Res., 83, 4975-4987, 1978.

Bird, P.: Continental delamination and the Colorado Plateau. J. Geophys. Res., 84, 7561-7571, 1979.

Bogdanova, S. V., Pashkevich, I. K., Gorbatschev, R., and Orlyuk, M. I.: Riphean rifting and major Palaeoproterozoic crustal boundaries in the basement of the East European Craton: geology and geophysics. Tectonophysics, 268, 1-21, 1996.

Bogdanova, S. V.: The Palaeoproterozoic terrane pattern in the western part of the East European Craton, Seventh EUROBRIDGE Workshop. Polish Geological Institute, Suwalki, Poland, 11-13, 1999.

Bogdanova, S. V., Gorbatschev, R., Stephenson, R. A., and Guterch A. (ed.): EUROBRIDGE: Palaeoproterozoic accretion of Fennoscandia and Sarmatia. Tectonophysics, 339, 1–2 , 2001.

Bogdanova, S., Gorbatschev, R., Grad, M., Janik, T., Guterch, A., Kozlovskaya, E., Motuza, G., Skridlaite, G., Starostenko, V., Taran, L., the EUROBRIDGE and POLONAISE Working Groups: EUROBRIDGE: new insight into the geodynamic evolution of the East European Craton. In: Gee, D.G., Stephenson, R.A. (Eds.), European Lithospheric Dynamics. Memoirs Number 32. Geological Society, London, 599–625, 2006.

Bormann, P (ed.): New Manual of Seismological Observatory Practice (NMSOP). GeoForschungsZentrum Potsdam, vol. 1, 2002.

Bruneton, M., Pedersen, H. A., Farra, V., Arndt, N. T., Vacher, P., Achauer, U., Alinaghi, A., Ansorge, J., Bock, G., Friederich,W., Grad, M., Guterch, A., Heikkinen, P., Hjelt, S.-E., Hyvönen, T. L., Ikonen, J.-P., Kissling, E., Komminaho, K., Korja, A., Kozlovskaya, E., Nevsky, M. V., Paulssen, H., Pavlenkova, N. I., Plomerová, J., Raita, T., Riznichenko, O. Y., Roberts, R. G., Sandoval, S., Sanina, I. A., Sharov, N. V., Shomali, Z. H., Tiikkainen, J., Wielandt, E., Wilegalla, K., Yliniemi, J., and Yurov, Y. G.: Complex lithospheric structure under the central Baltic Shield from surface wave tomography. Journal of Geophysical Research, vol. 109, B10303, doi:10.1029/2003JB002947, 2004.

Claesson, S., Bibikova, E. V., Bogdanova, S. V., and Gorbatschev, R.: Isotopic evidence of Plaeoproterozoic accretion in the basement of the East European Craton. Tectonophysics, 339, 1-18, 2001.

Cotte, N., Pedersen, H. A., and TOR Working Group: Sharp contrast in lithospheric structure across the Sorgenfrei–Tornquist zone as inferred by Rayleigh wave analysis of TOR1 project data. Tectonophysics, 360, 75–88, 2002.

Czuba, W., Grad, M., Luosto, U., Motuza, G., Nasedkin, V., and POLONAISE P5 Working Group: Crustal structure of the East European craton along the POLONAISE'97 P5 profile. Acta Geoph. Pol., 49 (2), 145–168, 2001.

Dadlez, R., Grad, M., and Guterch, A.: Crustal structure below the Polish Basin: Is it composed of proximal terranes derived from Baltica? Tectonophysics, 411, 111– 128, 2005.

Defant, M. J., and Kepezhinskas, P.: Adakites: some variations on a theme. Acta Petrol. Sinica, 18, 2, 129-142, 2002.

Dörr W., Belka Z., Marheine D., Schastok J., Valverde Vaquero P., and Wiszniewska J.: U–Pb and Ar–Ar geochronology of anorogenic granite magmatism of the Mazury complex NE Poland. In Precambrian Research, T. Rämo (ed.), Special issue, 119, 101–102, 2002.

Eaton, D. W., Darbyshire, F., Evans, R. L., Grütter, H., Jones, A. G., and Yuan, X.: The elusive lithosphere–asthenosphere boundary (LAB) beneath cratons. Lithos., 109, 1-22, 2009.

EUROBRIDGE SeismicWorking Group: Seismic velocity structure across the Fennoscandia-Sarmatia suture of the East European Craton beneath the EUROBRIDGE profile through Lithuania and Belarus. Tectonophysics, 314 (1–3), 193–217, 1999.

EUROBRIDGE Working Group, and EUROBRIDGE'95: Deep seismic profiling within the East European Craton. Tectonophysics, 339, 153-175, 2001.

Evans, J. R., and Achauer, U.: Teleseismic velocity tomography using the ACH method: theory and application to continental-scale studies. In Iyer, H. M., and Hirahara, K. (eds.), Seismic tomography: theory and practice. London, Chapman & Hall, 319-360, 1993.

Evans, J. R., Eberhart-Phillips, D., and Thurber, C. H: User's manual for SIMULPS12 for imaging $v_p$ and $v_p/v_s$; a derivative of the "Thurber" tomographic

inversion SIMUL3 for local earthquakes and explosions. U.S. Geological Survey, Open-file Report USGS-OFR-94-431, 1994.

Franke, W., and Zelazniewicz, A.: The Eastern Termination of the Variscides: Terrane Correlation and Kinematic Evolution in Orogenic processes: quantification and modelling in the Variscan Belt. Special Publications, 179, 63-85, edited by Franke W., Haak W., Oncken O., D. Tanner, Geological Society, London, 2000.

Garetskii, R. G., Boborykin, A. M., Bogino, V. A., German, V. A., Veres, S. A., Klushin, S. V., and Shafaruk, V. G.: Deep seismic sounding on the territory of Belorussia. Geophysical Journal International, 8, 439-448, 1990.

Gee, D. G., and Stephenson, R. A.: The European lithosphere: an introduction. In Gee, D. G., and Stephenson, R. A. (eds.), European Lithophere Dynamics. Geol. Soc. Lond. Mem., 32 (1-9), 2006.

Geissler, W. H., Sodoudi, F., and Kind, R.: Thickness of the central and eastern European lithosphere as seen by *S* receiver functions. Geophys. J. Int., 181 (2), 604-634, doi: 10.1111/j.1365-246X.2010.04548.x, 2010.

Giese, R.: Eine zweidimensionale Interpretation der Geschwindigkeitenstruktur der Erdkruste des sudwestlichen Teils der osteuropaischen Platform (Project Eurobridge): Scientific Technical Report STR98/16. Potsdam. 190, 1998.

Grad, M., and Tripolsky, A.: Crustal structure from P and S seismic waves and petrological model of the Ukrainian shield. Tectonophysics, 250, 89-112, 1995.

Grad, M., Keller, G. R., Thybo, H., Guterch, A., and POLONAISE Working Group: Lower lithospheric structure beneath the Trans-European Suture Zone from POLONAISE'97 seismic profiles. Tectonophysics, 360 (1–4), 153–168, 2002.

Grad, M., Janik, T., Guterch, A., Sroda, P., Czuba, W., EUROBRIDGE'94–97, POLONAISE'97 and CELEBRATION 2000 Seismic Working Groups:

Lithospheric structure of the western part of the East European Craton investigated by deep seismic profiles. Geological Quarterly, 50 (1), 9–22, 2006.

Gregersen, S., Pedersen, L. B., Roberts, R. G., Shomali, H., Berthelsen, A., Thybo, H., Mosegaard, K., Pedersen, T., Voss, P., Kind, R., Bock, G., Gossler, J., Wylegala, K., Rabbel, W., Woelbern, I., Budweg, M., Busche, H., Korn, M., Hock, S., Guterch, A., Grad, M., Wilde-Piorko, M., Zuchniak, M., Plomerova, J., Ansorge, J., Kissling, E., Arlitt, R., Waldhauser, F., Ziegler, P., Achauer, U., Pedersen, H., Cotte, N., Paulssen, H., and Engdahl, E. R.: Important findings expected from Europe's largest seismic array. Eos, Transactions American Geophysical Union, 80 (1), 1–6, DOI:10.1029/99EO00001, 1999.

Gregersen, S., Voss, P., Nielsen, L. V., Achauer, U., Busche, H., Rabbel, W., and Shomali, Z. H.: Uniqueness of modeling results from teleseismic P wave tomography in Project TOR. Tectonophysics, 481, 99-107, doi: 10.1016/j.tecto.2009.01.020, 2010.

Griffin, W. L., O'Reilly, S. Y., Abe, N., Aulbach, S., Davies, R. M., Pearson N. J., Doyle, B. J., and Kivi, K.: The origin and evolution of Archean lithospheric mantle, Precambrian Research, 127, 19–41, 2003.

Guterch, A., and Grad, M.: Seismic structure of the Earth's crust between Precambrian and Variscan Europe in Poland. Publs. Inst. Geophys. Pot. Acad. SC., M-18 (273), 67-73, 1996.

Guterch, A., Grad, M., Thybo, H., Keller, G.R., and the POLONAISE Working Group: POLONAISE'97—an international seismic experiment between Precambrian and Variscan Europe in Poland. Tectonophysics 314, 101–121, 1999.

Guterch, A., Grad, M., Keller, G. R., Posgay, K., Vozar, J., Spicak, A., Bruckl, E., Hajnal, Z., Thybo, H., Selvi, O., and CELEBRATION 2000 Experiment Team: CELEBRATION 2000 seismic experiment. Stud. Geophys. Geod., 47, 659-669, 2003.

Guterch, A., Grad, M., Keller, G. R., and POLONAISE'97, CELEBRATION 2000, ALP 2002, SUDETES 2003 Working Groups: Huge contrasts of the lithospheric structure revealed by new generation seismic experiments in Central Europe. Przegld Geologiczny, 52 (8/2), 2004.

Hansen, T. M., and Balling, N.: Upper-mantle reflectors: modeling of seismic wavefield characteristics and tectonic implications. Geophys. J. Int, 157, 664-682, 2004.

Jones, A. G., Plomerova, J., Korja, T., Sodoudi, F., and Spakman, W.: Europe from the bottom up: A statistical examination of the central and northern European lithosphere-asthenosphere boundary from comparing seismological and electromagnetic observations. Lithos, 120, 14-29, 2010.

Karousova, H., Plomerova, J., and Babuska, V.: Upper-mantle structure beneath the southern Bohemian Massif and its surroundings imaged by high-resolution tomography. Geophys. J. Int., doi: 10.1093/gji/ggt159, 2013.

Kennett, B. L. N., and Engdahl, E. R.: Traveltimes for global earthquake location and phase identification. Geophys. J. Int., 105, 429-465, 1991.

Kepezinskas, K., Rasteniene, V., and Suveizdis, P.: The Western Lithuanian geothermal anomaly. Institute of Geology, Vilnius, pp 68, 1996.

Knapmeyer-Endrun, B., Krüger, F., Legendre, C. P., Geissler, W. H., and PASSEQ Working Group: Tracing the influence of the Trans-European Suture Zone into the mantle transition zone. Earth and Planetary Science Letters, 363, 73-87, 2013a.

Knapmeyer-Endrun, B., Krüger, and PASSEQ Working Group: Imaging the lithosphere-asthenosphere boundary across the transition from Phanerozoic Europe to the East-European Craton with S-receiver functions. Geophysical Research Abstracts, 15, EGU2013-6972, 2013b.

Koch, M.: A numerical study on the determination of the 3-D structure of the lithosphere by linear and non-linear inversion of teleseismic travel times, Geophys, J. R. Astron. Soc., 80, 73-93, 1985.

Korja, T.: How is the European Lithosphere Imaged by Magnetotellurics? Surv. Geophys. 28, 239–272, doi: 10.1007/s10712-007-9024-9, 2007.

Kostyuchenko, S. L., Egorkin, A. V., and Solodilov, L. N.:Structure and genetic mechanisms of the Precambrian rifts of the East European Platform in Russia by integrated study of seismic, gravity, and magnetic data. Tectonophysics, 313, 9-28, 1999.

Koulakov, I., Kaban, M. K., Tesauro M., and Cloetingh S.: P- and S-velocity anomalies in the upper mantle beneath Europe from tomographic inversion of ISC data, Geophys. J. Int., 179, 345–366, 2009.

Legendre, C. P., Meier, T., Lebedev, S., Friederich, W., and Viereck-Götte, L.: A shear wave velocity model of the European upper mantle from automated inversion of seismic shear and surface waveforms. Geophys. J. Int., 191, 282–304, doi: 10.1111/j.1365-246X.2012.05613.x, 2012.

Majdański, M.: The structure of the crust in TESZ area by kriging interpolation. Acta Geophysica, vol. 60, issue 1, pp 59-75, doi:10.2478/s11600-011-0058-5, 2012.

Majorowicz, J. A., Čermak, V., Šafanda, J., Krzywiec, P.,Wróblewska, M., Guterch, A., and Grad, M.: Heat flow models across the Trans-European Suture Zone in the area of the POLONAISE'97 seismic experiment. Phys. Chem. Earth 28, 375–391, 2003.

Malinowski, M., Grad, M., Guterch, A., and CELEBRATION 2000 Working Group: Three-dimensional seismic modelling of the crustal structure between East European Craton and the Carpathians in SE Poland based on CELEBRATION

2000 data. Geophys. J. Int., 173, 546–565, doi: 10.1111/j.1365-246X.2008.03742.x, 2008.

Matzel, E., and Grand, S. P.: The anisotropic structure of the East European platform. Journal of Geophysical Research, 109, B01302, DOI: 10.1029/2001JB000623, 2004.

McKenzie, D. P.: Some remarks on the heat flow and gravity anomalies. Journal of Geophysical Research, 72, 6261-6273, 1967.

Menke, W.: Geophysical data analysis: Discrete inverse theory. Academic Press, Inc., Orlando, Fl., pp. 260, 1984.

Motuza, G., Nasedkin, V., Jacyna, J., and Korabliova, L.: The structure of the upper part of the lithosphere along the Eurobridge profile in Lithuania. Lithuanian Geological Survey Annual Report, Vilnius, 54-56, 2000.

Motuza, G.: Žemės plutos bei kristalinio pamato sandaros ir sudėties raida. In: Baltrūnas, V. (ed.), Lietuvos žemės gelmių raida ir ištekliai, UAB Petro ofsetas, Vilnius, 11-40, 2004.

Motuza, G.: Structure and formation of the crystalline crust in Lithuania. Mineralogical Society of Poland, Special Papers, 26, 67-79, 2005.

Motuza, G., and Staškus, V.: Seniausios Lietuvos uolienos. Geologijos akiračiai, ISSN 1392-0006, 3-4, 41-47, 2009.

Nolet, G., Zielhuis, A.: Low S velocities under the Tornquist–Teisseyre zone: evidence from water injection into the transition zone by subduction. J. Geophys. Res. 99, 15813–15820, 1994.

Oliver, J., and Murphy, L.: WWNSS: seismology's global network of observing stations. Science, 174, 254-261, 1971.

Oxburgh, E. R.: Flake tectonics and continental collision. Nature, 239, 202–204, 1972.

Pharaoh, T.C., England, R.W., Verniers. J. and Zelainiewicz, A.: Introduction: geological and geophysical studies in the Tram-European Suture Zone. Geol. Mug., 134 (5), pp. 585-590, 1997.

Pharaoh, T. C.: Paleozoic terranes and their lithospheric boundaries within the Trans-European Suture Zone (TESZ): a review. Tectonophysics 314, 17–41, 1999.

Pharaoh, T. C., and TESZ Project Core Group: EUROPROBE Trans-European Suture Zone project. British Geological Survey, EUROPROBE News 12, June 2000, 2000.

Plomerova J., Babuška V., Sileny J., Horalek J.: Seismic anisotropy and velocity variations in the mantle beneath the Saxothuringicum-Moldanubicum con- tact in central Europe. In Plomerova, J., Liebermann, R. C, and Babuška, V. (eds.), Geodynamics of Lithosphère and Earh's Mantle: Seismic Anisotropy as a Recird of the Past and Present Dynamic Processes. Pure and Appi. Geoph., Special issue, 151, 1998

Plomerova, J., and Babuska, V.: Seismic anisotropy of the lithosphere around the Trans-European suture zone (TESZ) based on teleseismic body-wave data of the TOR experiment. Tectonophysics, 360, 89-114, 2002a.

Plomerova, J., Kouba, D., Babuska, V.: Mapping the lithosphere-asthenosphere boundary (LAB) through changes in surface-wave anisotropy. Tectonophysics, 358, 175-185, 2002b.

Plomerova, J., Achauer, U., Babuska, V., Vecsey, L., and BOHEMA Working Group: Upper mantle beneath the Eger Rift (Central Europe): plume or asthenosphere upwelling? Geophys. J. Int., 169 (2), 675–682, DOI: 10.1111/j.1365-246X.2007.03361.x, 2007.

Plomerova, J., Babuska, V., Kozlovskaya, E., Vecsey, L., Hyvonen, L. T.: Seismic anisotropy - a key to resolve fabrics of mantle lithosphere of Fennoscandia. Tectonophysics, 462, 125-136, doi: 10.1016/j.tecto.2008.03.018, 2008.

Plomerova, J., Babuska, V.: Long memory of mantle lithosphere fabric – European LAB constrained from seismic anisotropy. Lithos, 120, 131-143, 10.1016/j.lithos.2010.01.008, 2010.

Rasteniene, V., Sliaupa, S., and Skridlaite, G.: The geothermal field of Lithuania. Proceedings of the international conference "The Earth's Thermal Field and Related Research Methods", Moscow, 230-233, 1998.

Rämö O. T., Huhma H., and Kirs J.: Radiogenic Isotopes of the Estonian and Latvian Rapakivi Granite Suite: New Data from the Concealed Precambrian of the East European Craton. Precambrian Research, 79, 209–226, 1996.

Sandoval Castano, S.: The Lithosphere-Asthenosphere System beneath Fennoscandia (Baltic Shield) by Body-wave Tomography. A dissertation submitted to the Swiss Federal Institute of Technology Zurich, 2002.

Sandoval, S., E. Kissling, and Ansorge, J.:High-resolution body wave tomography beneath the SVEKALAPKO array—II. Anomalous upper mantle structure beneath the central Baltic Shield. Geophys. J. Int., 157, 200–214, 2004.

Scherbaum, F.: Of poles and zeros, Fundamentals of digital seismology. Kluwer Academic, 1996.

Shomali, Z. H., Roberts, R. G., Pedersen, L. B., and the TOR Working Group: Lithospheric structure of the Tornquist Zone resolved by nonlinear P and S teleseismic tomography along the TOR array. Tectonophysics, 416, 133-149, 2006.

Skobelev, V. M.: Petrocheminstry and geochronology of the Precambrian formations of the north-western region of the Ukrainian Shield. Naukova Durnka, Kiev, 140, 1987.

Skridlaite, G., and Motuza, G.: Precambrian domains in Lithuania: evidence of terrane tectonics. Tectonophysics, 339, 113-133, 2001.

Spetzler, J., and Snieder, R.: The Fresnel volume and transmitted waves. Geophysics, 69, 653-663, 2004.

Sroda, P., and the POLCRUST and PASSEQ Working Groups: Seismic anisotropy and deformations of the TESZ lithosphere near the East European Craton margin in SE Poland at various scales and depths. EGU General Assembly 2014, Geophysical Research Abstracts, Vol. 16, EGU2014-6463-1, 2014.

Steck, L. K., and Prothero, W. A. J.: A 3-D raytracer for teleseismic bodywave arrival times, Bull. Seism. Soc. Am., 81, 1332-1339, 1991.

Stephenson, R. A., Bogdanova, S., and Julin, C.: Palaeozoic rifting in a 2.0 Ga Andean-type magmatic belt in the East European Craton: structural and rheological implications. Abstract of the 7th International Symposium on Deep Seismic Profiling of the Continents, 46, 1996.

Tesauro, M., Kaban, M. K., and Cloetingh, S. A. P. L.: EuCRUST-07: A new reference model for the European crust, Geophys. Res. Lett., 35, L05313, doi:10.1029/2007GL32244, 2008.

Thomson, C. J., and Gubbins, D.: Three-dimensional lithospheric modelling at NORSAR: linearity of the method and amplitude variations from the anomalies, Geophys. J. R. Astron. Soc., 71, 1-36, 1982.

Thurber, C.: Earthquake locations and three-dimensional crustal structure in the Coyote Lake area, central California, J. Geophys. Res., 88, 8226-8236, 1983.

Thybo, H.: Crustal structure and tectonic evolution of the Tornquist Fan region as revealed by geophysical methods. Bull. Geol. Soc. Den. 46, 145-160, 2000.

Thybo, H., Janik, T., and Omelchenko, V. D.: Upper lithospheric seismic velocity structure across the Pripyat Through and the Ukrainian Shield along the EUROBRIDGE'97 profile. Tectonophysics, 371, 41-79, 2003.

Vecsey, L., Plomerova, J., Babuska, V., and PASSEQ Working Group: Structure of the mantle lithosphere around the TESZ – from the East European Craton to the Variscan Belt. EGU General Assembly 2013, Geophysical Research Abstracts, Vol. 15, EGU2013-3133, 2013.

Vinnik, L. P., and Ryaboy, V. Z.: Deep structure of the East European platform according to seismic data. Physics of the Earth and Planetary Interiors, 25, 27-37, 1981.

Wagner, G. A., Gögen, K., Jonckheere, R., Wagner, I., and Woda, C.: Datingthe Quarternary volcanoes Komorní Huȯrka (Kammerbühl) and Železná Hȯrka (Eisenbühl), Czech Republic, by TL, ESR, alpha-recoil and fission track chronometry. Z.Geol.Wiss., 30, 191–200, 2002.

Weiland, Ch. M., Steck, L. K., Dawson, P. B., and Korneev, V. A.: Nonlinear teleseismic tomography at Long Valley caldera, using three-dimensional minimum travel time ray tracing. Journal of Geophysical Reseach, 100, B10, 20379-20390, 1995.

Wessel, P., and Smith, W.: Free software helps map and display data. EOS, Trans. Am. Union 72, 441, 1991.

Wilde-Piorko, M., Grad, M., and TOR Working Group: Crustal structure variation from the Precambrian to Palaeozoic platforms in Europe imaged by the inversion of teleseismic receiver functions – project TOR. Geophysical Journal International, 150, 261-270, 2002.

Wilde-Piórko, M., Geissler, W.H., Plomerová, J., Grad, M., Babuška, V., Brückl, E., Čyžienė, J., Czuba, W., Eengland, R., Gaczyński, E., Gazdova, R., Gregersen, S., Guterch, A., Hanka, W., Hegedűs, E., Heuer, B., Jedlička, P., Lazauskienė, J., Randy Keller, G., Kind, R., Klinge, K., Kolinsky, P., Komminaho, K., Kozlovskaya, E., Krűger, F., Larsen, T., Majdański, M., Málek, J., Motuza, G., Novotný, O., Pietrasiak, R., Plenefish, Th., Růžek, B., Šliaupa, S., Środa, P., Świeczak, M., Tiira, T., Voss, P., and Wiejacz, P.: PASSEQ 2006−2008: PASsive Seismic Experiment in Trans-European Suture Zone. Stud. Geophys. Geod., 52, 439−448, 2008.

Wilde-Piórko, M., Świeczak, M., Grad, M., and Majdański, M.: Integrated seismic model of the crust and upper mantle of the Trans-European Suture zone between the Precambrian craton and Phanerozoic terranes in Central Europe. Tectonophysics, 481, 108–115, 2010.

Winchester, J. A., and the PACE TMR Network Team: Paleozoic amalgamation of Central Europe: new results from recent geological and geophysical investigations. Tectonophysics, 360, 5–21, 2002.

Wüstefeld, A., Bokelmann, G., and Barruol, G.: Evidence for ancient lithospheric deformation in the East European Craton based on mantle seismic anisotropy and crustal magnetics. Tectonophysics, 481, 1-4, 16-28, 2010.

Yliniemi, J., Tiira, T., Luosto, U., Komminaho, K., Giese, R., Motuza, G., Nesedkin, V., Jacyna, J., Seckus, R., Grad, M., Czuba, W., Janik, T., Guterch, A., Lund, C.-E., and Doody, J. J.: EUROBRIDGE'95: Deep Seismic Profiling within the East European Craton. Tectonophysics, 339, 1-2, 2001.

Yliniemi, J., Kozlovskaya, E., Hjelt, S. E., Komminaho, K., and Ushakov, A.: Structure of the crust and uppermost mantle beneath southern Finland revealed by analysis of local events registered by the SVEKALAPKO seismic array. Tectonophysics, 394 (1–2), 41–67, 2004.

Zhang, H., and Thurber, C. H.: Estimating the model resolution matrix for large seismic tomography problems based on Lanczos bidiagonalization with partial reorthogonalization. Geophys. J. Int., 170 (1), 337-345, doi: 10.1111/j.1365-246X.2007.03418.x, 2007.

Zhu, H., Bozdağ, E., Peter, D., and Tromp, J.: Structure of the European upper mantle revealed by adjoint tomography. Nature Geosciences 5, 493–498, 2012.

# APPENDIX 1

Table 1. List of EQs used in the study for teleseismic tomography.

Time format – hour : minutes : seconds;

Latitude (lat) and longitude (long) in degrees;

Depth in kilometers;

Magnitude (M) was selected the highest value reported by the information source (ISC).

| nr. | year | month | day | time | lat | long | depth | M |
|---|---|---|---|---|---|---|---|---|
| 1 | 2006 | 6 | 18 | 18:28:00 | 32.9995 | -39.7009 | 8.6 | 6.0 |
| 2 | 2006 | 6 | 22 | 10:53:11 | 45.3023 | 149.4132 | 104.3 | 6.0 |
| 3 | 2006 | 6 | 27 | 18:07:21 | 6.4781 | 92.7356 | 25.8 | 6.3 |
| 4 | 2006 | 6 | 27 | 2:39:33 | 52.1552 | 176.1572 | 28.3 | 6.2 |
| 5 | 2006 | 6 | 28 | 21:02:09 | 26.8361 | 55.8060 | 15.1 | 5.8 |
| 6 | 2006 | 7 | 6 | 3:57:52 | 39.0233 | 71.7719 | 23.7 | 5.8 |
| 7 | 2006 | 7 | 8 | 20:39:57 | 51.1889 | -179.2640 | 3.2 | 6.6 |
| 8 | 2006 | 7 | 10 | 7:21:36 | -11.5727 | -13.4176 | 10.0 | 5.5 |
| 9 | 2006 | 7 | 12 | 14:44:44 | -8.5692 | 67.8158 | 10.0 | 5.7 |
| 10 | 2006 | 7 | 27 | 11:16:40 | 1.7244 | 97.1295 | 30.0 | 6.3 |
| 11 | 2006 | 7 | 29 | 19:53:41 | 23.5288 | -63.876 | 8.5 | 5.8 |
| 12 | 2006 | 8 | 6 | 14:26:17 | 37.4091 | 74.7119 | 4.9 | 5.6 |
| 13 | 2006 | 8 | 6 | 18:16:39 | 26.2558 | 143.9864 | 23.0 | 5.9 |
| 14 | 2006 | 8 | 11 | 14:30:39 | 18.4706 | -101.135 | 58.4 | 6.1 |
| 15 | 2006 | 8 | 16 | 18:38:58 | -28.8283 | 61.7726 | 10.0 | 5.9 |
| 16 | 2006 | 8 | 24 | 21:50:36 | 51.0679 | 157.5354 | 53.5 | 6.5 |
| 17 | 2006 | 9 | 1 | 12:04:21 | 53.9609 | -166.3610 | 75.6 | 5.9 |
| 18 | 2006 | 9 | 10 | 14:56:06 | 26.3900 | -86.5804 | 10.0 | 5.9 |
| 19 | 2006 | 9 | 24 | 22:56:21 | -17.6967 | 41.8104 | 17.2 | 5.7 |
| 20 | 2006 | 9 | 29 | 13:08:24 | 10.8486 | -61.7653 | 53.4 | 6.1 |
| 21 | 2006 | 9 | 30 | 17:50:22 | 46.1890 | 153.1761 | 19.4 | 6.6 |
| 22 | 2006 | 10 | 1 | 9:06:00 | 46.3193 | 153.3046 | 19.5 | 6.5 |
| 23 | 2006 | 10 | 9 | 10:01:47 | 20.7054 | 120.0645 | 17.3 | 6.3 |
| 24 | 2006 | 10 | 10 | 23:58:06 | 37.1616 | 142.8023 | 32.2 | 6.0 |
| 25 | 2006 | 10 | 21 | 18:23:20 | 13.3641 | 121.4278 | 18.0 | 5.9 |
| 26 | 2006 | 10 | 23 | 21:17:22 | 29.4110 | 140.3506 | 29.9 | 6.4 |
| 27 | 2006 | 11 | 17 | 18:03:11 | 28.5876 | 129.8655 | 23.1 | 6.2 |
| 28 | 2006 | 11 | 29 | 15:38:43 | 53.8157 | -35.4350 | 10.0 | 5.6 |

| | | | | | | | | |
|---|---|---|---|---|---|---|---|---|
| 29 | 2006 | 12 | 1 | 3:58:20 | 3.4573 | 99.1030 | 204.2 | 6.3 |
| 30 | 2006 | 12 | 25 | 20:00:59 | 42.0738 | 76.0856 | 15.2 | 5.8 |
| 31 | 2006 | 12 | 26 | 12:26:20 | 21.8354 | 120.5330 | 6.3 | 7.1 |
| 32 | 2006 | 12 | 30 | 8:30:47 | 13.2050 | 51.3376 | 10.0 | 6.6 |
| 33 | 2007 | 1 | 9 | 15:49:32 | 59.4467 | -137.1380 | 10.0 | 5.7 |
| 34 | 2007 | 1 | 17 | 23:18:48 | 10.0815 | 58.7013 | 10.0 | 6.2 |
| 35 | 2007 | 2 | 4 | 20:56:57 | 19.3369 | -78.3947 | 10.0 | 6.2 |
| 36 | 2007 | 2 | 19 | 2:33:42 | 1.6404 | 30.6974 | 27.3 | 5.6 |
| 37 | 2007 | 3 | 1 | 23:11:50 | 26.6058 | -44.6470 | 10.0 | 6.0 |
| 38 | 2007 | 3 | 6 | 3:49:38 | -0.5060 | 100.4824 | 21.2 | 6.4 |
| 39 | 2007 | 3 | 9 | 7:27:29 | -11.4284 | 66.2758 | 10.0 | 5.7 |
| 40 | 2007 | 3 | 9 | 3:22:42 | 43.2206 | 133.5123 | 439.5 | 6.0 |
| 41 | 2007 | 3 | 13 | 2:59:00 | 26.1733 | -110.6970 | 10.0 | 6.0 |
| 42 | 2007 | 3 | 18 | 2:11:03 | 4.6505 | -78.5033 | 1.1 | 6.2 |
| 43 | 2007 | 3 | 22 | 6:10:43 | -3.3420 | 86.7202 | 26.9 | 5.9 |
| 44 | 2007 | 3 | 25 | 0:41:56 | 37.3209 | 136.5686 | 4.0 | 6.7 |
| 45 | 2007 | 3 | 28 | 21:17:10 | -6.2242 | 29.6190 | 13.4 | 5.8 |
| 46 | 2007 | 4 | 3 | 3:35:06 | 36.4738 | 70.6405 | 215.5 | 6.2 |
| 47 | 2007 | 4 | 4 | 19:58:02 | -17.1836 | 66.8750 | 10.0 | 5.9 |
| 48 | 2007 | 4 | 5 | 3:56:49 | 37.3659 | -24.6358 | 16.2 | 6.3 |
| 49 | 2007 | 4 | 10 | 13:56:50 | 13.0113 | 92.5102 | 15.3 | 5.5 |
| 50 | 2007 | 4 | 13 | 5:42:21 | 17.2469 | -100.2410 | 33.4 | 6.0 |
| 51 | 2007 | 4 | 20 | 1:45:55 | 25.6879 | 125.0772 | 9.2 | 6.3 |
| 52 | 2007 | 5 | 4 | 12:06:51 | -1.3273 | -15.0009 | 10.0 | 6.2 |
| 53 | 2007 | 5 | 5 | 8:51:38 | 34.3079 | 81.9875 | 13.4 | 6.1 |
| 54 | 2007 | 5 | 7 | 11:59:46 | 31.3215 | 97.6605 | 12.0 | 5.5 |
| 55 | 2007 | 5 | 16 | 8:56:13 | 20.5565 | 100.7342 | 10.0 | 6.3 |
| 56 | 2007 | 5 | 23 | 19:09:13 | 21.9055 | -96.3184 | 1.7 | 5.6 |
| 57 | 2007 | 5 | 30 | 20:22:11 | 52.0987 | 157.2889 | 120.4 | 6.4 |
| 58 | 2007 | 6 | 2 | 21:34:58 | 23.0785 | 101.0073 | 11.0 | 6.1 |
| 59 | 2007 | 6 | 13 | 19:29:44 | 13.7024 | -90.6465 | 64.0 | 6.7 |
| 60 | 2007 | 6 | 15 | 18:49:51 | 1.7332 | 30.7452 | 20.1 | 5.9 |
| 61 | 2007 | 6 | 18 | 14:29:48 | 34.4568 | 50.8578 | 11.4 | 5.5 |
| 62 | 2007 | 7 | 3 | 8:25:59 | 0.7697 | -30.1971 | 10.0 | 6.3 |
| 63 | 2007 | 7 | 6 | 1:09:18 | 16.5781 | -93.6161 | 120.0 | 6.1 |
| 64 | 2007 | 7 | 13 | 21:54:43 | 51.8785 | -176.246 | 44.1 | 6.0 |
| 65 | 2007 | 7 | 15 | 13:08:00 | 52.4899 | -168.0320 | 12.5 | 6.1 |
| 66 | 2007 | 7 | 16 | 14:17:36 | 36.8660 | 134.7943 | 347.1 | 6.8 |

| | | | | | | | | |
|---|---|---|---|---|---|---|---|---|
| 67 | 2007 | 7 | 17 | 14:10:41 | -2.8260 | 36.2670 | 14.8 | 5.9 |
| 68 | 2007 | 7 | 20 | 10:06:52 | 42.9111 | 82.2962 | 19.1 | 5.6 |
| 69 | 2007 | 7 | 29 | 4:54:35 | 53.6067 | 169.7092 | 28.0 | 5.9 |
| 70 | 2007 | 7 | 30 | 22:42:05 | 19.3104 | 95.5410 | 15.9 | 5.6 |
| 71 | 2007 | 7 | 31 | 22:55:28 | -0.1482 | -17.7189 | 2.7 | 6.2 |
| 72 | 2007 | 8 | 2 | 13:37:27 | 12.4470 | 47.4593 | 10.0 | 5.7 |
| 73 | 2007 | 8 | 2 | 2:37:42 | 46.9248 | 141.8324 | 19.9 | 6.2 |
| 74 | 2007 | 8 | 2 | 5:22:16 | 46.7681 | 141.7716 | 6.9 | 5.8 |
| 75 | 2007 | 8 | 2 | 3:21:44 | 51.3075 | -179.9750 | 37.8 | 6.7 |
| 76 | 2007 | 8 | 7 | 0:02:21 | 27.3494 | 126.7991 | 4.4 | 6.0 |
| 77 | 2007 | 8 | 13 | 22:23:03 | -30.9737 | -13.4479 | 10.0 | 5.5 |
| 78 | 2007 | 8 | 15 | 20:22:11 | 50.2629 | -177.5540 | 17.8 | 6.5 |
| 79 | 2007 | 8 | 16 | 14:18:25 | -3.4566 | -12.1013 | 20.9 | 5.5 |
| 80 | 2007 | 8 | 20 | 22:42:28 | 8.1332 | -39.2186 | 10.0 | 6.5 |
| 81 | 2007 | 9 | 1 | 19:14:22 | 25.0103 | -109.6400 | 11.9 | 6.1 |
| 82 | 2007 | 9 | 3 | 16:14:52 | 45.7243 | 150.1509 | 98.6 | 6.2 |
| 83 | 2007 | 9 | 6 | 17:51:26 | 24.3526 | 122.2370 | 56.2 | 6.2 |
| 84 | 2007 | 9 | 10 | 1:49:12 | 3.0475 | -77.9501 | 27.6 | 6.8 |
| 85 | 2007 | 9 | 13 | 3:35:27 | -2.1560 | 99.5994 | 18.8 | 7 |
| 86 | 2007 | 9 | 13 | 2:30:01 | -1.6595 | 99.6100 | 24.0 | 6.5 |
| 87 | 2007 | 9 | 20 | 8:31:13 | -2.0015 | 100.0640 | 29.1 | 6.7 |
| 88 | 2007 | 9 | 26 | 18:39:33 | -7.0062 | -11.6291 | 10.0 | 5.6 |
| 89 | 2007 | 10 | 2 | 18:00:07 | 54.5033 | -161.7350 | 42.9 | 6.3 |
| 90 | 2007 | 10 | 4 | 12:40:29 | 2.5719 | 92.9055 | 34.7 | 6.2 |
| 91 | 2007 | 10 | 18 | 16:13:13 | 30.1823 | -42.6211 | 12.3 | 5.7 |
| 92 | 2007 | 10 | 24 | 21:02:50 | -3.9271 | 101.0147 | 28.2 | 6.8 |
| 93 | 2007 | 10 | 31 | 3:04:54 | 37.3720 | -121.7980 | 10.0 | 5.6 |
| 94 | 2007 | 11 | 7 | 7:10:20 | 22.1583 | 92.3702 | 29.7 | 5.5 |
| 95 | 2007 | 11 | 27 | 4:26:59 | 16.2324 | 119.8240 | 45.3 | 5.9 |
| 96 | 2007 | 12 | 6 | 17:12:03 | 22.7483 | -45.1418 | 15.9 | 5.8 |
| 97 | 2007 | 12 | 8 | 19:55:18 | -7.5221 | 37.6041 | 10.0 | 5.6 |
| 98 | 2007 | 12 | 12 | 23:39:58 | 52.1242 | -131.4370 | 10.0 | 5.8 |
| 99 | 2007 | 12 | 19 | 9:30:26 | 51.3295 | -179.5090 | 34.2 | 7.2 |
| 100 | 2007 | 12 | 25 | 14:04:33 | 38.4955 | 142.0641 | 48.1 | 6.1 |
| 101 | 2007 | 12 | 26 | 22:04:55 | 52.5351 | -168.2210 | 34.1 | 6.4 |

# APPENDIX 2

Table 1. List of seismic stations used in this study.

| station code | place | country | datalogger | seismometer | sampling rate, Hz | latitude | longitude | Altitude, m | depth, m | start date | end date |
|---|---|---|---|---|---|---|---|---|---|---|---|
| BRG | Sachsen | Germany | | STS-2/N | | 50.8732 | 13.9428 | 296 | 36 | | |
| BFO | Baden-Wurttemberg | Germany | | STS-2/N | | 48.3301 | 8.32956 | 589 | | | |
| BG03 (PP01) | Ilmenau | Germany | MARSLITE | LE3D-5s | 125 | 50.6604 | 10.9145 | | 0 | 01/08/2006 | 12/20/2006 |
| | | | PS6-Log | L4-3D | 100 | 50.6604 | 10.9145 | | 0 | 12/20/2006 | 03/27/2007 |
| | | | PS6-Log | L4-3D | 50 | 50.6604 | 10.9145 | | 0 | 03/27/2007 | 07/16/2007 |
| BG16 | Frankenberger Hoehe | Germany | PS6-Log | L4-3D | 100 | 49.8467 | 11.7407 | 533 | 0 | 17/08/2006 | 21/11/2006 |
| | | | PS6-Log | L4-3D | 100 | 49.8467 | 11.7407 | 533 | 0 | 21/11/2006 | 01/15/2007 |
| | | | PS6-Log | L4-3D | 50 | 49.8467 | 11.7407 | 533 | 0 | 01/15/2007 | 07/05/2007 |
| BSEG | Schleswig-Holstein | Germany | | STS-2/N | | 53.9353 | 10.3169 | 40 | | | |
| BUG | Nordrhein-Westfalen | Germany | | STS-2/N | | 51.4406 | 7.26928 | 85 | | | |
| CLL | Sachsen | Germany | | STS-2/N | | 51.3077 | 13.0026 | 230 | | | |
| DPC | Dobruska-Polom | Czech Republic | | STS-2/N | | 50.3502 | 16.3222 | 748 | | | |
| FUR | Bayern | Germany | | STS-2/N | | 48.1655 | 11.2763 | 565 | | | |
| GKP | Gorka Klasztorna | Poland | | STS-2/N | | 53.2697 | 17.2367 | 115 | | | |
| HSKC | Hora Svate Kateriny | Czech Republic | PS6-Log | Guralp-3ESPC | 100 | 50.6084 | 13.4368 | 593 | 0 | 20/11/2006 | 31/12/2008 |
| JAC | Jachymov | Czech Republic | RUP2004 | CMG-40T | 100 | 50.3718 | 12.9132 | 745 | 512 | 05/01/2006 | N/A |
| JAVC | Velka Javorina | Czech Republic | | STS-2/N | | 48.8591 | 17.6707 | 827.6 | | | |
| KHC | Kasperske Hory | Czech Republic | | STS-2/N | | 49.1309 | 13.5782 | 695 | | | |
| KRUC | Moravsky | Czech Republic | | STS-2/N | | 49.0619 | 16.3952 | 341 | | | |

| | | | | | | | | | | | |
|---|---|---|---|---|---|---|---|---|---|---|---|
| KSP | Ksiaz | Poland | | STS-2/N | | 50.8428 | 16.2931 | 353 | | | |
| KWP | Kalwaria Paclawska | Poland | | STS-2/N | | 49.6314 | 22.7075 | 448 | | | |
| MORC | Moravsky Beroun | Czech Republic | | STS-2/N | | 49.7768 | 17.5425 | 743 | | | |
| MOX | Thuringen | Germany | | STS-2/N | | 50.6447 | 11.6156 | 455 | | | |
| MTSE | Matsula | Estonia | | CMG-40T/30 | | 58.7144 | 23.8146 | 3.4 | | | |
| NKC | Novy Kostel | Czech Republic | | STS-2/N | | 50.2331 | 12.4479 | 564 | | | |
| OJC | Ojcow | Poland | | STS-2/N | | 50.2195 | 19.7984 | 391 | | | |
| OKC | Ostrava-Krasne | Czech Republic | | STS-2/N | | 49.8375 | 18.1472 | 272 | | | |
| OST | Ostas | Czech_Republic | RUP2004 | CMG-40T | 100 | 50.5565 | 16.2156 | 560 | 0 | 05/22/2006 | N/A |
| PA01 | Sixenhof Crailshof | Germany | Reftek | STS-2 | 100 | 49.1062 | 10.1688 | 538 | 0 | 24/08/2004 | 04/03/2007 |
| | | | Reftek | STS-2 | 20 | 49.1062 | 10.1688 | 538 | 0 | 04/03/2007 | 31/12/2008 |
| PA03 | Heppstaedt | Germany | MARSLITE | LE3D-5s | 125 | 49.6829 | 10.9029 | 409 | 0 | 11/30/2006 | 01/22/2007 |
| | | | PS6-Log | Guralp-3ESPC | 50 | 49.6829 | 10.9029 | 409 | 0 | 01/22/2007 | 07/02/2007 |
| PA07 | Komorn Hurka | Czech Republic | RUP2004 | CMG-40T | 100 | 50.1000 | 12.3360 | 480 | 0 | 05/01/2006 | N/A |
| PA10 | Prisecnice | Czech Republic | RUP2004 | CMG-40T | 100 | 50.4903 | 13.1355 | 730 | 8 | 05/01/2006 | N/A |
| PA20 | Wuischke | Germany | DM24 | Guralp-3ESPD | 100 | 51.1264 | 14.5454 | 380 | 0 | 07/09/2006 | 01/12/2007 |
| | | | DM24 | Guralp-3ESPD | 50 | 51.1264 | 14.5454 | 380 | 0 | 01/12/2007 | 31/12/2008 |
| PA64 | Grochowice | Poland | CMG-SAM | CMG-3TD/120 | 100 | 51.7915 | 16.0036 | 77 | 0 | 26/07/2006 | 17/11/2007 |
| PA65 | Turew | Poland | CMG-SAM | CMG-3TD/120 | 100 | 52.0766 | 16.8366 | 90 | 0 | 26/07/2006 | 18/11/2007 |
| PA66 | Graby | Poland | CMG-SAM | CMG-3TD/120 | 100 | 52.4092 | 17.4722 | 115 | 0 | 26/07/2006 | 18/11/2007 |
| PA67 | Kruszwica | Poland | CMG-DCM | CMG-3ESP/120 | 100 | 52.6573 | 18.3505 | 74 | 0 | 08/08/2006 | 14/05/2007 |
| | | | CMG-SAM | CMG-40T/30 | 100 | 52.6573 | 18.3505 | 74 | 0 | 09/07/2007 | 18/11/2007 |
| PA68 | Trutowo | Poland | CMG-DCM | CMG-3ESP/120 | 100 | 52.9606 | 19.0508 | 96 | 0 | 13/09/2006 | 10/06/2007 |
| | | | CMG-SAM | CMG-3ESP/120 | 100 | 52.9606 | 19.0508 | 96 | 0 | 26/06/2007 | 19/11/2007 |
| PA69 | Nowy Dwór | Poland | CMG-DCM | CMG-3ESP/120 | 100 | 53.2387 | 19.8420 | 142 | 0 | 12/09/2006 | 26/06/2007 |
| | | | CMG-SAM | CMG-40T/30 | 100 | 53.2387 | 19.8420 | 142 | 0 | 26/06/2007 | 19/11/2007 |

| | | | | | | | | | | | |
|---|---|---|---|---|---|---|---|---|---|---|---|
| PA70 | Wikno | Poland | CMG-SAM | CMG-3TD/120 | 100 | 53.4720 | 20.5229 | 157 | 0 | 16/11/2006 | 19/11/2007 |
| PA71 | Kołowinek | Poland | CMG-SAM | CMG-3TD/120 | 100 | 53.7424 | 21.4321 | 130 | 0 | 27/07/2006 | 20/11/2007 |
| PA73 | Pobondzie | Poland | CMG-SAM | CMG-3TD/120 | 100 | 54.3191 | 22.9493 | 148 | 0 | 28/07/2006 | 20/11/2007 |
| PA81 | Būdninkai | Lithuania | Orion | STS-2/N | 20 | 54.5513 | 23.7539 | 134 | 0 | 02/08/2007 | 09/22/2007 |
| PB04 | Pottenstein | Germany | PS6-Log | L4-3D | 100 | 49.7460 | 11.4245 | 394 | 0 | 17/08/2006 | 21/11/2006 |
| | | | PS6-Log | L4-3D | 100 | 49.7460 | 11.4245 | 394 | 0 | 21/11/2006 | 01/15/2007 |
| | | | PS6-Log | L4-3D | 50 | 49.7460 | 11.4245 | 394 | 0 | 01/15/2007 | 07/05/2007 |
| PB09 | Hirtstein | Germany | PS6-Log | L4-3D | 100 | 50.5358 | 13.1932 | 886 | 0 | 14/07/2006 | 22/09/2006 |
| | | | PS6-Log | L4-3D | 100 | 50.5358 | 13.1932 | 886 | 0 | 22/09/2006 | 05/28/2007 |
| | | | PS6-Log | L4-3D | 100 | 50.5358 | 13.1932 | 886 | 0 | 05/28/2007 | 09/09/2007 |
| PB14 | Lauenstein reservoir | Germany | PS6-Log | L4-3D | 100 | 50.7805 | 13.8336 | 510 | 0 | 18/07/2006 | 22/09/2006 |
| | | | PS6-Log | L4-3D | 100 | 50.7805 | 13.8336 | 510 | 0 | 22/09/2006 | 04/30/2007 |
| | | | PS6-Log | Guralp-3ESPC | 100 | 50.7805 | 13.8336 | 510 | 0 | 04/30/2007 | 08/30/2007 |
| | | | PS6-Log | L4-3D | 100 | 50.7805 | 13.8336 | 510 | 0 | 08/30/2007 | 31/12/2008 |
| PB16 | Heeselicht Mill | Germany | PS6-Log | L4-3D | 100 | 50.9965 | 14.1043 | 205 | 0 | 07/09/2006 | 23/09/2006 |
| | | | PS6-Log | L4-3D | 100 | 50.9965 | 14.1043 | 205 | 0 | 23/09/2006 | 04/28/2007 |
| | | | PS6-Log | Guralp-3ESPC | 100 | 50.9965 | 14.1043 | 205 | 0 | 04/28/2007 | 08/30/2007 |
| | | | PS6-Log | L4-3D | 100 | 50.9965 | 14.1043 | 205 | 0 | 08/30/2007 | 31/12/2008 |
| PB19 | Neukirch | Germany | PS6-Log | L4-3D | 100 | 51.0850 | 14.2905 | 381 | 0 | 15/07/2006 | 23/09/2006 |
| | | | PS6-Log | L4-3D | 100 | 51.0850 | 14.2905 | 381 | 0 | 23/09/2006 | 04/28/2007 |
| | | | PS6-Log | Guralp-3ESPC | 100 | 51.0850 | 14.2905 | 381 | 0 | 04/28/2007 | 09/10/2007 |
| | | | PS6-Log | L4-3D | 100 | 51.0850 | 14.2905 | 381 | 0 | 09/10/2007 | 31/12/2008 |
| PB22 | Weissenberg | Germany | PS6-Log | L4-3D | 100 | 51.1944 | 14.6635 | 180 | 0 | 08/08/2006 | 22/09/2006 |
| | | | PS6-Log | L4-3D | 100 | 51.1944 | 14.6635 | 180 | 0 | 22/09/2006 | 04/30/2007 |
| | | | PS6-Log | Guralp-3ESPC | 100 | 51.1944 | 14.6635 | 180 | 0 | 04/30/2007 | 08/30/2007 |
| | | | PS6-Log | L4-3D | 100 | 51.1944 | 14.6635 | 180 | 0 | 08/30/2007 | 31/12/2008 |
| PB23B | Diehsa | Germany | PS6-Log | Guralp-3ESPC | 100 | 51.2535 | 14.7784 | 160 | 0 | 17/11/2006 | 31/12/2008 |

| | | | | | | | | | | | |
|---|---|---|---|---|---|---|---|---|---|---|---|
| PB25 | Rothenburg | Germany | PS6-Log | L4-3D | 100 | 51.3560 | 14.9650 | 160 | 0 | 08/08/2006 | 25/09/2006 |
| | | | PS6-Log | L4-3D | 100 | 51.3560 | 14.9650 | 160 | 0 | 25/09/2006 | 04/30/2007 |
| PB41 | Polana | Poland | PS6-Log | MARK L4-3D | 100 | 51.3998 | 15.0891 | 158 | 0 | 13/07/2006 | 20/10/2006 |
| | | | PS6-Log | MARK L4-3D | 50 | 51.3998 | 15.0891 | 158 | 0 | 20/10/2006 | 27/03/2007 |
| | | | PS6-Log | MARK L4-3D | 50? | 51.3998 | 15.0891 | 158 | 0 | 27/03/2007 | 19/07/2007 |
| | | | PS6-Log | MARK L4-3D | 50 | 51.3998 | 15.0891 | 158 | 0 | 19/07/2007 | |
| PB42 | Klików | Poland | PS6-Log | MARK L4-3D | 100 | 51.4676 | 15.2055 | 134 | 0 | 13/07/2006 | 20/10/2006 |
| | | | PS6-Log | MARK L4-3D | 50 | 51.4676 | 15.2055 | 134 | 0 | 20/10/2006 | 26/03/2007 |
| | | | PS6-Log | MARK L4-3D | 50? | 51.4676 | 15.2055 | 134 | 0 | 26/03/2007 | 19/07/2007 |
| | | | PS6-Log | MARK L4-3D | 50 | 51.4676 | 15.2055 | 134 | 0 | 19/07/2007 | |
| PB43 | Mycielin | Poland | PSS | MARK L4-3D | 20 | 51.6310 | 15.7091 | 152 | 0 | 26/07/2006 | |
| PB44 | Pastuszyn | Poland | PSS | MARK L4-3D | 20 | 51.6889 | 15.8178 | 166 | 0 | 26/07/2006 | |
| PB45 | Koczury | Poland | PSS | MARK L4-3D | 20 | 51.9093 | 16.3877 | 106 | 0 | 26/07/2006 | 11/09/2007 |
| | | | RefTec130 | MARK L4-3D | 50 | 51.9093 | 16.3877 | 106 | 0 | 11/09/2007 | ??/01/2008 |
| PB46 | Pośmigiel | Poland | PSS | MARK L4-3D | 20 | 51.9817 | 16.4970 | 130 | 0 | 26/07/2006 | 16/05/2007 |
| PB47 | Niesłabin | Poland | PSS | MARK L4-3D | 20 | 52.1442 | 17.0076 | 58 | 0 | 27/07/2006 | |
| PB50 | Ciencisko | Poland | PSS | MARK L4-3D | 20 | 52.5738 | 18.1279 | 96 | 0 | 28/07/2006 | |
| PB54 | Wierzchownia | Poland | PSS | MARK L4-3D | 20 | 53.1601 | 19.6526 | 128 | 0 | 27/06/2006 | |
| PB55 | Filice | Poland | PSS | MARK L4-3D | 20 | 53.3032 | 20.1516 | 173 | 0 | 28/06/2006 | |
| PB56 | Bartoszki | Poland | PSS | MARK L4-3D | 20 | 53.3777 | 20.4885 | 178 | 0 | 28/06/2006 | |
| PB57 | Sasek | Poland | PSS | MARK L4-3D | 20 | 53.6294 | 20.9086 | 124 | 0 | 04/10/2006 | |
| PB58 | Jeleniewo | Poland | PSS | MARK L4-3D | 20 | 53.6965 | 21.1554 | 150 | 0 | 28/06/2006 | 19/04/2007 |
| | | | RefTec130 | Mark L22 (2 Hz) | 50? | 53.6965 | 21.1554 | 150 | 0 | 19/04/2007 | 23/05/2007 |
| | | | RefTec130 | MARK L4-3D | 50? | 53.6965 | 21.1554 | 150 | 0 | 23/05/2007 | ??/01/2008 |
| PB60 | Siemionki | Poland | RefTec130 | L22 (2 Hz) | 100? | 53.9503 | 22.0117 | 154 | 0 | 18/04/2007 | ??/01/2008 |
| PB82 | Žuvintai | Lithuania | RT-130 | CM-3 | 50 | 54.4571 | 23.6405 | 84 | 0 | 22/06/2006 | 09/03/2007 |
| PB83 | Kisieliškės | Lithuania | RT-72 A | Mark L4 | 50 | 54.6188 | 24.0973 | 110 | 0 | 21/06/2006 | 09/06/2007 |

| | | | | | | | | | | | |
|---|---|---|---|---|---|---|---|---|---|---|---|
| PB84 | Balceriškės | Lithuania | RT-130 | CM-3 | 50 | 54.7442 | 24.4874 | 143 | 0 | 21/06/2006 | 09/19/2007 |
| PB85 | Geibonys | Lithuania | RT-72 A | Mark L4 | | 54.7800 | 24.6800 | 101 | | 09/06/2006 | 10/24/2007 |
| PB86 | Glitiškės | Lithuania | RT-72 A | Mark L4 | | 54.9821 | 25.2389 | 140 | | 09/06/2006 | 02/01/20007 |
| PB87 | Dubingiai | Lithuania | RT-130 | Lennartz LE-3Dlite | 50 | 55.0601 | 25.4510 | 175 | 0 | 21/06/2006 | 08/21/2007 |
| PB88 | Januliškis | Lithuania | RT-72 A | Mark L4 | | 55.1669 | 25.8422 | 150 | 0 | 19/06/2006 | 09/19/2007 |
| PC21 | Primda | Czech Republic | GAIA | STS-2 | 20 | 49.6700 | 12.6780 | 732 | | 11/10/2006 | |
| PC23 | Nectiny | Czech Republic | RUP2004 | CMG-40T | 100 | 49.9774 | 13.1686 | 520 | 0 | 05/01/2006 | N/A |
| PC26 | Becov | Czech Republic | GAIA | STS-2 | 20 | 50.0860 | 12.8400 | 547 | | 05/10/2006 | 03/27/2007 |
| PC32 | Josefuv_dul | Czech Republic | RUP2004 | CMG-40T | 100 | 50.7915 | 15.1957 | 690 | 0 | 05/10/2006 | N/A |
| PD22 | Lomy | Czech Republic | GAIA | Le3D | 20 | 49.8600 | 12.9370 | 500 | | 05/10/2006 | 21/12/2006 |
| PD24 | Drahous | Czech Republic | GAIA | Le3D | 20 | 50.0810 | 13.4760 | 543 | | 13/09/2006 | |
| PD25 | Krasny Dvur | Czech Republic | GAIA | Le3D | 20 | 50.2520 | 13.3700 | 299 | | 08/09/2006 | |
| PD28 | Hazmburk | Czech Republic | GAIA | Le3D | 20 | 50.4340 | 14.0140 | 454 | | 05/09/2006 | |
| PD29 | Rip | Czech Republic | GAIA | Le3D | 20 | 50.3860 | 14.2900 | 255 | | 05/09/2006 | |
| PD30 | Hamr | Czech Republic | GAIA | Le3D | 20 | 50.6860 | 14.8520 | 342 | | 31/10/2006 | 05/17/2007 |
| PD31 | Doleni_Paseky | Czech Republic | GAIA | Le3D | 20 | 50.7120 | 14.9660 | 460 | | 10/10/2006 | |
| PD41 | Dębowy Gaj | Poland | PS6-log | MARK L4-3D | 100 | 51.0737 | 15.6368 | 270 | 0 | 13/07/2006 | 20/10/2006 |
| | | | PS6-log | MARK L4-3D | 50 | 51.0737 | 15.6368 | 270 | 0 | 20/10/2006 | 20/03/2007 |
| | | | PS6-log | MARK L4-3D | ??? | 51.0737 | 15.6368 | 270 | 0 | 20/03/2007 | 10/07/2007 |
| | | | PS6-log | MARK L4-3D | 50 | 51.0737 | 15.6368 | 270 | 0 | 10/07/2007 | 20/07/2007 |
| | | | PS6-log | MARK L4-3D | 50 | 51.0737 | 15.6368 | 270 | 0 | 20/07/2007 | 17/10/2007 |
| | | | PS6-log | MARK L4-3D | 50 | 51.0737 | 15.6368 | 270 | 0 | 17/10/2007 | |
| PD42 | Sitno | Poland | PS6-log | MARK L4-3D | 100 | 51.3799 | 16.3752 | 104 | 0 | 12/07/2006 | 19/10/2006 |
| | | | PS6-log | MARK L4-3D | 50 | 51.3799 | 16.3752 | 104 | 0 | 19/10/2006 | 10/07/2007 |
| | | | PS6-log | MARK L4-3D | 100 do 235.2007; ??? od 236.2007 | 51.3799 | 16.3752 | 104 | 0 | 10/07/2007 | 17/10/2007 |
| | | | PS6-log | MARK L4-3D | 50 | 51.3799 | 16.3752 | 104 | 0 | 17/10/2007 | |

| | | | | | | | | | | | |
|---|---|---|---|---|---|---|---|---|---|---|---|
| PD43 | Zygmuntowo | Poland | PS6-log | MARK L4-3D | 100 | 51.6553 | 17.2284 | 99 | 0 | 25/07/2006 | 19/10/2006 |
| | | | PS6-log | MARK L4-3D | 50 | 51.6553 | 17.2284 | 99 | 0 | 19/10/2006 | 26/03/2007 |
| | | | PS6-log | MARK L4-3D | 50 | 51.6553 | 17.2284 | 99 | 0 | 26/03/2007 | 11/07/2007 |
| | | | PS6-log | MARK L4-3D | 100 | 51.6553 | 17.2284 | 99 | 0 | 26/03/2007 | 11/07/2007 |
| | | | PS6-log | MARK L4-3D | ??? | 51.6553 | 17.2284 | 99 | 0 | 11/07/2007 | 24/10/2007 |
| | | | PS6-log | MARK L4-3D | 50 | 51.6553 | 17.2284 | 99 | 0 | 24/10/2007 | |
| PD44 | Piskory | Poland | PS6-log | MARK L4-3D | 100 | 51.9710 | 18.0363 | 105 | 0 | 08/07/2006 | 04/10/2006 |
| | | | PS6-log | MARK L4-3D | 50 | 51.9710 | 18.0363 | 105 | 0 | 04/10/2006 | 27/06/2007 |
| | | | PS6-log | MARK L4-3D | 100 | 51.9710 | 18.0363 | 105 | 0 | 27/06/2007 | 24/10/2007 |
| | | | PS6-log | MARK L4-3D | 50 | 51.9710 | 18.0363 | 105 | 0 | 24/10/2007 | |
| PD45 | Słubin | Poland | PS6-log | MARK L4-3D | 100 | 52.3633 | 18.8092 | 113 | 0 | 08/07/2006 | 19/07/2006 |
| | | | PS6-log | MARK L4-3D | 50 | 52.3633 | 18.8092 | 113 | 0 | 04/10/2006 | 27/06/2007 |
| | | | PS6-log | MARK L4-3D | 100 | 52.3633 | 18.8092 | 113 | 0 | 27/06/2007 | 24/10/2007 |
| | | | PS6-log | MARK L4-3D | 50 | 52.3633 | 18.8092 | 113 | 0 | 24/10/2007 | |
| PD46 | Brwilno | Poland | PS6-log | MARK L4-3D | 100 | 52.5791 | 19.6068 | 101 | 0 | 17/07/2006 | 07/11/2006 |
| | | | PS6-log | MARK L4-3D | 50 | 52.5791 | 19.6068 | 101 | 0 | 07/11/2006 | 06/03/2007 |
| | | | PS6-log | MARK L4-3D | 100 do 8:21 077.2007; ??? od 14:54 077.2007 | 52.5791 | 19.6068 | 101 | 0 | 06/03/2007 | 27/05/2007 |
| | | | PS6-log | MARK L4-3D | ??? | 52.5791 | 19.6068 | 101 | 0 | 27/06/2007 | 29/10/2007 |
| | | | PS6-log | MARK L4-3D | 50 | 52.5791 | 19.6068 | 101 | 0 | 29/10/2007 | |
| PD47 | Sujki | Poland | PS6-log | MARK L4-3D | 100 | 52.8765 | 20.3658 | 112 | 0 | 20/07/2006 | 07/11/2007 |
| | | | PS6-log | MARK L4-3D | 50 | 52.8765 | 20.3658 | 112 | 0 | 07/11/2006 | 06/03/2007 |
| | | | PS6-log | MARK L4-3D | ??? | 52.8765 | 20.3658 | 112 | 0 | 06/03/2007 | 01/11/2007 |
| | | | PS6-log | MARK L4-3D | 50 | 52.8765 | 20.3658 | 112 | 0 | 01/11/2007 | |
| PD48 | Budziska | Poland | PS6-log | MARK L4-3D | 100 | 53.1649 | 21.0910 | 106 | 0 | 20/07/2006 | 08/11/2008 |
| | | | PS6-log | MARK L4-3D | 50 | 53.1649 | 21.0910 | 106 | 0 | 08/11/2006 | 10/01/2007 |

| | | | | | | | | | | | |
|---|---|---|---|---|---|---|---|---|---|---|---|
| | | | PS6-log | MARK L4-3D | 100 | 53.1649 | 21.0910 | 106 | 0 | 10/01/2007 | 07/03/2007 |
| | | | PS6-log | MARK L4-3D | ??? | 53.1649 | 21.0910 | 106 | 0 | 07/03/2007 | 19/06/2007 |
| | | | PS6-log | MARK L4-3D | 50 | 53.1649 | 21.0910 | 106 | 0 | 07/03/2007 | |
| PD49 | Pupki | Poland | PS6-log | MARK L4-3D | 100 | 53.3622 | 21.7898 | 102 | 0 | 20/07/2006 | 08/11/2009 |
| | | | PS6-log | MARK L4-3D | 50 | 53.3622 | 21.7898 | 102 | 0 | 07/11/2006 | 07/03/2007 |
| | | | PS6-log | MARK L4-3D | 50 | 53.3622 | 21.7898 | 102 | 0 | 07/03/2007 | 03/08/2007 |
| | | | PS6-log | MARK L4-3D | 100 | 53.3622 | 21.7898 | 102 | 0 | 03/08/2007 | 15/11/2007 |
| | | | PS6-log | MARK L4-3D | 50 | 53.3622 | 21.7898 | 102 | 0 | 15/11/2007 | |
| PD50 | Kozłówka | Poland | PS6-log | MARK L4-3D | 100 | 53.6637 | 22.6811 | 117 | 0 | 20/07/2006 | 08/11/2006 |
| | | | PS6-log | MARK L4-3D | 50 | 53.6637 | 22.6811 | 117 | 0 | 08/11/2006 | 14/03/2007 |
| | | | PS6-log | MARK L4-3D | 100 | 53.6637 | 22.6811 | 117 | 0 | 14/03/2007 | 05/07/2007 |
| | | | PS6-log | MARK L4-3D | 50 | 53.6637 | 22.6811 | 117 | 0 | 08/08/2007 | |
| PD81 | Paliepis | Lithuania | RT-72 A | Mark L4 | | 54.0056 | 23.7865 | 113 | 0 | 17/06/2006 | 09/04/2007 |
| PD82 | Martinava | Lithuania | RT-72 A | Mark L4 | | 54.2990 | 24.4814 | 140 | 0 | 17/06/2006 | 09/04/2007 |
| PD83 | Mikašiūnai | Lithuania | RT-72 A | Mark L4 | | 54.4802 | 25.1464 | 140 | 0 | 18/06/2006 | 09/19/2007 |
| PF21 | Chudenice | Czech Republic | GAIA | Le3D | 20 | 49.4680 | 13.1740 | 580 | | 18/11/2006 | |
| PF22 | Tocnik | Czech Republic | GAIA | Le3D | 20 | 49.8900 | 13.8870 | 500 | | 13/09/2006 | 05/16/2007 |
| PF23A | Mcely | Czech Republic | GAIA | | 20 | 50.2965 | 15.0792 | 229 | | 04/12/2007 | |
| PF24 | Kumburk | Czech Republic | GAIA | Le3D | 20 | 50.4940 | 15.4460 | 642 | | 06/09/2006 | |
| PF41 | Bąków | Poland | PS6-log | MARK L4-3D | 100 | 51.2130 | 17.1550 | 137 | 0 | 09/07/2006 | 19/10/2006 |
| | | | PS6-log | MARK L4-3D | 50 | 51.2130 | 17.1550 | 137 | 0 | 19/10/2006 | 20/03/2007 |
| | | | PS6-log | MARK L4-3D | ??? | 51.2130 | 17.1550 | 137 | 0 | 20/03/2007 | 17/10/2007 |
| | | | PS6-log | MARK L4-3D | 50 | 51.2130 | 17.1550 | 137 | 0 | 17/10/2007 | |
| PF42 | Mikstat | Poland | PS6-log | MARK L4-3D | 100 | 51.5022 | 17.9694 | 188 | 0 | 09/07/2006 | 04/10/2006 |
| | | | PS6-log | MARK L4-3D | 50 | 51.5022 | 17.9694 | 188 | 0 | 04/10/2006 | 06/06/2007 |
| | | | PS6-log | MARK L4-3D | 100 | 51.5022 | 17.9694 | 188 | 0 | 06/06/2007 | 26/06/2007 |
| | | | PS6-log | MARK L4-3D | 50 | 51.5022 | 17.9694 | 188 | 0 | 23/10/2007 | |

| | | | | | | | | | | | |
|---|---|---|---|---|---|---|---|---|---|---|---|
| PF43 | Mianów | Poland | PS6-log | MARK L4-3D | 100 | 51.8198 | 19.0269 | 140 | 0 | 08/07/2006 | 04/10/2006 |
| | | | PS6-log | MARK L4-3D | 50 | 51.8198 | 19.0269 | 140 | 0 | 04/10/2006 | 06/06/2007 |
| | | | PS6-log | MARK L4-3D | ??? | 51.8198 | 19.0269 | 140 | 0 | 06/06/2006 | 08/10/2007 |
| | | | PS6-log | MARK L4-3D | 50 | 51.8198 | 19.0269 | 140 | 0 | 23/10/2007 | |
| PF44 | Januszew | Poland | PS6-log | MARK L4-3D | 100 | 52.3579 | 20.1613 | 73 | 0 | 17/07/2006 | 07/11/2011 |
| | | | PS6-log | MARK L4-3D | 50 | 52.3580 | 20.1612 | 59 | 0 | 07/11/2006 | 06/03/2011 |
| | | | PS6-log | MARK L4-3D | ??? | 52.3580 | 20.1612 | 59 | 0 | 06/03/2007 | 19/04/2007 |
| | | | RefTec130 | L22 (2 Hz) | 50 | 52.3578 | 20.1613 | 119 | 0 | 19/04/2007 | ??/01/2008 |
| PF45 | Obryte | Poland | PS6-log | MARK L4-3D | 100 | 52.7065 | 21.2280 | 100 | 0 | 21/07/2006 | 09/11/2012 |
| | | | PS6-log | MARK L4-3D | 50 | 52.7065 | 21.2280 | 100 | 0 | 09/11/2006 | 12/03/2007 |
| | | | PS6-log | MARK L4-3D | ??? | 52.7065 | 21.2280 | 100 | 0 | 12/03/2007 | 16/11/2007 |
| | | | PS6-log | MARK L4-3D | 50 | 52.7065 | 21.2280 | 100 | 0 | 16/11/2007 | |
| PF46 | Poryte Jabłoń | Poland | PS6-log | MARK L4-3D | 100 | 53.0239 | 22.2165 | 107 | 0 | 21/07/2006 | 09/11/2013 |
| | | | PS6-log | MARK L4-3D | 50 | 53.0239 | 22.2165 | 107 | 0 | 09/11/2006 | 07/03/2007 |
| | | | PS6-log | MARK L4-3D | 50 | 53.0239 | 22.2165 | 107 | 0 | 07/03/2007 | 03/08/2007 |
| | | | PS6-log | MARK L4-3D | 100 | 53.0239 | 22.2165 | 107 | 0 | 03/08/2007 | 15/11/2007 |
| | | | PS6-log | MARK L4-3D | 50 | 53.0239 | 22.2165 | 107 | 0 | 15/11/2007 | |
| PF47 | Ośrodek | Poland | PS6-log | MARK L4-3D | 100 | 53.3711 | 23.2324 | 189 | 0 | 21/07/2006 | 08/11/2006 |
| | | | PS6-log | MARK L4-3D | 50 | 53.3711 | 23.2324 | 189 | 0 | 08/11/2006 | 14/03/2007 |
| | | | PS6-log | MARK L4-3D | 100 | 53.3711 | 23.2324 | 189 | 0 | 14/03/2007 | 02/08/2007 |
| | | | PS6-log | MARK L4-3D | 50 | 53.3711 | 23.2324 | 189 | 0 | 02/08/2007 | |
| PG01 | Niederlippach | Germany | Reftek DAS130 | STS-2 | 100 | 48.4204 | 12.0779 | 449 | 0 | 17/10/2006 | 01/26/2007 |
| | | | Reftek DAS130 | STS-2 | 20 | 48.5871 | 12.0780 | 437 | 0 | 01/26/2007 | 02/16/2007 |
| | | | Reftek DAS130 | STS-2 | 20 | 48.5871 | 12.0780 | 437 | 0 | 02/16/2007 | 31/12/2008 |
| PG22 | Blanik | Czech Republic | GAIA | CMG-40T | 20 | 49.6430 | 14.8990 | 446 | | 25/06/2005 | |
| PG23 | Kuneticka Hora | Czech Republic | GAIA | STS-2 | 20 | 50.0810 | 15.8120 | 316 | | 19/05/2007 | |
| PG41 | Kolnica | Poland | GAIA | STS-2 | 20 | 50.7510 | 17.3330 | 137 | | 24/08/2006 | |

| | | | | | | | | | | | |
|---|---|---|---|---|---|---|---|---|---|---|---|
| | | | GAIA | STS-2 | 20 | 50.4507 | 17.2000 | 183 | 0 | 24/08/2006 | |
| PG42 | Sajdak | Poland | GAIA | STS-2 | 20 | 51.0980 | 18.0640 | 180 | | 23/08/2006 | |
| | Komorzno | Poland | GAIA | STS-2 | 20 | 51.0589 | 18.0382 | 181 | 0 | 23/08/2006 | |
| PG43 | Świerki | Poland | GAIA | STS-2 | 20 | 51.4720 | 18.7240 | 169 | | 23/08/2006 | |
| | | | GAIA | STS-2 | 20 | 51.2832 | 18.4341 | 173 | 0 | 23/08/2006 | |
| PG44 | Rzepki | Poland | GAIA | STS-2 | 20 | 51.6100 | 19.6530 | 185 | | 22/08/2006 | |
| | | | GAIA | STS-2 | 20 | 51.3660 | 19.3916 | 181 | 0 | 22/08/2006 | |
| PG45 | Osuchów | Poland | GAIA | STS-2 | 20 | 51.8880 | 20.5950 | 197 | | 22/08/2006 | |
| | | | GAIA | STS-2 | 20 | 51.5328 | 20.3572 | 197 | 0 | 22/08/2006 | |
| PG46 | Miednik | Poland | CMG-SAM | CMG-3TD/120 | 100 | 52.5271 | 21.9582 | 157 | 0 | 08/09/2006 | 25/06/2007 |
| PG47 | Markowo | Poland | CMG-SAM | CMG-40T/30 | 100 | 52.8021 | 22.7613 | 134 | 0 | 04/08/2006 | 25/06/2007 |
| PH49 | Pieńki | Poland | PS6-log | MARK L4-3D | 100 | 53.0588 | 23.6034 | 150 | 0 | 26/09/2006 | 09/11/2015 |
| | | | PS6-log | MARK L4-3D | 50 | 53.0588 | 23.6034 | 150 | 0 | 09/11/2006 | 14/03/2007 |
| | | | PS6-log | MARK L4-3D | ??? | 53.0588 | 23.6034 | 150 | 0 | 14/03/2007 | 24/06/2007 |
| | | | PS6-log | MARK L4-3D | 50 | 53.0588 | 23.6034 | 150 | 0 | 02/08/2007 | |
| PJ41 | Szemrowice | Poland | PS6-log | MARK L4-3D | 100 | 50.7411 | 18.3708 | 227 | 0 | 12/07/2006 | 18/10/2006 |
| | | | PS6-log | MARK L4-3D | 50 | 50.7411 | 18.3708 | 227 | 0 | 18/10/2006 | 20/03/2007 |
| | | | PS6-log | MARK L4-3D | ??? | 50.7411 | 18.3708 | 227 | 0 | 20/03/2007 | 16/10/2007 |
| | | | PS6-log | MARK L4-3D | 50 | 50.7411 | 18.3708 | 227 | 0 | 16/10/2007 | |
| PJ42 | Wola Blakowa | Poland | PS6-log | MARK L4-3D | 100 | 51.1275 | 19.3173 | 232 | 0 | 11/07/2006 | 18/10/2006 |
| | | | PS6-log | MARK L4-3D | 50 | 51.1275 | 19.3173 | 232 | 0 | 18/10/2006 | 21/03/2007 |
| | | | PS6-log | MARK L4-3D | 50 | 51.1275 | 19.3173 | 232 | 0 | 21/03/2007 | 11/07/2007 |
| | | | PS6-log | MARK L4-3D | ??? | 51.1275 | 19.3173 | 232 | 0 | 11/07/2007 | 16/10/2007 |
| | | | PS6-log | MARK L4-3D | 50 | 51.1275 | 19.3173 | 232 | 0 | 16/10/2007 | |
| PJ43 | Brzustów | Poland | PS6-log | MARK L4-3D | 100 | 51.5023 | 20.1832 | 167 | 0 | 11/07/2006 | 17/11/2006 |
| | | | PS6-log | MARK L4-3D | 50 | 51.5023 | 20.1832 | 167 | 0 | 17/11/2006 | 24/07/2007 |
| | | | PS6-log | MARK L4-3D | 50 | 51.5023 | 20.1832 | 167 | 0 | 24/07/2007 | |

| | | | | | | | | | | | |
|---|---|---|---|---|---|---|---|---|---|---|---|
| PJ44 | Orzechowo | Poland | PS6-log | MARK L4-3D | 100 | 51.7355 | 20.9964 | 147 | 0 | 24/08/2006 | 17/11/2006 |
| | | | PS6-log | MARK L4-3D | 50 | 51.7355 | 20.9964 | 147 | 0 | 17/11/2006 | 13/03/2007 |
| | | | PS6-log | MARK L4-3D | ??? | 51.7355 | 20.9964 | 147 | 0 | 13/03/2007 | 25/11/2007 |
| | | | PS6-log | MARK L4-3D | 50 | 51.7355 | 20.9964 | 147 | 0 | 25/11/2007 | |
| PJ45 | Jedlina | Poland | PS6-log | MARK L4-3D | 100 | 52.0432 | 21.9106 | 156 | 0 | 22/07/2006 | 17/11/2006 |
| | | | PS6-log | MARK L4-3D | 50 | 52.0432 | 21.9106 | 156 | 0 | 17/11/2006 | 08/03/2007 |
| | | | PS6-log | MARK L4-3D | 100 | 52.0432 | 21.9106 | 156 | 0 | 08/03/2007 | 24/07/2007 |
| | | | PS6-log | MARK L4-3D | 50 | 52.0432 | 21.9106 | 156 | 0 | 08/03/2007 | |
| PJ46 | Słochy Annopolskie | Poland | PS6-log | MARK L4-3D | 100 | 52.3817 | 22.8289 | 114 | 0 | 22/07/2006 | 09/11/2016 |
| | | | PS6-log | MARK L4-3D | 50 | 52.3817 | 22.8289 | 114 | 0 | 09/11/2006 | 14/03/2007 |
| | | | PS6-log | MARK L4-3D | ??? | 52.3817 | 22.8289 | 114 | 0 | 14/03/2007 | 16/11/2007 |
| | | | PS6-log | MARK L4-3D | 50 | 52.3817 | 22.8289 | 114 | 0 | 16/11/2007 | |
| PN01 | Wernstein | Germany | Reftek | STS-2 | 100 | 50.1154 | 11.3818 | 370 | 0 | 08/03/2006 | 14/02/2007 |
| | | | Reftek | STS-2 | 20 | 50.1154 | 11.3818 | 370 | 0 | 14/02/2007 | 31/12/2008 |
| PN09 | Neuhirschstein | Germany | MARSLITE | LE3D-5s | 125 | 51.2510 | 13.3990 | | 0 | 02/08/2006 | 17/01/2007 |
| | | | PS6-Log | Guralp-3ESPC | 100 | 51.2510 | 13.3990 | | 0 | 23/01/2007 | 12/04/2007 |
| | | | PS6-Log | L4-3D | 100 | 51.2510 | 13.3990 | | 0 | 20/09/2007 | 31/12/2008 |
| PN11 | Bischheim-Häslich | Germany | PS6-Log | L4-3D | 100 | 51.2499 | 14.0061 | 220 | 0 | 11/07/2006 | 22/09/2006 |
| | | | PS6-Log | L4-3D | 100 | 51.2499 | 14.0061 | 220 | 0 | 22/09/2006 | 04/30/2007 |
| | | | PS6-Log | Guralp-3ESPC | 100 | 51.2499 | 14.0061 | 220 | 0 | 04/30/2007 | 08/30/2007 |
| | | | PS6-Log | L4-3D | 100 | 51.2499 | 14.0061 | 220 | 0 | 08/30/2007 | 31/12/2008 |
| PN13 | Kahsel | Germany | MARSLITE | LE3D-5s | 125 | 51.6588 | 14.4604 | | 0 | 12/07/2006 | 01/15/2007 |
| PN41 | Kukadło | Poland | PS6-log | MARK L4-3D | 100 | 51.9417 | 15.1215 | 79 | 0 | 13/07/2006 | 20/10/2006 |
| | | | PS6-log | MARK L4-3D | 50 | 51.9417 | 15.1215 | 79 | 0 | 20/10/2006 | 27/03/2007 |
| | | | PS6-log | MARK L4-3D | 100 | 51.9417 | 15.1215 | 79 | 0 | 27/03/2007 | 19/07/2007 |
| | | | PS6-log | MARK L4-3D | 50 | 51.9417 | 15.1215 | 79 | 0 | 19/07/2007 | 28/11/2007 |
| PN42 | Buków | Poland | PS6-log | MARK L4-3D | 100 | 52.1417 | 15.6283 | 132 | 0 | 05/07/2006 | 21/10/2006 |

| | | | | | | | | | | | |
|---|---|---|---|---|---|---|---|---|---|---|---|
| | | | PS6-log | MARK L4-3D | 50 | 52.1413 | 15.6302 | 120 | 0 | 21/10/2006 | 27/03/2007 |
| | | | RefTec130 | L22 (2 Hz) | 50 | 52.1415 | 15.6301 | 138 | 0 | 15/05/2007 | ??/01/2008 |
| | | | PS6-log | MARK L4-3D | 50 | 52.1413 | 15.6302 | 120 | 0 | ??/01/2008 | |
| PN43 | Duszniki | Poland | PS6-log | MARK L4-3D | 100 | 52.4581 | 16.4361 | 89 | 0 | 05/07/2006 | 08/11/2017 |
| | | | PS6-log | MARK L4-3D | 50 | 52.4581 | 16.4361 | 89 | 0 | 08/11/2006 | 27/03/2007 |
| | | | PS6-log | MARK L4-3D | 100 | 52.4581 | 16.4361 | 89 | 0 | 27/03/2007 | 19/07/2007 |
| | | | PS6-log | MARK L4-3D | 50 | 52.4581 | 16.4361 | 89 | 0 | 19/07/2007 | |
| PN44 | Łoskoń Stary | Poland | PS6-log | MARK L4-3D | 100 | 52.6603 | 17.0552 | 91 | 0 | 15/07/2006 | 08/11/2006 |
| | | | PS6-log | MARK L4-3D | 50 | 52.6603 | 17.0552 | 91 | 0 | 08/11/2006 | 27/03/2007 |
| | | | PS6-log | MARK L4-3D | 100 | 52.6603 | 17.0552 | 91 | 0 | 27/03/2007 | 07/09/2007 |
| | | | PS6-log | MARK L4-3D | 50 | 52.6603 | 17.0552 | 91 | 0 | 07/09/2007 | 07/19/2007 |
| | | | PS6-log | MARK L4-3D | 50 | 52.6603 | 17.0552 | 91 | 0 | 07/19/2007 | |
| PN45 | Kornelin | Poland | PS6-log | MARK L4-3D | 100 | 53.0146 | 17.8370 | 64 | 0 | 15/07/2006 | 09/11/2006 |
| | | | PS6-log | MARK L4-3D | 50 | 53.0146 | 17.8370 | 64 | 0 | 09/11/2006 | 28/03/2007 |
| | | | PS6-log | MARK L4-3D | 50 | 53.0146 | 17.8370 | 64 | 0 | 28/03/2007 | 09/07/2007 |
| | | | PS6-log | MARK L4-3D | 100 do 287.2007 10:44; ??? od 287.2007 17:27 | 53.0146 | 17.8370 | 64 | 0 | 09/07/2007 | 29/11/2007 |
| | | | PS6-log | MARK L4-3D | 50 | 53.0146 | 17.8370 | 64 | 0 | 29/11/2007 | |
| PN46 | Płutowo | Poland | PS6-log | MARK L4-3D | 100 | 53.2770 | 18.3926 | 77 | 0 | 17/07/2006 | 27/11/2006 |
| | | | PS6-log | MARK L4-3D | 50 | 53.2770 | 18.3926 | 77 | 0 | 27/11/2006 | 02/04/2007 |
| | | | PS6-log | MARK L4-3D | 50 | 53.2770 | 18.3926 | 77 | 0 | 02/04/2007 | 14/07/2007 |
| | | | PS6-log | MARK L4-3D | 50 | 53.2770 | 18.3926 | 77 | 0 | 14/07/2007 | ??/03/2008 |
| PN47 | Świecie nad Osą | Poland | PS6-log | MARK L4-3D | 100 | 53.4519 | 19.0899 | 62 | 0 | 18/07/2006 | 27/11/2006 |
| | | | PS6-log | MARK L4-3D | 50 | 53.4519 | 19.0899 | 62 | 0 | 27/11/2006 | 02/04/2007 |
| | | | PS6-log | MARK L4-3D | 50 | 53.4519 | 19.0899 | 62 | 0 | 02/04/2007 | 14/07/2006 |
| | | | PS6-log | MARK L4-3D | 50 | 53.4519 | 19.0899 | 62 | 0 | 14/07/2006 | |

| | | | | | | | | | | | |
|---|---|---|---|---|---|---|---|---|---|---|---|
| PN48 | Sąpy | Poland | PS6-log | MARK L4-3D | 100 | 53.7092 | 19.6750 | 100 | 0 | 18/07/2006 | 28/11/2006 |
| | | | PS6-log | MARK L4-3D | 50 | 53.7092 | 19.6750 | 100 | 0 | 28/11/2006 | 12/03/2007 |
| | | | PS6-log | MARK L4-3D | ??? | 53.7092 | 19.6750 | 100 | 0 | 12/03/2007 | 10/10/2007 |
| | | | PS6-log | MARK L4-3D | 50 | 53.7092 | 19.6750 | 100 | 0 | 10/10/2007 | |
| PN49 | Sętal | Poland | PS6-log | MARK L4-3D | 100 | 53.9103 | 20.4865 | 131 | 0 | 19/07/2006 | 28/11/2006 |
| | | | PS6-log | MARK L4-3D | 50 | 53.9103 | 20.4865 | 131 | 0 | 28/11/2006 | 13/03/2007 |
| | | | PS6-log | MARK L4-3D | 100 | 53.9103 | 20.4865 | 131 | 0 | 13/03/2007 | 10/10/2007 |
| | | | PS6-log | MARK L4-3D | 50 | 53.9103 | 20.4865 | 131 | 0 | 10/10/2007 | |
| PN81 | Matarniai | Lithuania | RT-72 A | Mark L4 | | 54.7547 | 23.0052 | 40 | 0 | 16/06/2006 | 09/06/2007 |
| PN82 | Mozūriškiai | Lithuania | RT-130 | CM-3 | 50 | 54.9508 | 23.6694 | 85 | 0 | 20/06/2006 | 10/11/2007 |
| PN83 | Aklasis ežeras | Lithuania | RT-130 | CM-3 | 50 | 55.1474 | 24.4850 | 80.6 | 0 | 20/06/2006 | 09/03/2007 |
| PN84 | Adomiškėlis | Lithuania | RT-130 | CM-3 | 50 | 55.3099 | 25.3485 | 162 | 0 | 20/06/2006 | 10/10/2007 |
| PP05 | Roitzschjora | Germany | MARSLITE | LE3D-5s | 125 | 51.5852 | 12.4855 | | 0 | 09/02/2006 | 01/16/2007 |
| | | | PS6-Log | Guralp-3ESPC | 100 | 51.5852 | 12.4855 | | 0 | 01/16/2007 | 04/11/2007 |
| PP08 | Wiepersdorf | Germany | MARSLITE | LE3D-5s | 125 | 51.8813 | 13.2431 | | 0 | 12/07/2006 | 01/16/2007 |
| | | | PS6-Log | Guralp-3ESPC | 100 | 51.8813 | 13.2431 | | 0 | 16/01/2007 | 04/13/2007 |
| | | | MARSLITE | LE3D-5s | | 51.8813 | 13.2431 | | 0 | ??/??/2007 | |
| PP10 | Lindenberg | Germany | MARSLITE | LE3D-5s | 125 | 52.2076 | 14.1237 | | 0 | 02/08/2006 | 01/15/2007 |
| | | | PS6-Log | Guralp-3ESPC | 100 | 52.2076 | 14.1237 | | 0 | 01/15/2007 | 04/12/2007 |
| | | | MARSLITE | LE3D-5s | | 52.2076 | 14.1237 | | 0 | ??/??/2007 | |
| PP41 | Połęcko | Poland | PS6-Log | L4-3D | 100 | 52.4014 | 14.8756 | 67 | 0 | 07/04/2006 | 21/10/2006 |
| | | | PS6-Log | L4-3D | 50 | 52.4014 | 14.8756 | 67 | 0 | 21/10/2006 | 02/27/2007 |
| | | | PS6-Log | L4-3D | 50 | 52.4014 | 14.8756 | 67 | 0 | 02/27/2007 | 17/07/2007 |
| | | | PS6-log | MARK L4-3D | 50 | 52.4014 | 14.8756 | 67 | 0 | 17/07/2007 | 12/31/2008 |
| PP42 | Rapin | Poland | PS6-Log | L4-3D | 100 | 52.7665 | 15.7854 | 25 | 0 | 01/07/2006 | 09/10/2006 |
| | | | PS6-Log | L4-3D | 50 | 52.7665 | 15.7854 | 25 | 0 | 09/10/2006 | 31/12/2008 |
| PP43 | Stradun | Poland | PS6-Log | L4-3D | 100 | 53.0584 | 16.3906 | 85 | 0 | 01/07/2006 | 09/10/2006 |

| | | | | | | | | | | | |
|---|---|---|---|---|---|---|---|---|---|---|---|
| | | | PS6-Log | L4-3D | 50 | 53.0584 | 16.3906 | 85 | 0 | 09/10/2006 | 31/12/2008 |
| PP44 | Wymyslow | Poland | PS6-Log | L4-3D | 100 | 53.6082 | 17.9169 | 100 | 0 | 01/07/2006 | 08/10/2006 |
| | | | PS6-Log | L4-3D | 50 | 53.6082 | 17.9169 | 100 | 0 | 08/10/2006 | |
| | | | PS6-Log | L4-3D | 100 | 53.6082 | 17.9169 | 100 | 0 | 01/07/2006 | 08/10/2006 |
| | | | PS6-Log | L4-3D | 50 | 53.6082 | 17.9169 | 100 | 0 | 08/10/2006 | 31/12/2008 |
| PP45 | Cisowa Góra | Poland | PS6-log | MARK L4-3D | 100 | 53.7445 | 18.5186 | 90 | 0 | 18/07/2006 | 27/11/2006 |
| | | | PS6-log | MARK L4-3D | 50 | 53.7445 | 18.5186 | 90 | 0 | 27/11/2006 | 02/04/2007 |
| | | | PS6-log | MARK L4-3D | 50 | 53.7445 | 18.5186 | 90 | 0 | 02/04/2007 | |
| PP46 | Chartowo | Poland | PS6-log | MARK L4-3D | 100 | 53.9930 | 19.2812 | 44 | 0 | 18/07/2006 | 28/11/2006 |
| | | | PS6-log | MARK L4-3D | 50 | 53.9930 | 19.2812 | 44 | 0 | 28/11/2006 | 03/04/2007 |
| | | | PS6-log | MARK L4-3D | ??? | 53.9930 | 19.2812 | 44 | 0 | 03/04/2007 | 10/10/2007 |
| | | | PS6-log | MARK L4-3D | 50 | 53.9930 | 19.2812 | 44 | 0 | 10/10/2007 | |
| PP47 | Kiersiny | Poland | PS6-log | MARK L4-3D | 100 | 54.2879 | 20.0599 | 108 | 0 | 19/07/2006 | 28/11/2006 |
| | | | PS6-log | MARK L4-3D | 50 | 54.2879 | 20.0599 | 108 | 0 | 29/11/2006 | 13/03/2007 |
| | | | PS6-log | MARK L4-3D | ??? | 54.2879 | 20.0599 | 108 | 0 | 13/03/2007 | 08/08/2007 |
| | | | PS6-log | MARK L4-3D | 50 | 54.2879 | 20.0599 | 108 | 0 | 10/10/2007 | |
| PP81 | Mantviliai | Lithuania | RT-72 A | Mark L4 | | 55.1496 | 22.6523 | 31 | 0 | 16/06/2006 | 09/06/2007 |
| PP82 | Paliepai | Lithuania | RT-130 | Lennartz LE-3Dlite | | 55.3525 | 23.5543 | 100.5 | 0 | 15/06/2006 | 01/10/2008 |
| PP83 | Ustronė | Lithuania | RT-130 | Lennartz LE-3Dlite | | 55.6155 | 24.1015 | 40 | 0 | 16/06/2006 | 01/09/2008 |
| PP84 | Gudgailys | Lithuania | RT-130 | Lennartz LE-3Dlite | | 55.8217 | 24.7507 | 69 | 0 | 15/06/2006 | 01/09/008 |
| PQ01 | Sondershausen | Germany | Reftek | STS-2 | 100 | 51.3685 | 10.8466 | 117 | 0 | 15/08/2006 | 03/26/2007 |
| | | | Reftek | STS-2 | 20 | 51.3685 | 10.8466 | 117 | 0 | 03/26/2007 | |
| PQ05 | Neu-Rietz | Germany | PS6-Log | Guralp-3ESPC | 100 | 52.0700 | 12.7686 | | 0 | 12/12/2006 | 04/11/2007 |
| | | | PS6-Log | Guralp-3ESPC | | | | | 0 | ??/05/2007 | 12/31/2008 |
| | | | PS6-Log | Guralp-3ESPC | | | | | 0 | ??/05/2007 | 12/31/2008 |
| PQ11 | Neutrebbin | Germany | DM24 | CMG-3ESP/120 | 50 | 52.6621 | 14.1982 | 3 | 0 | 07/06/2006 | 05/12/2006 |

| | | | | | | | | | | | |
|---|---|---|---|---|---|---|---|---|---|---|---|
| | | | PS6-Log | Guralp-3ESPC | 100 | 52.6621 | 14.1982 | 3 | 0 | 12/05/2006 | 08/31/2007 |
| | | | PS6-Log | Guralp-3ESPC | 50? | 52.6621 | 14.1982 | 3 | 0 | 08/31/2007 | 31/12/2008 |
| PQ46 | Dyszno | Poland | DM24 | CMG-3ESP/120 | 100 | 52.8270 | 14.7348 | - | 0 | 07/08/2006 | 06/10/2006 |
| | | | DM24 | CMG-3ESP/120 | 50 | 52.8270 | 14.7348 | - | 0 | 06/10/2006 | |
| PQ47 | Zeliszewo | Poland | DM24 | CMG-3ESP/120 | 100 | 53.1973 | 15.5412 | | 0 | 08/06/2006 | 10/07/2006 |
| | | | DM24 | CMG-3ESP/120 | 50 | 53.1973 | 15.5412 | | 0 | 10/07/2006 | 28/02/2007 |
| | | | DM24 | CMG-3ESP/120 | 50 | 53.1973 | 15.5412 | | 0 | 02/03/2007 | 09/11/2007 |
| | | | DM24 | CMG-3ESP/120 | 50 | 53.1973 | 15.5412 | | 0 | 18/03/2008 | 31/12/2008 |
| PQ48 | Rakowo | Poland | DM24 | CMG-3ESP/120 | 100 | 53.6051 | 16.3349 | | 0 | 08/05/2006 | 10/07/2006 |
| | | | DM24 | CMG-3ESP/120 | 50 | 53.6051 | 16.3349 | | 0 | 10/07/2006 | 01/03/2007 |
| | | | DM24 | CMG-3ESP/120 | 50 | 53.6051 | 16.3349 | | 0 | 01/03/2007 | 16/07/2007 |
| | | | DM24 | CMG-3ESP/120 | 50 | 53.6051 | 16.3349 | | 0 | 16/07/2007 | 31/12/2008 |
| PQ49 | Przechlewo | Poland | DM24 | CMG-3ESP/120 | 100 | 53.8390 | 17.2479 | | 0 | 05/08/2006 | 08/10/2006 |
| | | | DM24 | CMG-3ESP/120 | 50 | 53.8390 | 17.2479 | | 0 | 08/10/2006 | 31/12/2008 |
| PQ81 | Radvietis | Lithuania | REFTEK-130 | STS-2/N | 50 | 55.5111 | 21.9334 | 99 | 0 | 02/11/2006 | 22/09/2007 |
| PQ82 | Jaugėlai | Lithuania | REFTEK-130 | STS-2/N | 50 | 55.7658 | 23.4980 | 150 | 0 | 03/11/2006 | 22/09/2007 |
| PR03 | Petersberg | Germany | MARSLITE | LE3D-5s | 125 | 51.5962 | 11.9545 | 244 | 0 | 14/02/2006 | 01/11/2007 |
| | | | PS6-Log | Guralp-3ESPC | 100 | 51.5962 | 11.9545 | 244 | 0 | 01/11/2007 | 04/11/2007 |
| | | | MARSLITE | LE3D-5s | 125 | 51.5962 | 11.9545 | 244 | 0 | 04/11/2007 | |
| PR04 | Golm | Germany | MARSLITE | LE3D-5s | 125 | 52.4098 | 12.9744 | | 0 | 30/11/2006 | 31/12/2008 |
| PR07 | Wuensdorf | Germany | PS6-Log | L4-3D | 100 | 52.1554 | 13.4845 | | 0 | 09/05/2006 | 06/11/2006 |
| | | | PS6-Log | L4-3D | 50 | 52.1554 | 13.4845 | | 0 | 06/11/2006 | 10/05/2007 |
| | | | PS6-Log | Guralp-3ESPC | 50 | 52.1554 | 13.4845 | | 0 | 10/05/2007 | 31/08/2007 |
| | | | PS6-Log | L4-3D | 50 | 52.1554 | 13.4845 | | 0 | 31/08/2007 | ??/11/2007 |

| | | | | | | | | | | | |
|---|---|---|---|---|---|---|---|---|---|---|---|
| | | | MARSLITE | LE3D-5s | | 52.1554 | 13.4845 | | 0 | ??/??/2007 | 31/12/2008 |
| PR09 | Liebenhof Sternwarte | Germany | PS6-Log | L4-3D | 100 | 52.5512 | 14.0179 | | 0 | 09/05/2006 | 06/11/2006 |
| | | | PS6-Log | L4-3D | 50 | 52.5512 | 14.0179 | | 0 | 06/11/2006 | 10/05/2007 |
| | | | PS6-Log | Guralp-3ESPC | 50 | 52.5512 | 14.0179 | | 0 | 10/05/2007 | 31/08/2007 |
| | | | PS6-Log | L4-3D | 50 | 52.5512 | 14.0179 | | 0 | 31/08/2007 | 31/12/2008 |
| PR41 | Rogaczewo | Poland | PS6-Log | L4-3D | 100 | 52.7604 | 14.4312 | 35 | 0 | 06/08/2006 | 06/10/2006 |
| | | | PS6-Log | L4-3D | 50 | 52.7604 | 14.4312 | 35 | 0 | 06/10/2006 | 31/12/2008 |
| PR42 | Miedzyn | Poland | PS6-Log | L4-3D | 100 | 53.0166 | 15.0145 | 55 | 0 | 01/07/2006 | 06/10/2006 |
| | | | PS6-Log | L4-3D | 50 | 53.0166 | 15.0145 | 55 | 0 | 06/10/2006 | 31/12/2008 |
| PR44 | Zofiowka | Poland | PS6-Log | L4-3D | 100 | 53.4109 | 15.9458 | 90 | 0 | 01/07/2006 | 07/10/2006 |
| | | | PS6-Log | L4-3D | 50 | 53.4109 | 15.9458 | 90 | 0 | 07/10/2006 | 31/12/2008 |
| PR45 | Gwda | Poland | PS6-Log | L4-3D | 100 | 53.7112 | 16.8493 | 135 | 0 | 01/07/2006 | 07/10/2006 |
| | | | PS6-Log | L4-3D | 50 | 53.7112 | 16.8493 | 135 | 0 | 07/10/2006 | 31/12/2008 |
| PR46 | Trzebun | Poland | PS6-Log | L4-3D | 50 | 54.0194 | 17.7060 | ? | 0 | 16/07/2007 | ??/??/???? |
| | | | PS6-Log | L4-3D | 50 | 54.0194 | 17.7060 | ? | 0 | ??/??/???? | 31/12/2008 |
| PR81 | Lašinskiai | Lithuania | RT-130 | Lennartz LE-3Dlite | | 55.6588 | 22.8915 | 150 | 0 | 14/06/2006 | 01/09/2008 |
| PR82 | Narteikai | Lithuania | RT-130 | Lennartz LE-3Dlite | | 56.0482 | 24.1764 | 40 | 0 | 15/06/2006 | 01/09/2008 |
| PRU | Pruhonice | Czech Republic | | | | 49.9883 | 14.5417 | 302 | | | |
| PT81 | Žarėnai | Lithuania | RT-130 | Lennartz LE-3Dlite | 40 | 55.8361 | 22.2079 | 160 | 0 | 14/06/2006 | 10/02/2007 |
| PVCC | Panska Ves | Czech Republic | | | | 50.5282 | 14.5689 | 311 | | | |
| ROC | | | | | | | | | | | |
| SLA | | | | | | | | | | | |
| SUW | Suwalki | Poland | | | | 54.0125 | 23.1808 | 152 | | | |
| TNS | Hessen | Germany | | | | 50.2225 | 08.4473 | 815 | | | |
| VRAC | Vranov | Czech Republic | | | | 49.3083 | 16.5935 | 475 | | | |
| WAR | Warsaw | Poland | | | | 52.2417 | 21.0236 | 110 | | | |
| WDRB | Werdau | Germany | MARSLITE | LE3D-5s | 125 | 50.7274 | 12.4149 | | 0 | 07/04/2006 | 01/16/2007 |

| | | | | | | | | | | | |
|---|---|---|---|---|---|---|---|---|---|---|---|
| (PN05) | | | PS6-Log | L4-3D | 100 | 50.7274 | 12.4149 | | 0 | 16/01/2007 | 27/02/2007 |
| | | | PS6-Log | L4-3D | 50 | 50.7274 | 12.4149 | | 0 | 27/02/2007 | 19/03/2007 |
| WEBG (PN07) | Wechselburg | Germany | MARSLITE | LE3D-5s | 125 | 51.0043 | 12.7706 | | 0 | 26/01/2006 | 31/12/2008 |
| | | | PS6-Log | Guralp-3ESPC | 100 | 51.0043 | 12.7706 | | 0 | 26/01/2006 | 04/12/2007 |
| WET | Bayern | Germany | | | | 49.1440 | 12.8782 | 613 | | | |
| ZVI | | Czech Republic | | | | 49.4392 | 14.1928 | 373 | | | |

**Papers related to the theses:**

1. **Janutyte, I.,** Kozlovskaya, E., Majdanski, M., Voss, P. H., Budraitis, M., and PASSEQ Working Group: Traces of the crustal units and the upper mantle structure in the southwestern part of the East European Craton, Solid Earth, 5, 821–836, doi:10.5194/se-5-821-2014, 2014.
2. **Janutyte, I.,** Majdanski, M., Voss, P. H., Kozlovskaya, E., and Working Group, PASSEQ: Upper mantle structure around the Trans-European Suture Zone obtained by teleseismic tomography, Solid Earth Discuss., 6, 1723-1763, doi:10.5194/sed-6-1723-2014, 2014.
3. **Janutyte, I.,** Kozlovskaya, E., Motuza, G., and PASSEQ Working Group: Study of local seismic events in Lithuania and adjacent areas using data from the PASSEQ experiment. Pure and applied geophysics, Vol. 170, Issue 5, pp. 797-814, DOI: 10.1007/s00024-012-0458-8, 2012

**Conferences:**

1. **Janutyte, I.,** Majdanski, M., Voss P. H., Kozlovskaya, E., and PASSEQ Working Group (2014), Upper Mantle Structure Around the Trans-European Suture Zone. EGU General Assembly 2014, Geophysical Research Abstracts, Vol. 16, EGU2014-4463.
2. **Janutyte, I.,** Voss, P. H., Kozlovskaya, E., Majdanski, M., and PASSEQ Working Group (2013), Results of teleseismic tomography across the Trans-European Suture Zone. CTBT Science and Technology 2013 Conference, Hofburg Palace, Vienna, Austria, 17-21 June 2013, Book of abstracts, pp. 39, poster No. T1-P49.
3. **Janutyte, I.,** Voss, P. H., Kozlovskaya, E., and PASSEQ Working Group (2012), Preliminary results of teleseismic tomography across the Trans-European Suture Zone. European Seismological Commision 33rd General Assembly, Moscow, Russia, August 19-24, 2012, Programme and abstract book.